

# Rapid Proptotyping and Tooling of Automotive Seal Mouldings

By  
*Iestyn Evans*

Submitted to Swansea University in fulfilment of the requirements for the  
Degree of *MSc by Research*



Prifysgol Abertawe  
Swansea University

*Swansea University*  
2019



## **Abstract**

EPDM exterior automotive seals are currently only manufactured by injection moulding or extrusion, both requiring expensive tooling which are produced by traditional machining. Aston Martin and other automotive companies regularly need a small number of seals to be produced, upwards of 100 for prototype testing and small production runs required for limited edition vehicle programs. This project looks at whether rapid prototyping techniques can be used to manufacture tooling for injection moulding of EPDM used for short production runs, reducing cost and lead time associated with traditional machining.


A novel rapid prototype tooling methodology is proposed which optimises rapid prototyping techniques, combining rapid tooling techniques of metal powder and epoxy. Mechanical and thermal properties of the proposed novel rapid prototype tooling are validated by computational simulation performed in ANSYS 19.1 software. An optimum rapid prototype tooling is deduced from displacement, stress, and thermal footprint results.

It has been shown through computational modelling that the proposed novel rapid tooling methodology produces a number of tooling that would be capable of small production runs of EPDM seals by injection moulding. 5mm thick titanium shell with reinforcement is proposed as the optimum rapid prototype tooling which would be capable of producing upwards of 100 EPDM seals by injection moulding. A total cost saving of 210% could be made when utilising rapid prototyping techniques in the manufacture of tooling for injection moulding of EPDM.

# Declaration and Statements

## DECLARATION

This work has not previously been accepted in substance for any degree and is not being concurrently submitted in candidature for any degree.

Signed: 

Date: 10/06/2020

## STATEMENT 1

This thesis is the result of my own investigations, except where otherwise stated. Other sources are acknowledged by footnotes giving explicit references. A bibliography is appended.

Signed: 

Date: 10/06/2020

## STATEMENT 2

I hereby give consent for my thesis, if accepted, to be available for photocopying and for inter-library loan, and for the title and summary to be made available to outside organisations.

Signed: 

Date: 10/06/2020

# Contents

- 1 Introduction** **13**
  
- 2 Literature Review** **15**
  - 2.1 Ethylene Propylene Diene Monomer . . . . . 15
    - 2.1.1 Properties of EPDM . . . . . 15
    - 2.1.2 Production of EPDM . . . . . 16
    - 2.1.3 Composite EPDM Material . . . . . 18
  - 2.2 Rubber Manufacture . . . . . 20
    - 2.2.1 Mixing . . . . . 20
    - 2.2.2 Forming . . . . . 22
    - 2.2.3 Vulcanising . . . . . 26
  - 2.3 Rapid Prototyping . . . . . 29
    - 2.3.1 Stereolithography . . . . . 30
    - 2.3.2 Digital Light Processing . . . . . 31
    - 2.3.3 Selective Laser Sintering . . . . . 32
    - 2.3.4 Fused Deposition Modelling . . . . . 33
    - 2.3.5 Laminated Object Manufacture . . . . . 35
    - 2.3.6 Material Jetting . . . . . 36
    - 2.3.7 Binder Jetting . . . . . 37
    - 2.3.8 Summary of Rapid Prototyping Techniques . . . . . 38
  - 2.4 Rapid Tooling . . . . . 39
    - 2.4.1 Direct Tooling . . . . . 40
    - 2.4.2 Indirect Tooling . . . . . 45
    - 2.4.3 Summary of Rapid Tooling Techniques . . . . . 55
  - 2.5 Computational Modelling . . . . . 56
  - 2.6 Proposed Novel Rapid Tooling Methodology . . . . . 59
  
- 3 ANSYS Computational Method Analysis** **62**
  - 3.1 Overview . . . . . 62
  - 3.2 Methodology . . . . . 63
    - 3.2.1 Tool Selection . . . . . 63
    - 3.2.2 Computational Model . . . . . 65
  - 3.3 Results . . . . . 74
  - 3.4 Conclusion . . . . . 81

<b>4</b>	<b>Computational Validation of Proposed Novel Rapid Tooling</b>	<b>83</b>
4.1	Overview . . . . .	83
4.2	Methodology . . . . .	83
4.2.1	Physical Model . . . . .	83
4.2.2	Computational Model . . . . .	84
4.3	Results . . . . .	88
4.3.1	Mechanical . . . . .	88
4.3.2	Thermal . . . . .	96
4.4	Conclusion . . . . .	103
<b>5</b>	<b>Evaluation of Proposed Novel Rapid Tooling</b>	<b>104</b>
5.1	Tool Life . . . . .	104
5.2	Production Cost . . . . .	105
5.2.1	Individual Part . . . . .	106
5.2.2	Whole Tool . . . . .	108
<b>6</b>	<b>Conclusion</b>	<b>110</b>
6.1	Project Outcomes . . . . .	110
6.2	Future Work . . . . .	111
	<b>References</b>	<b>112</b>

## **Acknowledgments**

I would firstly like to thank my academic supervisor Dr Andrew Rees on all his guidance and help throughout this project. A special thanks also goes to all staff at Swansea University who have helped me throughout the year.

I would also like to thank my sponsoring company Aston Martin for the wonderful experience of working with them. They have been very supportive throughout the project and most welcoming on visits to Gaydon. Enrico Mariconda deserves a special mention for all his time and expertise throughout which has been invaluable in ensuring a successful project.

I would also like to thank everybody at the M2A team for all their hard work which often goes unnoticed. Their support has been invaluable in ensuring the smooth running of the project. I am also very grateful to M2A, EPSRC, ESF, and Aston Martin for all the funding that I have received.

Finally I would like to thank all my friends and family for their support during this year, without which I would not have been able to complete the project.

## List of Tables

2.1	Physical, mechanical, and thermal properties of EPDM rubber [7]. . .	16
2.2	Strengths and weaknesses of EPDM rubber. . . . .	16
2.3	Comparison of the different rapid prototyping processes. . . . .	39
2.4	Comparison of the different rapid tooling processes. . . . .	55
3.1	Typical parameters for injection moulding of EPDM exterior automotive seals. . . . .	66
3.2	Summary of the ANSYS computational model analysis, displaying maximum and average displacement and stress values at the fluid-solid interface, along with the computational time for each model. . . . .	75
4.1	Typical parameters for injection moulding of EPDM using Aston Martin 614690 – 1 – AM305 roadster header mould tool. . . . .	84
4.2	Material and their properties to be used in computational simulations.	86
4.3	Thermal Footprint of 2mm thick aluminium shell with backing rapid prototype tooling, 8mm thick aluminium shell without backing rapid prototype tooling, and benchmark part at 45s, 86s, 120s, and 150s. . .	100
4.4	Average heating and cooling rates of various aluminium rapid prototype and benchmark tooling. . . . .	102
5.1	Summary of the manufacturing cost for the ALM shell components of 2mm and 8mm thickness. . . . .	106
5.2	Total cost for the manufacture of complete rapid prototype tooling. . .	106
5.3	Production cost for the 5mm thick titanium shell with reinforcement rapid prototype tooling. . . . .	107
5.4	Traditional machining manufacturing cost for the benchmark part form various companies. . . . .	107

## List of Figures

1.1	3D printing process from 3D CAD model to 3D object. . . . .	14
2.1	Chemical structure of ethylene propylene diene monomer. . . . .	15
2.2	Chemical structures of commercially used dienes in the production of ethylene propylene diene monomer: (a) 5-ethylidene-2-norbornene, (b) dicyclopentadiene, (c) 1,4-hexadiene. . . . .	15

2.3	Variation of: (a) density, (b) hardness, (c) tensile strength, (d) elongation, and (e) DC electrical conductivity of EPDM against carbon black loading at 25°C [20]. . . . .	20
2.4	Schematic of a two-roll mill. . . . .	21
2.5	Schematic of (a) internal mixer, and two types of rotors used in internal mixers; (b) tangential and (c) intermeching. . . . .	21
2.6	Schematic of calendering coating of fabric. . . . .	22
2.7	Schematic of a screw extruder. . . . .	23
2.8	Schematic of the calendering process. . . . .	24
2.9	Schematic of the moulding processes; (a) compression, (b) transfer and (c) injection. . . . .	26
2.10	Typical fatigue, hardness, tensile strength and elongation of rubber as a function of crosslinking density [27]. . . . .	27
2.11	3D printing process from 3D CAD model to 3D object. . . . .	29
2.12	Schematic of the stereolithography process. . . . .	30
2.13	Schematic of the digital light processing process. . . . .	31
2.14	Schematic of the selective laser sintering process. . . . .	32
2.15	Schematic of the fused deposition modelling process. . . . .	34
2.16	Schematic of the laminated object manufacture process. . . . .	36
2.17	Schematic of the material jetting process. . . . .	37
2.18	Schematic of the binder jetting process. . . . .	38
2.19	Schematic of the laser engineered net shaping process. . . . .	45
2.20	Schematic of the spray metal tooling process. . . . .	50
2.21	Schematic of the electroforming tooling process. . . . .	52
2.22	Process routes of rapid investment casting [46]. . . . .	53
2.23	Schematic of the 3D Keltool process. . . . .	55
2.24	Classification of the rapid tooling processes. . . . .	56
2.25	Cross sectional view of the stereolithography injection moulding tool inserts [91]. . . . .	57
2.26	Scaffolding assembly structure used in mechanical evaluation [88]. . . . .	58
2.27	Three-dimensional FEM model for half of the die [81]. . . . .	59
2.28	Manufacturing route of the proposed novel rapid tooling technique; (a) CAD model of tooling, (b) CAD model of tooling's shell, (c) additive layer manufacture of shell, and (d) filling of shell with epoxy resin. . . . .	61



2.29	Figure of an example tool made by the proposed novel rapid tooling technique. . . . .	61
3.1	Schematic of information flow in 1-way and 2-way coupled fluid structure interaction. . . . .	62
3.2	CAD model of Aston Martin 6G33 - L20708 - A - 22 - WEATHER STRIP ASSY – DOOR PRIM exterior automotive seal used as benchmark part for ANSYS computational methods analysis. . . . .	63
3.3	Cross-section for simplified part which has been taken from original part. . . . .	64
3.4	Complete simplified part which is used to create the cavity for the mould used in computational model analysis. . . . .	64
3.5	Transparent isometric view of the simplified tool for the computational model analysis. . . . .	65
3.6	Static structural computational model with loads and boundary conditions. . . . .	67
3.7	Project schematic for the 1-way coupled thermal-structural computational model. . . . .	67
3.8	Steady-state thermal computational model, with A representing the tool-melt interface temperature and B representing the external plate temperature. . . . .	68
3.9	Loads and boundary conditions for the structural component of the 1-way coupled thermal-structural computational model, which differs to the structural computational model due to the inclusion of imported body temperature. . . . .	69
3.10	Project schematic of the 1-way coupled fluent-structural computational model. . . . .	69
3.11	Model for the fluent simulations along with its named selections; inlet and fluid-tool boundary. . . . .	70
3.12	Loads and boundary conditions for the transient structural component of the 1-way coupled fluent-structural computational model. . . . .	71
3.13	Project schematic of the 1-way coupled fluent-thermal-structural computational model. . . . .	72
3.14	Loads and boundary conditions for the transient structural component of the 1-way coupled fluent-thermal-structural computational model. . . . .	73

3.15	Project schematic of the 2-way coupled fluent-structural computational model. . . . .	73
3.16	Maximum and average displacement results from each computational model at fluid-solid interface. . . . .	75
3.17	Maximum and average stress results from each computational model at fluid-solid interface. . . . .	76
3.18	Computational time for each computational model. . . . .	76
3.19	Displacement plot including location of maximum and minimum displacement for the structural computational model. . . . .	77
3.20	Displacement plot including location of maximum and minimum displacement for the 1-way coupled FSI fluent-thermal-structural computational model. . . . .	78
3.21	Displacement plot including location of maximum and minimum displacement for the 2-way coupled FSI fluent-structural computational model. . . . .	78
3.22	Stress plot including location of maximum and minimum stress for the structural computational model. . . . .	79
3.23	Stress plot including location of maximum and minimum stress for the 1-way coupled FSI fluent-thermal-structural computational model. . . . .	79
3.24	Stress plot including location of maximum and minimum stress for the 2-way coupled FSI fluent-structural computational model. . . . .	80
4.1	Exploded view of the Aston Martin 614690 – 1 – AM305 roadster header mould tool. . . . .	84
4.2	Isometric view of a CAD model of the single part chosen from the commercial tool for computational validation. . . . .	85
4.3	Physical setup of the mechanical simulation which includes a pressure and fixed geometries. . . . .	87
4.4	Physical setup of the thermal simulation which includes a temperature and thermal radiation. . . . .	87
4.5	Temperature profile at the fluid-solid interface. . . . .	88
4.6	Summary of the mechanical mesh sensitivity analysis, comparing (a) maximum and average displacement, (b) maximum and average stress, and (c) computational time against number of elements for linear and quadratic type mesh. . . . .	90
4.7	Histogram of node stress in the linear and quadratic mesh. . . . .	90

4.8	Mesh used for the mechanical simulations of an 8mm thick shell without reinforcement. . . . .	91
4.9	Comparison of maximum displacement of additive layer manufactured parts with different shell thicknesses, material, and with or without reinforcement. . . . .	92
4.10	Comparison of average displacement of additive layer manufactured parts with different shell thicknesses, material, and with or without reinforcement. . . . .	92
4.11	Comparison of maximum stress of additive layer manufactured parts with different shell thicknesses, material, and with or without reinforcement. . . . .	93
4.12	Comparison of average stress of additive layer manufactured parts with different shell thicknesses, material, and with or without reinforcement. . . . .	94
4.13	Percentage of mesh nodes with stress greater than the ultimate tensile strength of the material. . . . .	94
4.14	Percentage of mesh nodes with stress greater than the ultimate tensile strength of the material with a safety factor of 2. . . . .	95
4.15	Summary of the thermal mesh sensitivity analysis, comparing (a) maximum and average temperature, and (b) computational time against number of elements for linear and quadratic type mesh. . . . .	96
4.16	Mesh used for the thermal simulations of an 8mm thick shell without reinforcement rapid prototype tooling. . . . .	97
4.17	Maximum and average temperature profile for 2mm thick shell with reinforcement rapid prototype tooling. . . . .	98
4.18	Maximum and average temperature profile for 8mm thick shell ALM parts without reinforcement. . . . .	98
4.19	Temperature profile of the two components, shell and reinforcement, in the 2mm thick aluminium shell with reinforcement rapid prototype tooling. . . . .	99
4.20	Average temperature of rapid prototype tooling 2mm thick aluminium shell with reinforcement material of epoxy composite including 0vol.%, 10vol.%, 30vol.%, and 50vol.% aluminium powder, compared against 8mm thick aluminium shell without reinforcement rapid prototype tooling and benchmark parts. . . . .	101

4.21	Average temperature of rapid prototype tooling 2mm thick titanium shell with reinforcement material of epoxy composite including 0vol.%, 10vol.%, 30vol.%, and 50vol.% aluminium powder, compared against 8mm thick titanium shell without reinforcement rapid prototype tooling and benchmark parts. . . . .	101
5.1	S-N curve for solution treated aged Ti-6Al-4V [7]. . . . .	105
5.2	CAD drawings of simple components from the Aston Martin 614690 – 1 – AM305 Vantage Roadster header mould tool. . . . .	108
5.3	CAD drawings of complex components from the Aston Martin 614690 – 1 – AM305 Vantage Roadster header mould tool. . . . .	109

# Nomenclature

## Abbreviations

2D . . . . . Two Dimensional  
3D . . . . . Three Dimensional  
3DP . . . . . Three Dimensional Printing  
ABS . . . . . Acrylonitrile Butadiene Styrene  
AHP . . . . . Analytic Hierarchy Process  
ALM . . . . . Additive Layer Manufacture  
BBO . . . . . Binder Burn Out  
BJ . . . . . Binder Jetting  
BPM . . . . . Ballistic Particle Manufacture  
CAD . . . . . Computer Aided Design  
CAE . . . . . Computer Aided Engineering  
CAM . . . . . Computer Aided Manufacturing  
CFD . . . . . Computational Fluid Dynamics  
CNC . . . . . Computer Numerically Controlled  
CTE . . . . . Coefficient of Thermal Expansion  
DC . . . . . Direct Current  
DCPD . . . . . Dicyclopentadiene  
DLP . . . . . Digital Light Processing  
DSPC . . . . . Direct Shell Production Casting  
EDM . . . . . Electrical Discharge Machining  
ENB . . . . . 5-Ethylidene-2-Norbornene  
EPDM . . . . . Ethylene Propylene Diene Monomer  
FDM . . . . . Fused Deposition Modelling  
FDMet . . . . . Fused Deposition of Metals  
FEM . . . . . Finite Element Methods  
FSI . . . . . Fluid Structure Interaction  
HCF . . . . . High Cycle Fatigue  
HV . . . . . Vickers Hardness  
LCF . . . . . Low Cycle Fatigue  
LENS . . . . . Laser Engineered Net Shape  
LMT . . . . . Laminated Metal Tooling  
LOM . . . . . Laminated Object Manufacture  
MBT . . . . . Mercaptobenzthiazole  
MJ . . . . . Material Jetting  
PC . . . . . Polycarbonate  
phr . . . . . Part Per Hundred Part Rubber  
PLA . . . . . Polyactic Acid  
PP . . . . . Polypropylene

PU . . . . . Polyurethane  
QFD . . . . . Quality Function Deployment  
RP . . . . . Rapid Prototyping  
RT . . . . . Rapid Tooling  
RTV . . . . . Room Temperature Vulcanisation  
SFF . . . . . Solid Freedom Fabrication  
SGC . . . . . Solid Ground Curing  
SL . . . . . Stereolithography  
SLA . . . . . Stereolithography  
SLM . . . . . Selective Laser Melting  
SLS . . . . . Selective Laser Sintering  
STL . . . . . Stereolithography  
TMTD . . . . . Tetramethyl Thiuram Disulphide  
TPE . . . . . Thermoplastic Elastomers  
TPV . . . . . Thermoplastic Vulcanisates  
UV . . . . . Ultraviolet  
vol . . . . . Volume  
wt . . . . . Weight  
YAG . . . . . Yttrium Aluminum Garnet  
ZDMC . . . . . Zinc Dimethyl Dithiocarbamate

## Symbols

$\text{Al}_2\text{O}_3$  . . . . . Aluminium Oxide  
Bi . . . . . Bismuth  
C . . . . . Celsius  
 $\text{CO}_2$  . . . . . Carbon Dioxide  
g . . . . . Gram  
K . . . . . Kelvin  
m . . . . . Meter  
Pa . . . . . Pascal  
Ra . . . . . Roughness Average  
Rz . . . . . Average Maximum Height  
Sb . . . . . Antimony  
 $\text{SiO}_2$  . . . . . Silicon Dioxide  
Sn . . . . . Tin  
W . . . . . Watt  
 $\text{ZnO}$  . . . . . Zinc Oxide

# 1 Introduction

During product development it is necessary to manufacture prototype production parts for validation and testing. Vehicle exterior seals are made from EPDM and currently, injection moulding and extrusion is their only viable manufacturing method. Injection moulding is necessary for manufacture of parts with complex geometry. Tooling for injection moulding of EPDM exterior seals are traditionally machined from steel which have high costs and lead times, typically with lead times of 16-26 weeks and cost upward of £80,000. EPDM is a very viscous material which requires high mould pressure during injection moulding. Part design is often modified during product development which results in scrapping or expensive modification costs of tooling.

Polyurethane (PU) prototype parts are currently used in product development, but are not useful for all required testing. Material improvement or rapid prototyping of tooling are two possible avenues for improving prototype parts in the product development stage, saving costs and time. A material could be developed that has replicable properties to EPDM with parts being made by a less expensive and quicker manufacturing route. The other possible method is to utilise rapid prototyping to manufacture tooling that could be used for the injection moulding of EPDM parts. This research focuses on the development of rapid prototyping to manufacture tooling for injection moulding as this could produce prototype EPDM parts which are manufactured using production technique.

Additive Layer Manufacture (ALM), also known as Rapid Prototyping (RP) or 3D printing, is the fast manufacture of a 3D part. It offers an alternative to traditional machining to produce tooling for injection moulding. Firstly, a model of the part is created on a Computer Aided Design (CAD) program which is exported as a stereolithography file to a slicing software package such as Cura. The slicing software slices the part and calculates the tool path, i.e. the build sequence. A part file is now ready to be sent to an additive layer manufacturing machine for fabrication. A schematic of the process from a CAD model to a 3D object is shown in Figure 1.1.

There are seven main categories that ALM techniques fall under; stereolithography, digital light processing, selective laser sintering, fused deposition modelling, laminated object manufacture, material jetting and binder jetting. Under each of these seven categories there are numerous variations, each with their own advantages and disadvantages. Material properties, part size, accuracy, surface finish and cost are some of the parameters that need to be considered when selecting the ALM technique to be used when creating rapid prototype tooling [1–3].

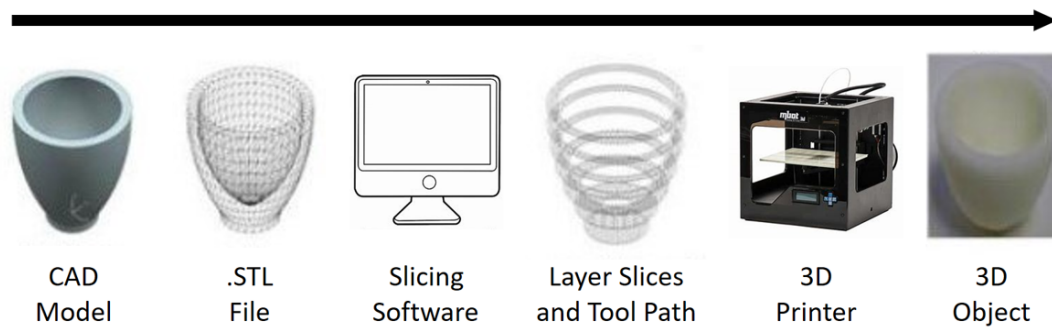


Figure 1.1: 3D printing process from 3D CAD model to 3D object.

Rapid tooling is the term used to describe the process of producing tooling using ALM, either creating the tool directly or creating a master model from which the tool is created, categorising rapid tooling into direct and indirect [4–6]. Utilising rapid tooling can significantly reduce the lead time and cost when compared to traditional machining [4–6]. During the product development stage, when time is at a premium, rapid tooling offers a prominent alternative to traditional machining of injection moulding tooling. Design changes are easier to accommodate when using rapid tooling, allowing for quicker part improvements and consequentially reducing product lead time [4–6]. This thesis investigates whether ALM is a viable method for producing tooling used in injection moulding of EPDM exterior automotive seals. Specifically, a proposed novel rapid prototype tooling method that combines metal powder and epoxy, which uses ALM methods of selective laser sintering or binder jetting. The proposed novel rapid prototype tooling is made from two components; an outer metal shell which is reinforced by an inner epoxy resin composite.

Evaluation of analysis systems available on ANSYS 19.1 software which can simulate the injection moulding process is undertaken to find the most appropriate computational model for validation of the rapid prototype tooling. Singular, 1-way coupled Fluid Structural Interaction (FSI), and 2-way coupled FSI computational models will be evaluated by looking at their results and computational times. The most appropriate computational model will be used for validation of the mechanical and thermal properties of the rapid prototype tooling. Shell thickness, shell material, and reinforcement are the independent parameters for the computational simulation of the proposed novel rapid tooling. From the computational models, an optimum tool will be suggested that has adequate mechanical and thermal properties for injection moulding of EPDM. Tool life and production cost of the rapid prototype tooling will also be evaluated.

## 2 Literature Review

### 2.1 Ethylene Propylene Diene Monomer

EDPM, a thermosetting elastomer rubber, is an unsaturated terpolymer of ethylene (45-75wt.%), propylene (20-50wt.%) and a non-conjugated diene (4.5-9.0wt.%) [7]. Figure 2.1 shows the chemical structure of EDPM and Figure 2.2 shows the chemical structures of commercially used diene monomers; 5-ethylidene-2-norbornene (ENB), dicyclopentadiene (DCPD), and 1,4-Hexadiene [7-9]. The diene monomer provides the unsaturation in EPDM which serves as the site for crosslinking. A non-conjugated diene is a hydrocarbon that contains two carbon double bonds that are separated by two or more single bonds. Non-conjugated dienes are less stable than their isomeric conjugated dienes. Crosslinking is commonly achieved by either sulphur or peroxide vulcanisation [8]. Typical use of EDPM for automotive applications includes seals, gaskets, roofing and hoses.

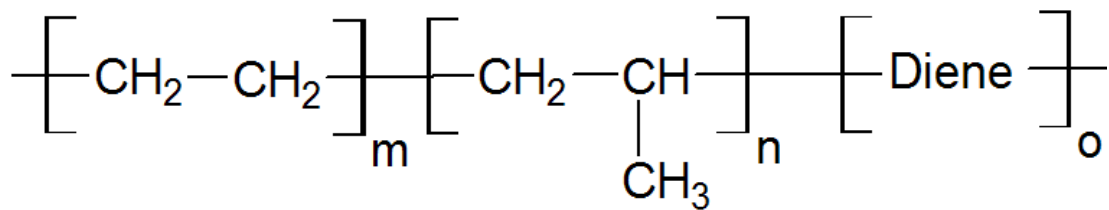


Figure 2.1: Chemical structure of ethylene propylene diene monomer.

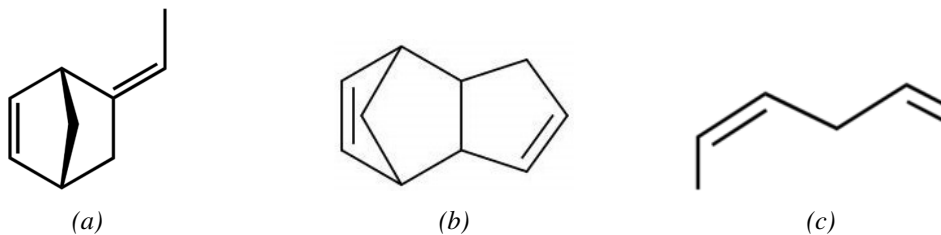


Figure 2.2: Chemical structures of commercially used dienes in the production of ethylene propylene diene monomer: (a) 5-ethylidene-2-norbornene, (b) dicyclopentadiene, (c) 1,4-hexadiene.

#### 2.1.1 Properties of EPDM

Vulcanised (cured) EPDM has a saturated polymer backbone which results in excellent resistance to oxygen, ozone, UV and heat, making it a perfect material for outdoor products such as seals, roofing and hoses [8]. Physical, mechanical and thermal prop-



erties of EPDM is shown in Table 2.1, whilst strengths and weaknesses of EPDM are shown in Table 2.2 [7].

Table 2.1: Physical, mechanical, and thermal properties of EPDM rubber [7].

<b>Property</b>	<b>Value</b>
<i>Physical</i>	
<i>Density</i>	860–880 $\text{kgm}^{-3}$
<i>Mechanical</i>	
<i>Young's Modulus</i>	7e-4–0.0017 GPa
<i>Yield Strength</i>	1.5–2.5 MPa
<i>Elongation</i>	500–700 %strain
<i>Compressive Modulus</i>	7e-4–0.0017 GPa
<i>Flexural Modulus</i>	7e-4–0.0017 GPa
<i>Shear Modulus</i>	2.4e-4–5.7e-4 GPa
<i>Bulk Modulus</i>	1.5–2 GPa
<i>Poisson's Ratio</i>	0.48–0.495
<i>Hardness - Vickers</i>	1–2 HV
<i>Thermal</i>	
<i>Glass Temperature</i>	–60––45 °C
<i>Maximum Service Temperature</i>	150–177 °C
<i>Minimum Service Temperature</i>	–51––45 °C
<i>Thermal Conductivity</i>	0.15–0.2 $\text{Wm}^{-1}\text{°C}^{-1}$
<i>Specific Heat Capacity</i>	2.01e3–1.12e4 °C
<i>Thermal Expansion Coefficient</i>	200–300 $\mu\text{strain}^{\circ}\text{C}^{-1}$

Table 2.2: Strengths and weaknesses of EPDM rubber.

<b>Property</b>	<b>Rating</b>
<i>Ozone Resistance</i>	Excellent
<i>Atmospheric Aging Resistance</i>	Excellent
<i>Weather Resistance</i>	Excellent
<i>Oxidation Resistance</i>	Excellent
<i>Heat Resistance</i>	Excellent
<i>Water/Steam Resistance</i>	Excellent
<i>Oil Resistance</i>	Poor
<i>Flame Resistance</i>	Poor

### 2.1.2 Production of EPDM

Commercial production of EPDM is achieved by three main polymerisation techniques; solution, slurry-phase and gas-phase [10]. Polymerisation of EPDM is an

exothermic reaction which is carefully controlled to maintain safety. Heat generated from the exothermic reaction increases the reaction rate which in turn generates even more heat which can lead to out of control reactions called autoacceleration. Adequate heat dissipation systems are required to avoid autoacceleration reaction which can be very dangerous.

#### **2.1.2.1 Solution**

Solution polymerisation begins by dissolving ethylene, propylene and diene monomers alongside a catalyst system in a non-reactive hydrocarbon solvent. Heat generated by the exothermic reaction is easily dispersed by the solvent which allows for good reaction rate control. Once the polymerisation is complete the solvent and any unreacted monomers are removed by mechanical devolatilization, hot water or steam. Particles of EPDM are left which are dried by any acceptable method, such as hot air or low-pressure dryers.

#### **2.1.2.2 Slurry Phase**

Polymerisation of EPDM by slurry phase is a modification of the bulk polymerisation technique where a propylene filled reactor is fed monomers and catalysts [10]. Polymerisation is fast, and granules of EPDM polymer are formed which are not soluble in propylene. Precise and stable temperature control is achievable as the slurry has low viscosity. The major advantage of the process is its ability to produce high molecular weight polymer without reducing production as the process is not limited by solution viscosity.

#### **2.1.2.3 Gas Phase**

Gas phase polymerisation is a technique commonly used for gaseous monomers such as ethylene and propylene. Gases of the monomers, catalysts and nitrogen are fed into a reactor. Nitrogen gas is included to circulate the reactor to remove heat from the exothermic reaction and to fluidise the polymer bed. Carbon black is fed in large quantities into the reactor to act as a partitioning aid which prevents the polymer granules from sticking to each other and to the reactor wall. Gas phase polymerisation eliminates the need for solvents and thus costly and time consuming processes of solvent removal and polymer drying.

### **2.1.3 Composite EPDM Material**

This section will highlight composite EPDM materials that are being used commercially and those that are being developed. These composite materials improve the properties and processability of EPDM which can result in lower manufacturing time and cost.

#### **2.1.3.1 Polypropylene and EPDM Blend**

Polypropylene and EPDM (PP/EPDM) blends are classified as thermoplastic elastomers (TPEs) and more specifically classed as thermoplastic vulcanizates (TPVs). Particles of cured EPDM are dispersed in PP, which is a thermoplastic, creating a thermoplastic and elastomer composite material. TPVs combine the processability of thermoplastics with the elastic and mechanical properties of vulcanised rubbers [11, 12]. Production of TPVs require simultaneously mixing and crosslinking of rubber with a thermoplastic at an elevated temperature [11, 13].

Reducing the interparticle distance of EPDM increase the strength of PP/EPDM material [14, 15]. This could be achieved by either increasing the volume or reducing the particle size of EPDM. Increasing the EPDM content increases the Izod impact strength but reduces the tensile and flexural strength of PP/EPDM blends [16]. The Izod impact test increased by 5 times when the EPDM weight content increased from 4% to 20% [14, 16]. Both the tensile and flexural strength of PP/EPDM blend decrease by half with the weight increase from 0% to 40% of EPDM [16]. Adding 5wt.% of silicon dioxide ( $\text{SiO}_2$ ) to the PP/EPDM blend increases the tensile and flexural strength by around 15% and increases the Izod impact strength of the PP/EPDM blend [16].

#### **2.1.3.2 EPDM-Organoclay Hybrids**

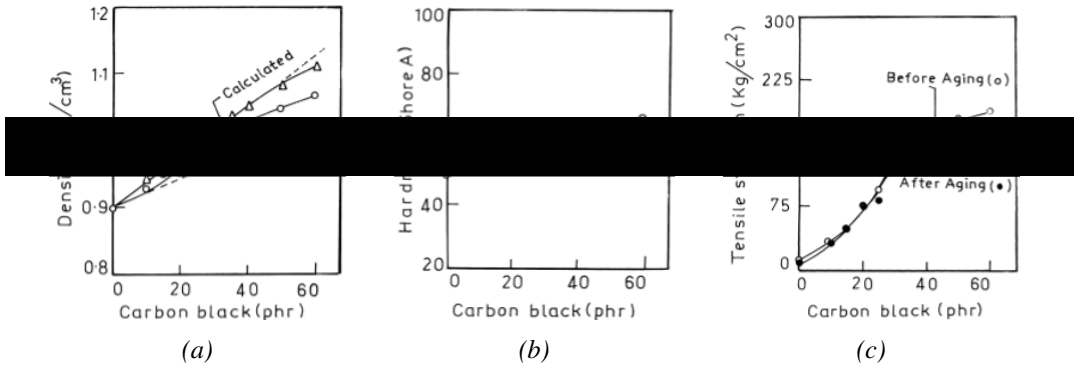
EDPM-organoclay hybrids are being developed predominantly for the nanotechnology sector, but they could be used in any other sector. Organoclays are organically modified clays whose surface have been altered. There are several different methods to prepare organoclays, such as adsorption, binding of inorganic and organic anions, and grafting of organic compounds, but the preferred method to prepare organoclays is with ion exchange with alkylammonium [17]. Vulcanisation process and melt interaction technique are two common methods of producing EPDM-organoclay hybrids [18, 19].

An addition of 4wt.% organoclay to EPDM increases the tensile strength from 5MPa to 10.1MPa but decreases the permeability by 30% [18]. The effect of organoclay on the elongation of EPDM depends on the vulcanisation accelerator used. When

zinc dimethyldithiocarbamate vulcanisation accelerator was used the elongation increased by 86% but when N-cyclohexyl-2-mercaotibenzothiazole vulcanisation accelerator was used the elongation decreased by 62% when used with the addition on 4wt.% of organoclay in EPDM [18]. The difference in elongation is due to the different dispersibility of the organoclay in EPDM, which is affected by the vulcanisation accelerator used [18]. Increasing the organoclay part per hundred part of rubber by weight (phr) from 0 to 5 increased the tensile strength from 4.5MPa to 12MPa, but further increases of organoclay above 5 phr gradually decreases the tensile strength [19].

**2.1.3.3 Carbon Black Filled EPDM**

Carbon black is a paracrystalline carbon that is produced by incomplete combustion of petroleum. It has a high surface area to volume ratio which makes it a good reinforcing filler material in many rubber products. The structure of the particles are graphitic with a size range from 10nm to 400nm in diameter, where the smaller ones are less graphitic [9]. Particle size and surface area, structure, physical nature of the surface, chemical nature of the surface, and particle porosity are the five most important parameters of carbon black [9]. The addition of 40 phr of carbon black to EPDM increases the density, hardness and tensile strength by 15%, 28% and 150-fold respectively [20]. At carbon black loading above 40 phr the hardness and tensile strength level off. Elongation at break reaches a maximum of 650% at carbon black loading of 30 phr [20]. DC electrical conductivity is also increase drastically with the addition of carbon black [20, 21]. Figure 2.3 shows the variation of density, hardness, tensile strength, elongation and DC electrical conductivity of EPDM against carbon black loading at 25°C [20].



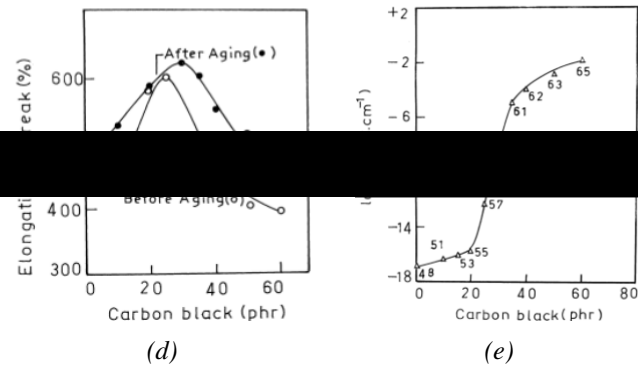


Figure 2.3: Variation of: (a) density, (b) hardness, (c) tensile strength, (d) elongation, and (e) DC electrical conductivity of EPDM against carbon black loading at 25°C [20].

## 2.2 Rubber Manufacture

Production of rubber can be divided into three stages; mixing, forming and vulcanising. Each stage has several different processing methods to accommodate the variety of rubbers being produced. The most common processing methods for each of the three stages of rubber manufacture are described below.

### 2.2.1 Mixing

Every rubber part is made from four main ingredients; polymers, fillers, processing aids, and vulcanising additives. The first stage in rubber manufacture is to thoroughly mix all ingredients to achieve uniform dispersion which ensures no defects in the final product. Tow-roll mills and internal mixers are two commercially used rubber mixers.

#### 2.2.1.1 Two-Roll Mill

Two-roll mills have been used since the beginning of rubber manufacturing and are still used today. The two-roll mill comprises of two rolls that are horizontal and parallel to each other with the distance between them adjusted for different composites. The main disadvantage of two-roll mill mixing is the dependence on the operator skill. A schematic of the two-roll mill is shown in Figure 2.4.

Friction ratio is the ratio of the front roll speed to the back roll speed and is crucial to achieve correct mixing [22]. Friction ratio of 1:1.25 is common for natural rubbers, high friction ratios such as 1:3 are used for refining compounds, and a ratio of 1:1 or inverse is best for synthetic rubbers [9, 23]. Two-roll mills can either be double geared or more commonly be single geared. Cheaper manufacture of single geared mills is the significant factor for its popularity over double geared mills. Care is needed when

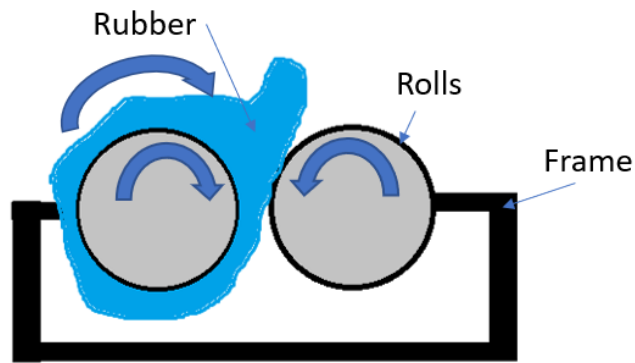


Figure 2.4: Schematic of a two-roll mill.

using single geared mills to avoid striping the teeth if the distance between the two roll is too great.

### 2.2.1.2 Internal Mixer

Internal mixers are characterised to have greater versatility, faster mixing, and larger throughput compared to two-roll mills which makes the internal mixer a preferred option for batch mixes compared to two-roll mill [9]. The internal mixer has two rotors that are encased within a chamber wall. A Schematic of an internal mixer is shown in figure 2.5. Banbury and Intermix are the two main types of internal mixers which have

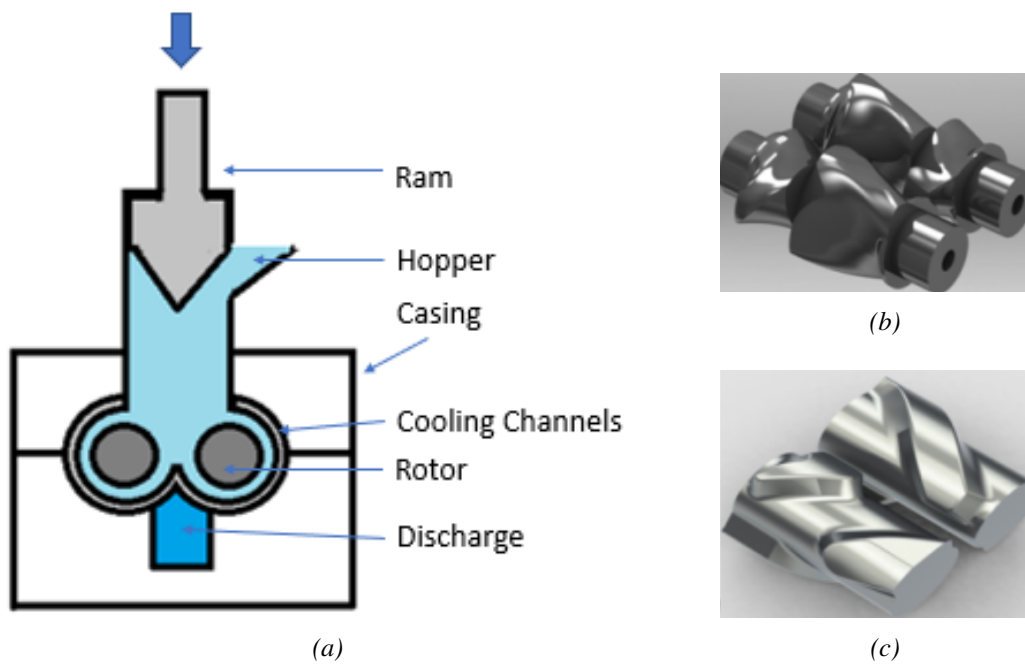


Figure 2.5: Schematic of (a) internal mixer, and two types of rotors used in internal mixers; (b) tangential and (c) intermeshing.

different rotor shapes which effect the location of mixing. The Banbury mixer has a tangential rotor type where around 80% of mixing work takes place between the rotor and the chamber wall, and the Intermix mixer has a intermeshing rotor type where around 80% of the mixing work takes place between rotors. Rotor speeds are different in the Banbury mixers which create a friction ratio, but rotor speeds are the same in the intermix mixers and the friction ratio is created by the rotors geometry. Figure 2.5 shows the rotor blades used in the Banbury and Intermix internal mixers.

## 2.2.2 Forming

Forming the material into its final shape is the second stage of rubber manufacture. There are numerous methods of rubber forming, but they can all be grouped under four basic categories; spreading, extruding, calendering and moulding [9]. The forming method used depends on the final product, with some products needing only one forming method and some needing several.

### 2.2.2.1 Spreading

Spreading is known as coating of textile fabrics in rubber manufacture. Waterproof and protective clothing, tarpaulin, electrical insulation and blackout curtains and blinds are a few examples of everyday products that are manufactured using coating of fabrics. Rubber is applied directly to the surfaces of the fabric by solvent dispersion or latex, or by calendering or frictioning [9, 24]. Good adhesion must exist between the rubber

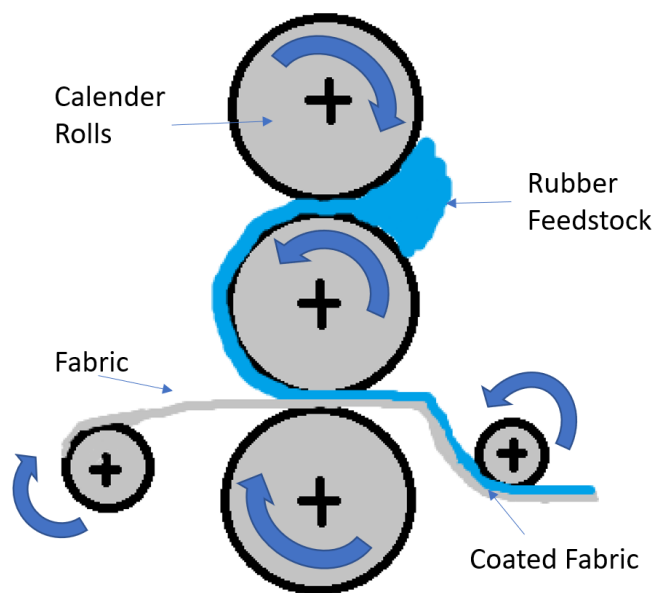


Figure 2.6: Schematic of calendering coating of fabric.

and the fabric to maximise their properties. It is necessary to chemically treat some synthetic fibres to achieve good adhesion with the rubber. A schematic of calendaring coating of fabrics is shown in Figure 2.6.

**2.2.2.2 Extruding**

Extruders are machines that use pressure to force material through a die to form the cross-sectional shape of the part. There are two types of extruders, screw and ram which are distinguished by their method of producing the pressure. Screw extruder is the most commonly used extruder in industry with the ram extruder tending only to be used for shorter runs. A schematic of a screw extruder is shown in Figure 2.7.

The material can be supplied hot or cold into the hopper but the length to diameter of the screw changes significantly for either. Screw length to diameter ratio is usually around 4.5:1 for hot material and around 17.5:1 for cold material [9]. The length of the screw is significantly longer for the cold material compared to the hot material due to the necessity to heat the material within the barrel. Temperature and pressure are two very important parameters that need to be control carefully to avoid any defects in the final part. Temperature and pressure depends on the feed rate of material which is determined by the screw geometry and rotational speed. At low pressures the screw with not be full at the discharge end which will result in surges of material arriving at the head which will affect the dimensional accuracy of the extruded part, and at high pressures chocking is seen which is very undesirable.

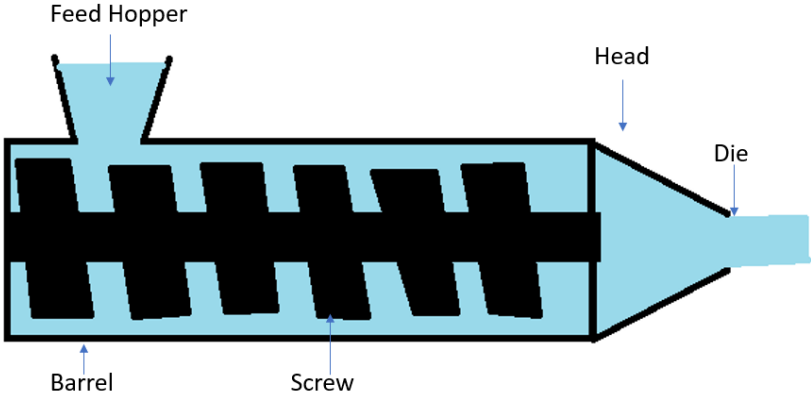
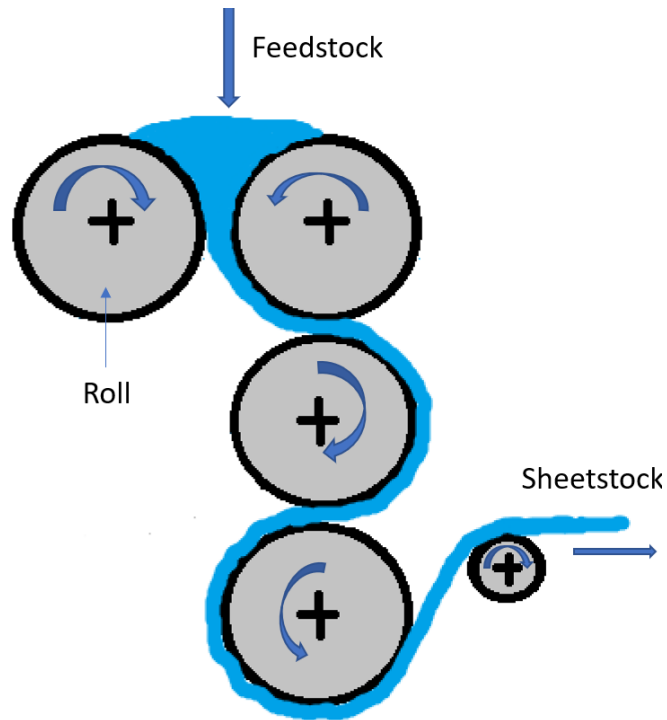


Figure 2.7: Schematic of a screw extruder.

**2.2.2.3 Calendering**

A calender produces sheets of material by passing material through a series of rolls. The distance between the rolls are adjusted to form sheet material of correct thickness.





*Figure 2.8: Schematic of the calendaring process.*

The rolls, bearings, and framework of the calendaring machine need to be sufficiently strong and robust as high loads are involved in processing rubber. Figure 2.8 shows a schematic of the calendaring process.

To achieve sheeting of uniform thickness the rubber material must have constant viscosity alongside even distribution across the rolls. Uneven distribution of material across the rolls results in areas having excess material and consequently thicker gauge. Viscosity of the rubber material is mainly affected by temperature, thus maintaining constant viscosity requires controlled temperature of the material and the calender rolls.

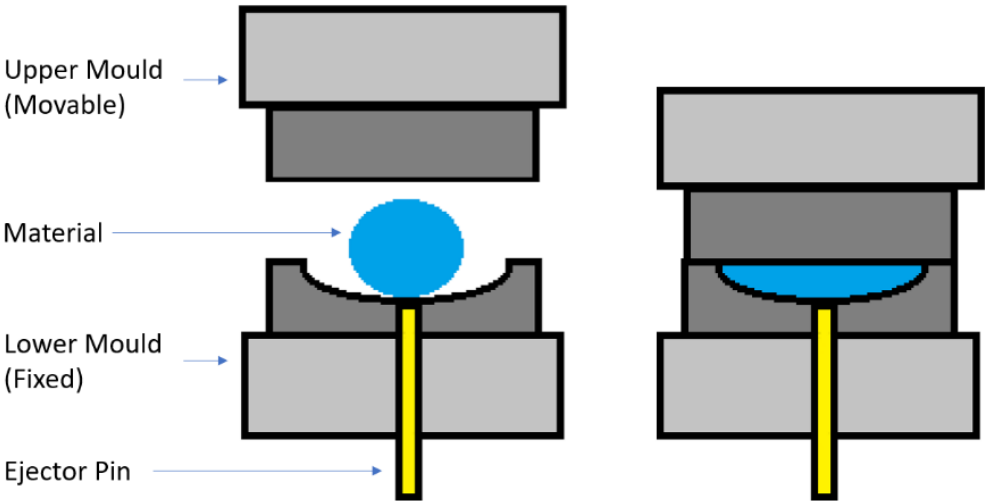
#### **2.2.2.4 Moulding**

The moulding process holds rubber in a mould under elevated temperature and pressure to shape and vulcanise the rubber material. Compression, transfer, and injection are the three main moulding processes which differ by the method of supplying material into the mould. Compression moulding is the best moulding technique for very large parts and can mould dissimilar materials. When complex metallic inserts are required, transfer moulding is the best moulding technique to use which also requires minimal post processing. Injection moulding would be the preferred moulding technique for high volume small to medium sized parts. The major advantage of injection moulding

over compression and transfer moulding is the elimination of blank preparation. A schematic of the three moulding processes is shown in Figure 2.9.

Large production runs require the mould to be manufactured from hardened steel to withstand the high temperature and pressure with aluminium moulds acceptable for low production runs. These moulds are expensive and tend to take around two weeks to fabricate. During the product development stage it is often required to manufacture a handful of prototype parts using the same process as full-scale manufacture. This is a problem for moulding as traditional moulds are very expensive to manufacture and changes to the design would incur high costs to rectify or refabricate the mould. Rapid tooling is a technique that can be utilised to fabricate low cost moulds at reduced time for moulding in the product development stage. A detailed described of rapid tooling is given in section 2.4.

Every material has a coefficient of thermal expansion which means that the size of the part will differ at moulding temperatures and ambient temperature. Shrinkage is the term used to describe the difference in dimension at ambient temperature of the mould and the parts produced from it. Differences in dimensions are due to the difference in coefficient of thermal expansion of the mould material and rubber. Steel is a common mould material which has a coefficient of thermal expansion of  $12\mu\text{strain}^\circ\text{C}^{-1}$  whilst EPDM rubber has a coefficient of thermal expansion of  $250\mu\text{strain}^\circ\text{C}^{-1}$ . The range of shrinkage is commonly between 1.5-3.0% and depends on the polymer type and filler loading [9].



(a)

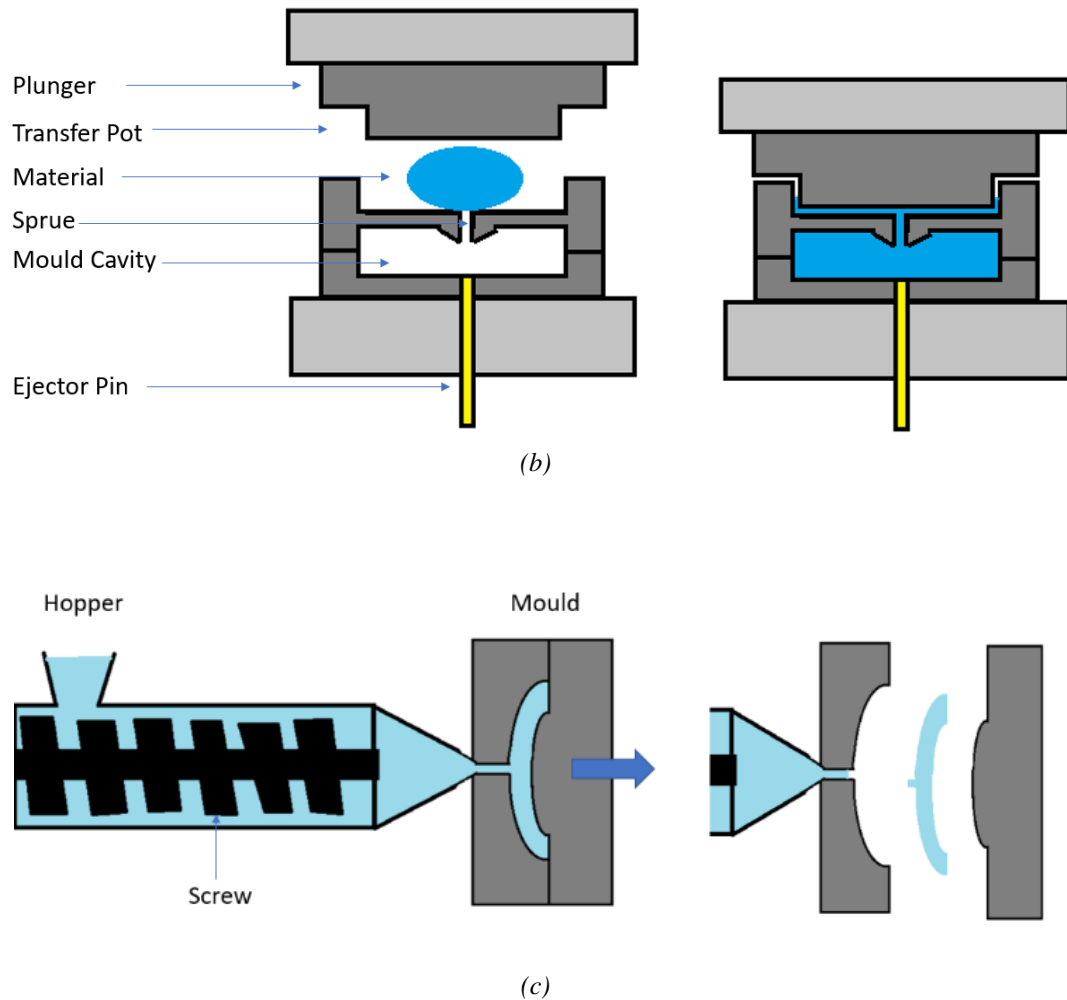


Figure 2.9: Schematic of the moulding processes; (a) compression, (b) transfer and (c) injection.

### 2.2.3 Vulcanising

Vulcanising “curing” is the last stage in rubber manufacture. Curing of rubber is a chemical reaction that crosslinks chains of rubber polymer which is achieved by heating, radiation exposition, or exposition to external chemicals [25]. Optimum cure is achieved by finding the perfect balance of temperature and time. Avoiding over-cure is crucial as it leads to thermal degradation of material. Pressure is often applied alongside temperature to avoid voids occurring in the rubber due to volatilised gases. Rubbers are vulcanised to improve their properties such as strength, elasticity, resistance to solvents and heat.

Accelerated sulphur vulcanisation is used for more than 90% of all rubbers [26]. Usually sulphur vulcanisation is performed in the presence of activators, such as ZnO and stearic acid, and accelerators such as MBT, TMTD and ZDMC [8]. A typical sulphur

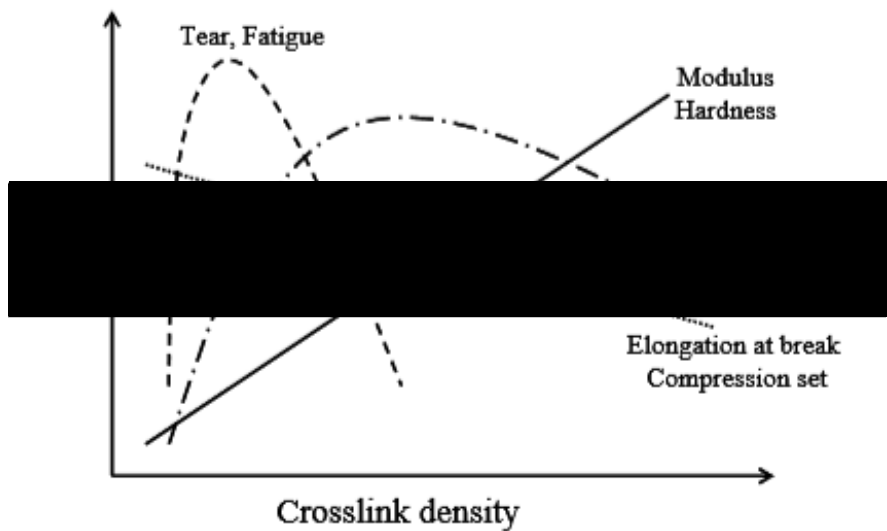


Figure 2.10: Typical fatigue, hardness, tensile strength and elongation of rubber as a function of crosslinking density [27].

curing system for EPDM would comprise of 5phr of ZnO, 0.5phr of MBT, 1.5phr of TMTM and 1.5phr of Sulphur which would be cured after 25 minutes at 165°C [9].

Fatigue, hardness, tensile strength and elongation at break are four important rubber characteristics that change with crosslinking density. With increasing crosslinking density of a typical rubber, the modulus of hardness increases but the elongation at fracture decreases. The tensile strength at fracture and tear fatigue of typical rubbers increase with crosslinking density up to a point, but then decrease again with further increase in crosslinking density. Figure 2.10 is a plot of typical fatigue, hardness, tensile strength and elongation at break of rubber as a function of crosslinking density [27].

Vulcanisation is a chemical reaction which can be classified by the activating energy source which is split into three categories, heating, radiation exposure, and exposure to external chemicals [25]. The vulcanisation method used will depend on the rubber material and the desired characteristics of the cured rubber. Mould forming processes cures the rubber inside the mould at elevated temperature usually avoiding any post curing which makes it the favoured rubber forming process. Parts fabricated by methods other than moulding require post cure shaping.

### 2.2.3.1 Heating

Heat is by far the most commonly used energy source for vulcanisation. Liquids, gasses and electricity are three commercially used heat sources for vulcanisation. There

are numerous different techniques that utilise heat to start the vulcanisation chemical reaction.

The moulding process commonly uses liquid as the source for mould heating and cooling. Moulds have networks of cavities beneath the surface where hot and cold liquid can flow. The development of additive layer manufacture of moulds, as described in section 2.4, allows for more intricate mould cavities to be fabricated that allows for better heating and cooling which produces better parts in shorter cycle times.

Autoclave, which is also called steam pan, is used for the vulcanisation of components that are unsuitable for moulding, such as extrusions and sheeting. Steam is the heat source used to achieve the required temperature and pressure. There are two variations of autoclave, a jacketed and unjacketed method. The jacketed autoclave consists of two pressure vessels with one inside the other. The inner pressure vessel is filled with an inert gas, commonly nitrogen to prevent polymer degradation by oxidation, whilst the outer pressure vessel is filled with high pressure steam that acts as the heating medium. The unjacketed autoclave is simply a singular pressure vessel that is filled with high pressure steam that acts as the heating medium.

Both moulding and autoclave are known as batch vulcanising techniques. Continuous vulcanisation methods such as hot air tunnel, fluidised bed and continuous drum core are used with extrusion and calendaring fabrication processes to continuously vulcanise the rubber product. Hot air tunnels are usually electrically heated and used for extrusion of silicone part where dimensional tolerances are not important. The setup cost of the hot air tunnel is very high but running costs are very low. Fluidised bed consists of inert material, such as sand or glass in a hot airstream which heats the rubber component. Fluidised bed is used for a variety of extrusions and is cheap and efficient to run. Cleaning of the rubber component to remove the inert material will be required post curing. The vulcanisation of sheet material is commonly achieved by a continuous drum roll. Sheet material is fed between large heated drums where the speed of the drums is controlled to achieve perfect vulcanisation.

#### **2.2.3.2 Radiation Exposure**

Radiation exposure is a source of energy that can be applied to start the vulcanising chemical reaction. Microwave, UV, electron beam and gamma radiation are commonly used types of radiation which have common advantages and disadvantages. Radiation exposure is often combined with hot air heating to maximise the process. The vulcanisation chemical reaction is achieved very quickly, in the order of seconds with radiation exposure. They are easy to use, straight forward to automate, less expensive

than other processes and offer long shelf life at room temperature as curing only arises with exposure to radiation. Drawbacks of the radiation exposure vulcanisation process is that only certain polymers can be cured, and part thickness is limited. Great care is needed to ensure safeguard of operatives from harmful radiation when using radiation exposure to cure rubber.

### 2.2.3.3 Exposure to External Chemicals

Exposing rubber to chemicals is a method of producing the vulcanising chemical reaction. Cold curing is a process of vulcanising thin rubber products by immersion in a carbon bisulphide solution of sulphur chloride or exposure to its vapour [9]. The peachy process is a variation of cold curing where the thin rubber is firstly exposed to sulphur dioxide gas and then to hydrogen sulphide. The major advantage of cold curing is that no heat or steam is necessary so bright-coloured rubbers can be vulcanised without losing any brilliance.

## 2.3 Rapid Prototyping

Rapid Prototyping (RP) is the fast manufacture of a 3D part. Firstly, a model of the part is created on a Computer Aided Design (CAD) programme. The 3D CAD model is then changed to a stereolithography (STL) file which uses triangles to describe only the surface geometry of a 3D part. The part is then sliced into layers and a tool path chosen which is done on a slicing software such as Cura. The part file is now ready to be sent to an additive layer manufacturing machine for fabrication. A schematic of the process from a CAD model to a 3D object is shown in Figure 2.11. Additive layer

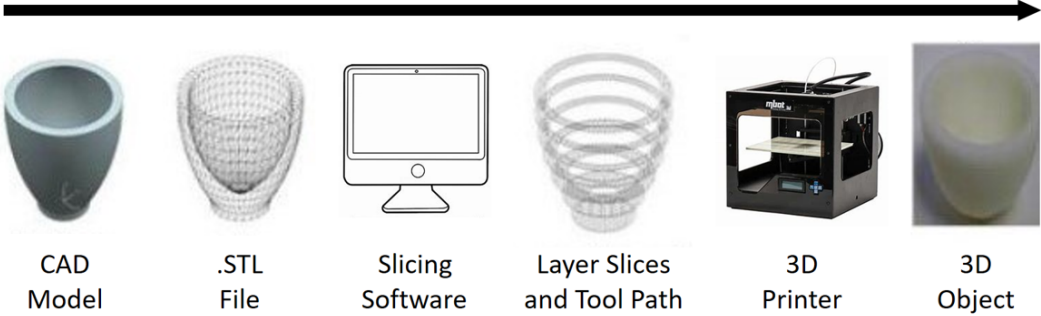


Figure 2.11: 3D printing process from 3D CAD model to 3D object.

manufacturing techniques all build the part one layer at a time. RP has seven main process technology, with each technology having several variations. Detailed process description of the main seven RP processes along with their advantages and limitations are given below.

### 2.3.1 Stereolithography

Stereolithography (SLA) (SL) uses an ultraviolet laser to cure photopolymer resin to build a part. A high accuracy laser traces out the first layer of the part on a platform that sits in a vat of photopolymer. Photopolymers are sensitive to ultraviolet light and solidify with the passing of the laser. Once the bottom layer is cured “printed”, the platform lowers ready for the next layer. Layer thickness depends on the magnitude that the platform lowers, which is typically around  $50\mu\text{m}$ . The process continues until the part is complete. A schematic of the process is shown in Figure 2.12.

The main advantage of stereolithography is its capability of producing high resolution parts. Resolution depends largely on the optic apparatus and the diffusion in the photopolymer. The resolution is commonly between  $50\mu\text{m}$  and  $150\mu\text{m}$  along the XYZ axes with accuracy of 0.1% [1].

A disadvantage of the technology is the need for support structures during printing to

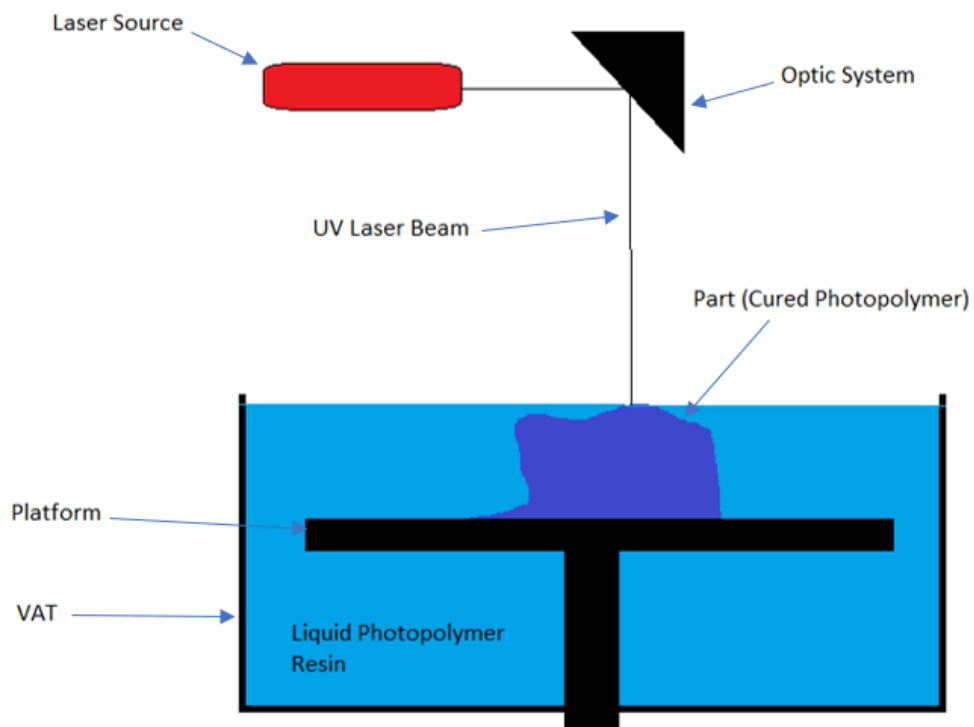


Figure 2.12: Schematic of the stereolithography process.

prevent deflection of overhanging sections. These support structures must be removed manually after printing, which is costly and time consuming. Photopolymer material can be expensive and is more difficult to change compared to other layer additive manufacturing techniques such as FDM.

### 2.3.2 Digital Light Processing

Digital Light Processing (DLP) is also commonly known as Solid Ground Curing (SGC). The technology used by DLP is very similar to that used by SLA. Both technologies can be described as using UV light to cure photopolymer resin into a part. SLA uses a UV laser to trace out the layer whereas DLP uses a digital light projector to cure a whole layer at once. The projector is a digital screen which means that the projected image of each layer is composed of square pixels. Each layer therefore will be formed from small rectangular blocks called voxels. After each layer is cured the excess photopolymer is removed and any empty spaces are filled with wax. The build platform then lowers, and a layer of photopolymer is reapplied. This process continues until the completion of the part. A schematic of the process is shown in Figure 2.13. DLP and SLA uses similar technology, thus they share many common advantages and limitation, but there are a few differences. DLP has the advantage of faster print times

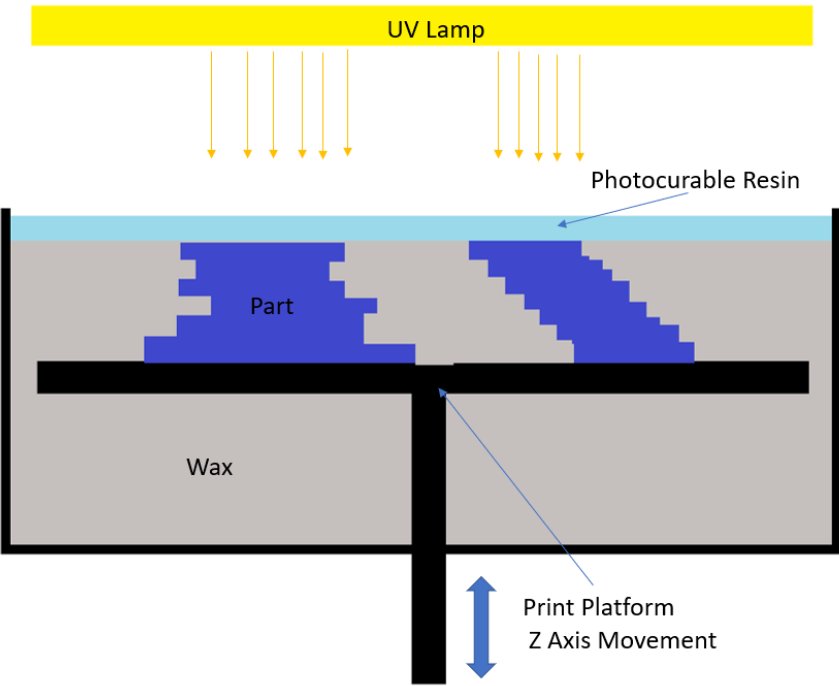


Figure 2.13: Schematic of the digital light processing process.



compared to SLA due to each individual layer being cured in one photo rather than being traced out with a laser point as with SLA. Using wax as the support material allows for easier and quicker post processing removal compared to printed support structure as with SLA, saving time and cost [28]. Another advantage of DLP is that it requires shallower vat of resin compared to SLA which generally reduces waste and running costs.

### 2.3.3 Selective Laser Sintering

Selective Laser Sintering (SLS) uses a high-power laser to selectively sinter "fuse" small particles of plastics, metals, ceramics, or glasses into a part. A small amount of powder is spread evenly across a platform which is scanned by the laser. Once the layer has been scanned and fused, the platform lowers, and another layer of powder is deposited. This process continues until the completion of the part. SLS typically uses a pulsed laser as the final density of the part depends on the peak laser power and not its duration. The bulk powder is heated close to its melting point to make it easier for the laser to raise the temperature above the melting point of the selected material.

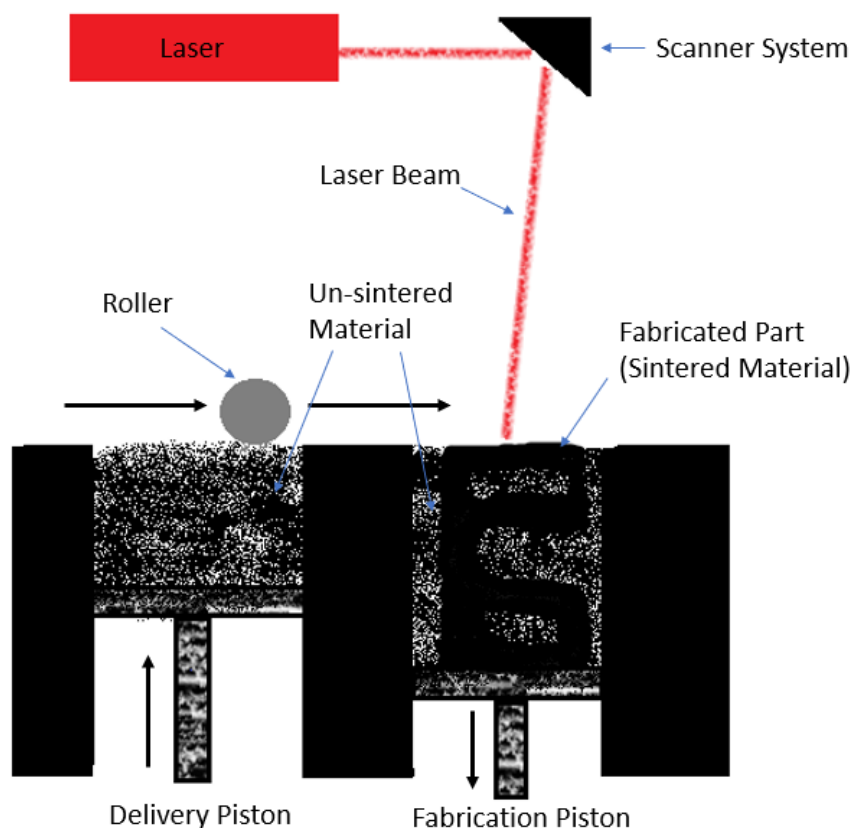


Figure 2.14: Schematic of the selective laser sintering process.

Layer thickness is typically around  $75\mu\text{m}$  and a tolerance of  $\pm 200\mu\text{m}$  is achieved with well-designed parts [1]. Figure 2.14 shows a schematic of the SLS process.

One major advantage of SLS over other additive layer manufacturing techniques is its ability to produce parts without any support structure. The un-sintered material acts as the support material for any sections of the part that would usually require support structure. This allows complex parts to be created that would not be possible with other techniques, but more importantly it saves post processing of support material, which reduces time and costs.

A disadvantage of SLS is that the parts inherently have porous surfaces which require additional processes to seal the part. An evolved technology from SLS, selective laser melting (SLM), melts the powder instead of sintering, giving a solid final part. The process is very similar to SLS except for the power and duration setting of the laser. Parts produced by SLM have no voids which makes them stronger than parts fabricated from SLS, allowing for functional testing.

### **2.3.4 Fused Deposition Modelling**

Fused Deposition Modelling (FDM) is a process that uses a continuous feed of filament to fabricate the 3D part. The filament is predominantly a thermoplastic material, although clever innovations are currently being developed. The filament is feed through a heated printer extruder head which heats the material past its glass transition temperature and deposits material on the print platform. The material solidifies after being deposited to form the solid part. The printer head and its path are controlled by a Computer Aided Manufacturing (CAM) software package. Once each layer is complete the print platform lowers, and the next layer is printed. Depending on the material chosen, a layer thickness of between  $180\mu\text{m}$ - $250\mu\text{m}$  is achievable with a tolerance of around  $\pm 200\mu\text{m}$  [3]. Careful consideration is needed when choosing the part print orientation as it has a significant effect on the accuracy and surface finish of the finished part, but also the amount of support material needed [29]. By number of machines, FDM is the most popular 3D process for hobby grade fabrication. A schematic of FDM process is shown in Figure 2.15.

Advantages of FDM compared to other 3D methods are as follows; Speed of fabrication is much quicker which saves time and costs. Changing material is very straight forward with FDM which can be difficult with other additive layer manufacturing methods. The FDM machines are easy to use and this explains the popularity of the process with the public.

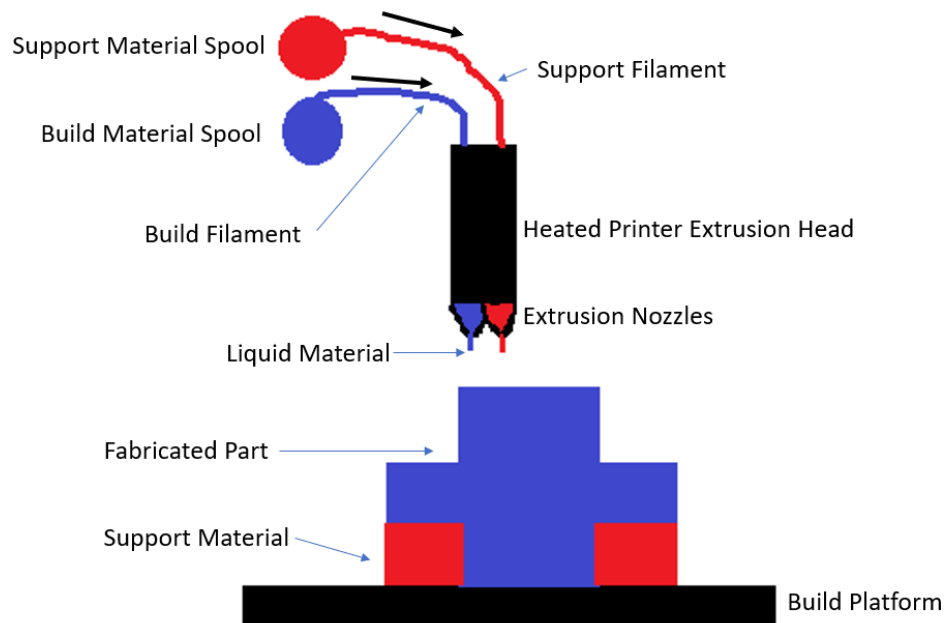


Figure 2.15: Schematic of the fused deposition modelling process.

A disadvantage of the process is the limited material that can be used. The quality of the final fabricated part is not good as achieved by SLA or SLS techniques. SLA, SLS and other additive layer manufacturing are better at producing fine detail. When support structures are required a second extruder head is required to deposit the support material which adds complexity and costs to the process.

#### 2.3.4.1 Alternatives to Thermoplastic Filament

As previously mentioned, thermoplastic material is by far the most used filament in FDM. Thermoplastics are polymers that melt above a certain temperature and then solidify when cooled without adversely affecting its mechanical properties, thus making it the perfect material for FDM. Commonly used materials are acrylonitrile butadiene styrene (ABS) and polylactic Acid (PLA). Fused Deposition of Metals (FDMet) is a branch of FDM that 3D prints metal objects. Successful fabrication of parts has been made with alloys such as tin-bismuth which have relatively low melting points. The main issue with FDMet is the high melting point of most metals which makes the process difficult, limiting the process to use alloys with low melting temperature which often have low strength. Precautions must also be made to avoid oxidation during fabrication due to the lack of environmental control. Using metal filament for fabrication of parts has therefore a limited capacity.

A more prosperous branch of FDMet is with the development of hybrid mixture of thermoplastic and metal material filament [30, 31]. There are three main steps in FDMet

technology, feedstock preparation, green fabrication, and post processing. Feedstock preparation involves using ball milling to create a fine powder of your desired metal with an average particle size in the region of  $20\mu\text{m}$  and then mixing with an appropriate thermoplastic binder to create your filament. This hybrid filament is used in the same way as any other filament to create the green metal part of thermoplastic and metal material. Post processing can be used to create more functional part, which involves the removal of the thermoplastic binder in a process called Binder Burn Out (BBO), leaving a porous metal part which is then sintered. This process can produce parts from any material that is available in powder form.

Thermoplastic Elastomers (TPEs) have very useful properties that could be used to directly print rubber like parts. TPEs combine the elastic and mechanical properties of crosslinked rubbers with the melt processability of thermoplastics. Blends of polypropylene (PP) and ethylene propylene diene monomer (EPDM) are currently being used successfully in industry that can produce rubber like parts [11].

### **2.3.5 Laminated Object Manufacture**

Laminated Object Manufacture (LOM) can fabricate parts from paper, plastics or metals. A continuous sheet of material is drawn by feed rollers across a build platform. As with any additive layer manufacturing method, the 3D object is sliced into layers. In LOM each layer is represented by the sheet material which is typically around  $100\mu\text{m}$  in thickness [32]. Material is drawn across the build platform and bonded to the platform and then cut. A laser is used to crosshatch the non-part material to facilitate waste removal on completion of part. The build platform then moves down, and another layer of material is drawn across and bonded to the previously layer and then cut, which continuous until the completion of the part. A schematic of the LOM process is shown in Figure 2.16.

Advantages of LOM include high manufacturing speeds due to only the circumference of the part being processed, differing to most additive layer manufacture where the whole part volume needs to be processed. There is also no chemical reaction or no enclosed chamber which makes it possible to build large parts. When the material temperature is maintained during fabrication and gradually lowered on completion, parts fabricated through LOM exhibits much smaller internal stress compared to parts fabricated by SLA, SLS and DLP [33]. Material for LOM is inexpensive, consistent, readily available, and well understood compared to other layer additive manufacturing techniques.

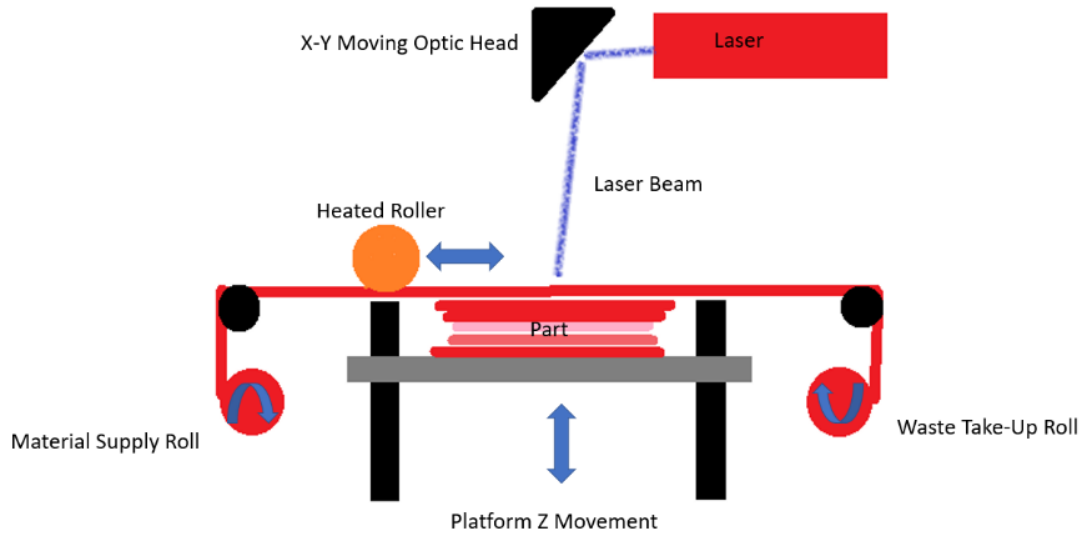


Figure 2.16: Schematic of the laminated object manufacture process.

The ability to produce good bond between layers is the main disadvantage of the LOM technology. Hollow parts cannot be manufactured as waste material needs to be removed on completion of part. LOM usually produces poor surface finish that usually requires finish machining to remove steps between layers.

### 2.3.6 Material Jetting

Material Jetting (MJ) is also commonly known as Ballistic Particle Manufacture (BPM). MJ comprises of a print nozzle jetting droplets of material onto a build platform in a similar process as used by a 2D printer. Commonly used material are photopolymers, plastics and waxes. It uses either a continuous or drop on demand technique, which depends on the layer geometry. When liquid droplets of photopolymer material are deposited, it is solidified under UV light source that is attached to the nozzle, building the part. When plastic and wax materials are used the part solidifies when the material cools. Each layer is built one at a time until the completion of the part. A second print nozzle is needed to deposit support material during the print which can be easily removed post processing by hand or with water. A schematic of the process is shown in Figure 2.17. Application of parts fabricated by material jetting include visual and fit testing prototypes, and for casting patterns.

Material Jetting is one of the most accurate 3D printing methods, with a typical layer height of  $16\mu\text{m}$  and dimensional accuracy of  $\pm 0.1\%$  which results in high resolution parts [34]. Warping of parts is minimised due to printing at near room temperatures,

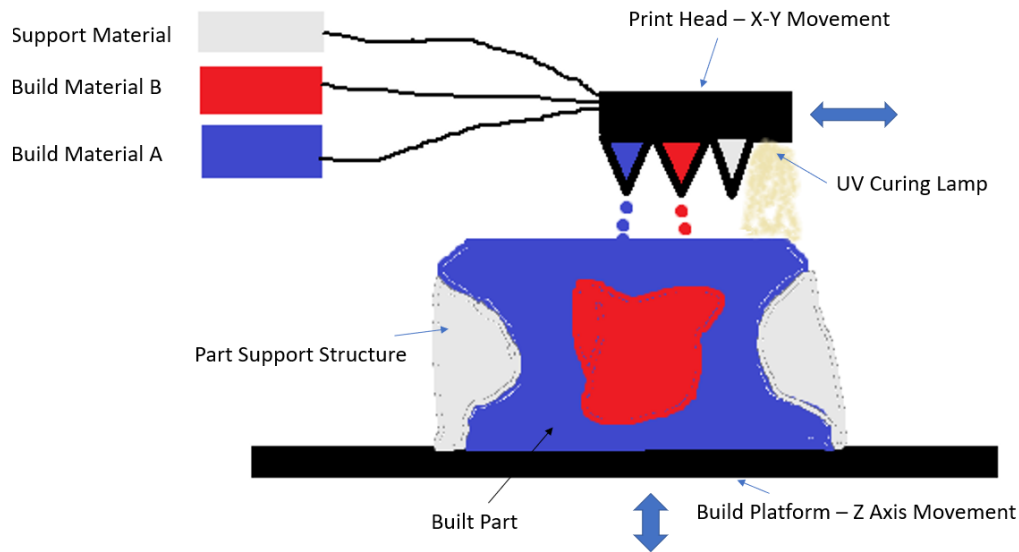


Figure 2.17: Schematic of the material jetting process.

which can be a problem with other technologies such as FDM and SLS. Material jetting can produce parts that have surface finish comparable the injection moulding with very high dimensional accuracy. The process also allows for multiple material and colour parts to be created.

Parts have poor mechanical properties that limit their use to only non-functional prototypes. Only limited materials, photopolymers and waxes, can be used, which tend to produce fragile parts with poor mechanical properties.

### 2.3.7 Binder Jetting

Binder Jetting (BJ) is also commonly known as three-dimensional printing (3DP). BJ binds powdered material to form the final part. Like SLS, a thin layer of powder is spread out on a build platform and the desired layer shape is bonded. In BJ the powder is bonded using a liquid bonding agent instead of laser sintering as is used in SLS. The liquid bonding agent is jetted through a printing head until the completion of the layer at which point the build platform drops a layer thickness and more powder is deposited. Each drop of liquid bonding agent is approximately  $80\mu\text{m}$  in diameter, allowing for good resolution of parts. This process is repeated until the completion of the part, at which point the part is left to cure and gain strength. Often further processing, infiltration and sintering is completed to create more functional and useful parts. Typically, parts with layer thickness of  $90\mu\text{m}$  and a tolerance of  $\pm 130\mu\text{m}$  are produced by BJ. Figure 2.18 shows a schematic of the BJ process.

BJ, in the same way as SLS, does not require any support structures. This is due to

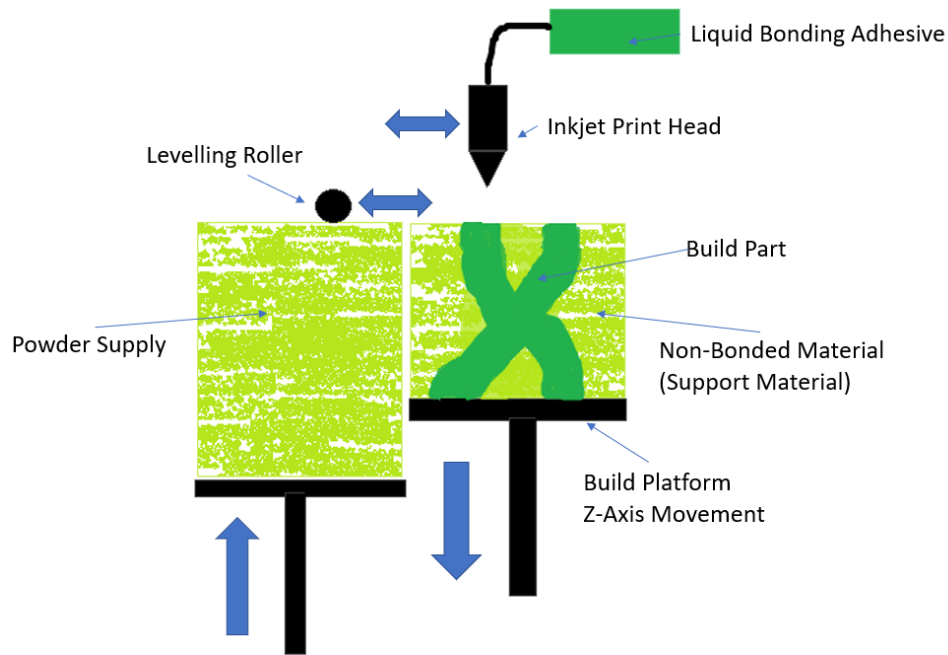


Figure 2.18: Schematic of the binder jetting process.

the non-bonded powder acting as the support during printing and is removed during post processing, saving support material, time and cost. An advantage of BJ is its capability of processing any material that is available in powder form [35]. BJ is faster, simpler and cheaper than many other additive layer manufacturing techniques due to its processing bonding powder at room temperature. Due to the processing temperature, dimensional distortions such as warping are not seen which are apparent in parts produced by other additive layer manufacturing techniques. This allows for large parts to be fabricated without compromising on dimensional accuracy.

Parts produced by BJ are fragile and exhibit limited mechanical properties if no additional post processing techniques are used. Fine detail is difficult to print with BJ due to its fragile nature. Extensive post processing such as curing, de-powdering, sintering, infiltration, annealing, and finishing are often required to achieve the desired finished part [36]. Often the post processing takes longer to complete than the print, which adds considerable time and cost to the overall process.

### 2.3.8 Summary of Rapid Prototyping Techniques

Comparison of the different rapid prototyping processes is shown in Table 2.3. The data has been collected from commonly used rapid prototyping machines in industry which gives a fair representation of each rapid prototyping process [3, 6, 28, 37].

Table 2.3: Comparison of the different rapid prototyping processes.

RP Process	Materials	Maximum Part Size (mm)	Support Material	Layer Thickness ( $\mu\text{m}$ )	Accuracy ( $\mu\text{m}$ )	Cost/Part	Ra ( $\mu\text{m}$ )
<i>SLA</i>	Photocurable Resins	1500x600x500	Yes	50	$\pm 100$	Medium	3.7
<i>DLP</i>	Photocurable Resins	650x650x450	Yes	100-200	$\pm 500$	Medium	9.8
<i>SLS</i>	Metal, Ceramic, Thermoplastics	700x380x580	No	76	$\pm 51$	Medium/High	18.4
<i>FDM</i>	Thermoplastic	914x610x914	Yes	50-762	$\pm 127$	Low/Medium	11.0
<i>LOM</i>	Paper, Polymer, Metal, Ceramic	550x800x500	No	76-203	$\pm 127$	Low/Medium	4.0
<i>MJ</i>	Photopolymer, Thermoplastic, Wax	1000x800x500	Yes	13-130	$\pm 25$	Medium	3.1
<i>BJ</i>	Thermoplastic, Ceramic, Metal	4000x2000x1000	No	177	$\pm 127$	Low	6.0

## 2.4 Rapid Tooling

Rapid tooling is the process of utilising rapid prototyping techniques to produce tooling for a variety of manufacturing systems. Rapid prototyping is used to produce a master model or to directly fabricate a tool.

During product development prototypes are fabricated to test, evaluate and develop a concept before full scale production. Prototype parts need to exhibit similar properties to the full-scale production parts to fully utilise the product development stage. This often means that prototype parts need to be manufactured using the same process as the full-scale parts. Full scale production processes commonly require some sort of tooling which is usually machined from steel or aluminium. Traditional tooling is expensive and time consuming to produce, which would incur high costs and long lead times during the prototyping stage. Rapid tooling offers an alternative to traditional tooling, with some methods having a tooling time one-fifth of conventional tooling, alongside significantly smaller costs [4, 38].

Rapid tooling is classified into direct, indirect, and soft and hard. Direct tooling is the process where the tool is made using any of the rapid prototyping methods. Indirect tooling is where a rapid prototyping technique is used to make a master model, which is then used to create the tooling. There is a bit of ambiguity with the definition of soft and hard tooling. The best way to interpret between soft and hard tooling is by the volume of parts that they can produce. A tool is said to be soft if it can only produce up to 100 parts and described as hard if it can produce more than 100 parts.



## **2.4.1 Direct Tooling**

### **2.4.1.1 Resin Tooling**

Resin tools are soft tools that can be fabricated directly using any rapid prototyping technique, but most commonly by stereolithography. Resin materials range from thermoplastic material such as polyvinyl, polystyrene and polyethylene to thermosetting material such as polyesters, epoxies and silicones. These tools are typically fabricated for the injection moulding of thermoplastic materials. They are not generally used for injection moulding of thermosetting polymers and metals as their glass transitional temperature is not sufficiently high. Due to their manufacture by stereolithography the tools have very good tolerances. Development of resins with higher glass transitional temperature is giving the possibility for short runs of thermosetting material to be manufactured by injection moulding. Resin moulds have limited strength which causes rapid tool wear limiting the number of possible cycles to around a maximum of 100.

An alternative to a solid resin tool is a composite tool which compromises of two parts. A shell with the required surface geometry of the tool, fabricated by SLA, and a reinforced filled epoxy resin that reinforces the shell. Manufacturing only the shell from stereolithography save a lot of time and cost. Thermal conductivity and strength of the tool can also be improved with the addition of filler material in the epoxy resin. Reinforced epoxy composite is used extensively in the field of RT within many different techniques. A detailed review of reinforced epoxy composites is given in section 2.4.2.2.

Advancements are being made with resins that can produce green ceramic and metal parts directly from stereolithography [39]. Ceramic or metal particles of between 40-80vol.% are dispersed in a photocurable resin that when cured form a composite part. The addition of either ceramic or metal particles to a resin mould would increase its mechanical and thermal properties making it more suitable for injection moulding. The green parts could be developed further with post processing sintering. Placing the green parts in a furnace and burning out the resin would leave a sintered porous part that could subsequently be infiltrated to achieve a fully dense part.

The addition of multi-walled carbon nanotubes into the photocurable resin has a significant impact on the tensile strength and fracture strength of the fabricated stereolithography part. With the addition of only 0.10wt.% of multi-walled nanotubes an increase of 7.5% in tensile strength and a 33% increase in failure strength is achieved [40]. This is a remarkable improvement in material property with minimal addition of filler.

Injection moulding tool inserts can be fabricated by using fused deposition modelling that produce quality parts [31]. As discussed in the alternatives to thermosetting filament in section 2.3.4.1, filaments comprising of polymer and metal are available. If the hybrid polymer and metal filament is fabricated correctly the fused deposition machine would require no modifications and the print times would be the same as when using traditional thermoplastic filament [31]. Tensile strength, tensile modulus and elongation of the tooling depends heavily on the volume and size of the metal particles [41]. Nylon and iron filament, 60% and 40% by volume respectfully, with the iron particle size  $<30\mu\text{m}$  has been used to successfully fabricate an injection moulding tool insert which created 40 parts from ABS with 99% of the measurements within  $\pm 76\mu\text{m}$  range [31].

#### **2.4.1.2 Metal Powder Tooling**

Using selective laser sintering or binder jetting, metal tools can be fabricated directly from a CAD file. Iron based metals are common for this process as they produce high quality tools. With selective laser sintering, the iron-based metal is first ball milled into a fine powder that is then coated with a thermoplastic binder. SLS is then used to selectively fuses the binder to create the green part. Binder jetting creates the green part straight from the raw powder material as described in section 2.3.7. After the green parts have been fabricated by either selective laser sintering or binder jetting they undergo the same post processing. Any un-sintered material is removed, and the part is placed in a furnace where the temperature is increased at a rate of around  $100^{\circ}\text{C}$  per hour. At a temperature around  $300^{\circ}\text{C}$  the thermoplastic binder will have been burned out leaving only the iron based metal part. As the temperature reaches around  $1000^{\circ}\text{C}$ , the iron based metal will start to sinter. Whilst at high temperature a second metal, usually copper or bronze, is introduced via capillary action into the green part to create a fully dense part. The temperature of the furnace is then reduced at a rate of  $150^{\circ}\text{C}$  per hour until around  $100^{\circ}\text{C}$  where the furnace cools at its natural rate. The final composition of the tool is commonly around 60% iron based metal and 40% second infused metal [42].

This method of rapid tooling produces hard tooling which can produce up to 50,000 parts. The tool manufacture time is five times smaller compared to traditional machining, which reduces the product lead time. Creating a tool that can produce 50,000 parts is acceptable, but for prototyping it is over engineered. The metal powder tool technique could be used to fabricate a thin metal shell that would be reinforced by an epoxy resin composite. This would reduce the fabrication time and save on expensive

powdered material making the tool even more appealing.

Tool creation through selective sintering of metal powders or binder jetting requires extensive post processing, which includes infiltration to create a fully dense part which increases its lead time and cost. The similar rapid prototyping technique of selective laser melting has been developed to create fully dense tools directly without the need for extensive post processing [43]. Another advantage of selective laser melting is its capability of processing material without any binder material and pre-treatment, which includes material such as stainless steel (1.4332, 1.4404) and tool steel (1.2343) [44]. The only requirement for the powdered material is that it is spherical in shape and between 20-50 $\mu\text{m}$  in size [44].

During selective laser melting, significant volume change in material occurs during cooling which results in thermal stress and undesirable metallic structure of the parts. A dual laser system, comprising of a YAG and CO<sub>2</sub> lasers is used to improve the ductility of the formed part [43]. The YAG laser is used to melt and solidify the part whilst the CO<sub>2</sub> laser is used to reheat the part after an appropriate time delay. The dual laser system of selective laser melting has been tested on aluminium, copper, iron, stainless steel, chromium and nickel-based alloy material, with the nickel-based alloy producing the best tool [43].

The main issue with selective laser melting is the possibility of spherical structures forming which leads to an undesirable porous structure. Spherical structures can form in the interaction zone of molten metal and laser beam due to the relatively high surface tension of the molten metal [44]. Laser power, scan speed, hatch distance, and layer thickness are the four main parameters that effect the formation of the spherical structure. Correct setting of these four parameters results in parts with porosity of less than 10% [44, 45].

#### **2.4.1.3 Ceramic Powder Tooling**

Ceramic powder tools are fabricated to be used in investment casting, where the process is called Direct Shell Production Casting (DSPC). Directly fabricating the ceramic shell eliminates the pattern production stage which results in reduced product lead time along with cost savings when compared to a traditional investment casting process [4, 46]. There are two rapid prototyping methods available for DSPC fabrication, binder jetting and selective laser sintering [4, 46, 47].

Binder jetting creates the ceramic powder tooling by jetting a binder material onto the ceramic powder, whilst with selective laser sintering the ceramic powder is coated with a binder material which is selectively sintered to create the part. Process description

of selective laser sintering and binder jetting are available in sections 2.3.3 and 2.3.7 respectfully. Both processes create a green part which are post processed to create the final casting shell. The post processing process from both methods are the same. The green part is placed in a furnace to remove the binder material and the ceramic shell is fired.

The ceramic shell has been fabricated by binder jetting, where alumina was the powdered material and the binder material was colloidal silica, which was successfully used for the casting of nickel superalloy at 1660°C [48]. To ensure accurate castings it is important to minimise shell shrinkage during firing. Whilst using powder alumina with silica binder it has been reported that the shrinkage during firing is minimal [48]. Selective laser sintering has been used to create a ceramic shell from zirconium silicate powders. The surface quality of the ceramic shell was between 30-50 $\mu$ m Rz with an accuracy of below  $\pm 0.6\%$  [49]. Successful castings were carried out that indicated a time reduction of 95% compared to traditional investment casting process [49].

#### **2.4.1.4 Laminated Metal Tooling**

Laminated Metal Tooling (LMT) process is an extension of the laminated object manufacturing which is described in section 2.3.5. Using any suitable cutting method such as CO<sub>2</sub> laser, water jet, milling, etc, sheets of any metals can be cut and processed. As with LOM each sheet represents one layer of the final part. Differing to the LOM process the layers are not bonded before they are cut, but they are assembled post cutting and then bonded [50]. Mechanical fasteners, adhesive bonding, soldering, brazing, diffusion, laser beam welding and hot isostatic pressing are seven common bonding methods [51,52]. The bonding used for laminated metal tooling for injection moulding is usually either high temperature epoxy adhesives or brazing using low temperature metals such as Copper or Silver [51]. Mechanical fasteners are not used because they only provide localised bonding and not the interlaminar bonding required for injection moulding. Insufficient impact properties of soldering dismiss it as a bonding method and hot isostatic pressing is often dismissed due to its size limitation and costs.

LMT has high manufacturing speeds due to only the circumference of the part being processed, differing to most additive layer manufacture where the whole part needs to be processed. Due to the “cut-stack-bond” method rather than “Stack-bond-cut” method used by LOM, LMT can produce parts with higher accuracy and smoother finishes. It also allows for easy manufacture of hollow parts. The major disadvantages with the process is the difficulty of producing good bonds between layers. Also “cut-stack-bond” compared to the “stack-bond-cut” method is more difficult to automate.

The major advantage of laminated metal tooling over conventional tooling is its ability to include complex conformal cooling channels within a mould [53]. Cooling channels would be drilled in traditionally machined moulds which prohibits complex and optimised channels. The complex cooling channels available with laminated metal tooling allows for variable cooling which can influence the solidification direction and mechanical properties of the moulded part [53]. With optimised cooling channels it is possible to achieve homogeneous tool temperature which reduces part distortions and cycle times.

Flux coated aluminium alloy 2.5mm thick sheets are commonly used in laminated metal tooling due to the low bonding temperature required. After the sheets have been cut, deburred, cleaned, and pressed together using bolts and two plates, they are placed in a furnace which is heated to a specific temperature that will melt the flux. Upon cooling the bolts and plates are removed and the parts is complete. Shrinkage is typically expected to be between 1-1.5% in the z direction (direction of the stacked layers) [53]. Fibre-metal laminates are being developed in the aerospace industry which have advantages of better damage tolerance to fatigue crack growth and impact damage compared to metal laminates [54]. Adhesively bonded fibre-metal laminates are shown to have better fatigue resistance compared to mechanically bonded laminates [54]. To ensure good bonding between layers when adhesive is used it is crucial that the correct surface preparation of the layers has been used, such as chemical etching.

#### **2.4.1.5 Laser Engineered Net Shaping Tooling**

Laser Engineered Net Shaping (LENS) is also known as laser cladding and direct metal deposition. Powder material is delivered to the surface of the print bed by a gas jet which has a laser beam focused coaxially with the flow of material [55]. The powdered material is fused by the high energy laser. Steels, nickel alloys, titanium alloys, cobalt alloys and aluminium alloys are typical materials used with LENS. Temperature of the molten material and thus the tempering effects is the most important parameter to control during LENS process to ensure a quality end part [56,57]. A schematic of the LENS process is shown in Figure 2.19.

Fully dense, geometrically complex parts with mechanical properties compatible to traditional machining processes are achievable [58]. Common average laser power in a LENS process is 1.75kW, compared with 0.5kW used in selective laser melting and 0.05kW used in selective laser sintering [58]. The laser operating cost is higher for the LENS process compared to selective laser sintering and melting but overall part fabrication cost is smaller due to the minimised post processing required.

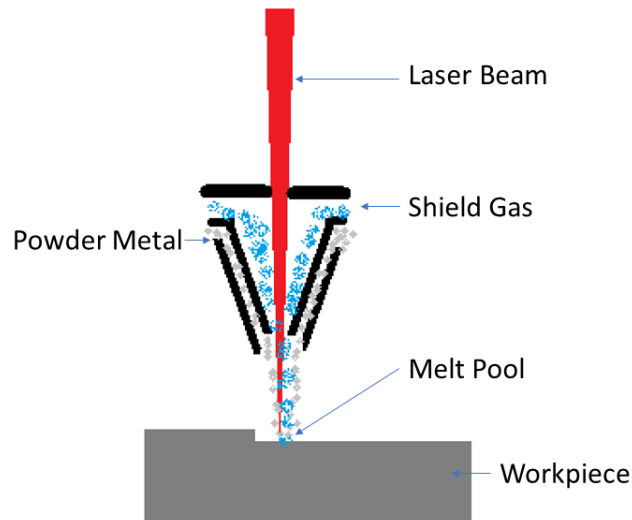


Figure 2.19: Schematic of the laser engineered net shaping process.

## 2.4.2 Indirect Tooling

### 2.4.2.1 Room Temperature Vulcanisation Tooling

Room Temperature Vulcanisation (RTV) tooling is also referred to as silicone tooling. As with any indirect rapid tooling technique, RTV starts with the fabrication of a master pattern using any of the appropriate rapid prototyping techniques. The master pattern is then coated in a release agent to assist removal of mould after curing. Vents and gating is added to allow air to exit the tool during casting, avoiding defects such as voids. The mould will be made of two parts, requiring parting lines which are marked out prior to pouring of mould material. A frame is fabricated around the master pattern to hold the material in place during casting. The mould material is then poured and is left to cure. Once curing has completed the mould is cut along the parting lines and the master pattern is removed. Cutting along the parting lines after curing works fine for transparent materials but poses difficulties for opaque material. Another more time-consuming method to produce the mould is to fabricate one side at a time. Plasticine is used to mark out the parting line and one side of the mould is casted, which is repeated for the other side.

The accuracy of the mould is as good as the accuracy of the master pattern which depends on the method of fabrication, with tolerances of  $50\mu\text{m}$  achievable when using stereolithography. RTV moulds have significant time and cost saving compared to traditional tooling. Fine detail can be produced due to the liquid silicone having low viscosity, ensuring an exact copy of the master pattern in the mould. Silicone moulds typically only exhibits between 0.2% and 0.4% shrinkage during curing. RTV tooling

can be used for reaction injection moulding process with thermosetting material to create up to 50 parts [59]. Catalysts, cross-linking agent, filler, cure temperature and time are the most important factors that determine the properties of the final mould [59].

Adding filler material has vast impact on the mould properties, which depends on the filler material and quantity. Boron Nitride reinforced silicone rubber composite has been studied with the direct aim to reduce the problem with heat dissipation with electronic devices [60]. The addition of Boron Nitride to the silicone matrix decreases the tensile strength, strain at break, and coefficient of thermal expansion, whilst increasing Young's modulus, hardness, and thermal conductivity [60]. The effect of aspect ratio of the Boron nitride is crucial in achieving high thermal conductivity, with an approximate aspect ratio of 20 giving the highest thermal conductivity among all the different types tested [60]. The main issue with the addition of boron nitride is the decrease of tensile strength of the silicon composites, which can be attributed to the poor interfacial interaction between silicone and Boron Nitride.

In a similar manner to the study of Boron Nitride reinforced silicone composite, the effect of  $\text{Al}_2\text{O}_3$  (aluminium oxide) particle size on the properties of reinforced silicone composite rubber have been studied [61]. The effects that the amount, size, and the mixing mass ratio of the filler particles had on the thermal conductivity and mechanical properties of the silicone composite rubber was investigated. The thermal conductivity of  $\text{Al}_2\text{O}_3$  and silicone rubber are  $30\text{-}40\text{Wm}^{-1}\text{K}^{-1}$  and  $0.2\text{Wm}^{-1}\text{K}^{-1}$  respectfully, thus adding  $\text{Al}_2\text{O}_3$  to silicone rubber is going to increase its thermal conductivity. An increase in mechanical properties of the silicone composite was seen at concentrations of  $\text{Al}_2\text{O}_3$  up to 55vol.%, but then decreased at concentrations above 55vol.%. It was also noted that silicone filler composite with less than 50vol.% of  $\text{Al}_2\text{O}_3$  had higher thermal conductivity with bigger sized particles. The hardness of the silicone  $\text{Al}_2\text{O}_3$  filled composites increased with  $\text{Al}_2\text{O}_3$  filler percentage volume but was unchanged by the size of filler particles [61].

Graphite nanoplatelets reinforced silicone composite has been developed and tested [62]. With the addition of 20wt.% of graphite nanoplatelets to the silicone composite a 11-fold increase in thermal conductivity and a 2-fold increase in the compressive modulus was achieved. Likewise to the Boron Nitride reinforced silicone composite, the addition of 20 wt % of graphite nanoplatelets decreased the strength by 2-fold which is attributed to the weak bonding at the graphite nanoplatelets-silicone interface. Improving the interface bonding between silicone and the filler material would yield a better composite, allowing for silicone composites to be used in a wider field.

### 2.4.2.2 Composite Epoxy Tooling

A composite epoxy tool is fabricated using the same methodology as RTV tooling for opaque silicone material as described in section 2.4.2.1. The master pattern, which is produced by a suitable rapid prototyping technique, is placed in a moulding box where plasticine is used to mark the parting line. Care is required when packing the plasticine to ensure that all regions are filled to avoid creating any undercut features or empty pockets. A full evaluation of the master pattern is needed to ensure that it is fully satisfactory before mould production, as any kind of deformity or discrepancy present in the surface of the master pattern will be transferred into the core surface of the mould. Epoxy material is either painted or poured around the master pattern producing one half of the mould. This is repeated for the other side of the mould. During the epoxy moulding process, the master pattern can often be destroyed. To overcome this problem an interim RTV mould is made from the master pattern which is used to create a polyurethane reproduction. The polyurethane reproduction is an exact copy of the master pattern that was fabricated by a rapid prototyping technique and is used in the casting of the composite epoxy tooling. Post processing is often required to machine any gates and vents that could not be moulded, and intricate core detail is added with machined aluminium or steel inserts.

The mechanical and thermal properties of the tool depends on the resin used but also any filler material used. Aluminium oxide, silicon carbide and silicone dioxide are typical filler material used, which improves thermal stability, glass transition temperature and dimensional stability of the epoxy tool. A composite epoxy tooling is classified between tooling produced by RTV and machined aluminium. Composite epoxy tooling has quicker time and smaller expense associated with RTV moulds and the capability to use production material for prototyping injection moulded parts associated with machined aluminium tooling. A typical composite epoxy tooling would be suitable to produce between 100 and 200 parts made by injection moulding.

As with RTV tooling, the composite epoxy tooling can easily reproduce fine detail from the master pattern. The accuracy of the mould is as accurate as the master pattern which requires the correct rapid prototyping technique to be used in the production of the master pattern. Typically, the cost of a composite epoxy tooling is less than 40% of a conventional tooling, and the lead time is usually significantly less. Compared to traditional tooling, composite epoxy tooling tends to produce more flash during injection moulding which increases the post processing costs. Sink marks can also be a problem with parts produced by composite epoxy tooling due to the decreased packing pressure



when compared to traditional tooling.

An epoxy resin mould that can be used at 200°C has been successfully fabricated [63]. The epoxy tooling comprises of bisphenol-A epoxy, a trifunctional aromatic epoxy, anhydride catalyst, imidazole catalyst, and a filler system comprising of particles having different sizes that are interstitially matched. When interstitially matched filler is used the viscosity of the epoxy composite can be maintained at a constant level without increasing with added volume of filler. Filler particle size was carefully chosen such that the smaller particles would fit between the larger particles. This is important to maintain low viscosity and hence pourability of the epoxy composite at high filler volume. The filler material was comprised of silicon carbide and silicon dioxide with particle sizes ranging from 0.5 $\mu\text{m}$  to 203 $\mu\text{m}$  [63]. Silicon carbide was used due to its abrasion resistance resulting in a tool with enhanced durability, and silicon dioxide was used due to its rigidity and low cost [63]. At filler level of 75vol.%, a mould temperature as high as 200°C could be used [63]. The importance of mixing under vacuum to degas and avoid any defects in the material is also mentioned in the report [63].

Reinforcing epoxy composites with carbon nanotubes has been investigated [64–66]. Good interface bonding is required between the epoxy and the filler material to maximise the mechanical and thermal properties of the filler material. Load transfer from the epoxy matrix to the nanotubes is limited due to nanotubes having atomically smooth surface which results in minimal interfacial bonding between the epoxy matrix and the nanotubes. Nanotubes have also very low solubility in most solvents due to intrinsic van der Waals forces, resulting in very poor dispersion when mixed with epoxy composites. A method of producing interfacial interaction between nanotubes and epoxy polymer and the ability to disperse the nanotubes homogeneously throughout the matrix to take full advantage of the exceptional properties of nanotubes has been developed [66]. Covalent integration of the nanotubes into the epoxy matrix has been achieved which results in the nanotubes becoming part of the crosslinking structure rather than just a separate component. Ultimate strength of the epoxy composite matrix increased by 30-70% with the addition of 1-4wt.% of nanotubes and also exhibited an increase in strain to failure which suggests higher toughness [66]. With the addition of 16.5wt.% of carbon nanotubes loading to an epoxy composite, the Young's modulus and tensile strength increased by 716% and 160% respectfully [65].

A comparison of injection moulding a part using an epoxy composite mould and a traditional mould is evaluated against cost, turnaround time and quality [67]. A mobile telephone front housing is used as the case study, which has many intricate features.

Successful rapid tooling of epoxy composite mould for this complex part would indicate that simpler parts could be produced with relative ease. The methodology of producing the epoxy composite tooling is described in extensive detail [67]. EP250 tooling resin (marketed by HEK-GMBH) that comprised of 75% aluminium powder and 25% epoxy was used in their work. They specified that thorough mixing is required prior to mould production to ensure uniform distribution of aluminium powder in the mixture, as nonuniform distribution of aluminium would cause soft spots to form on the mould and render it unsuitable for moulding operations. Due to the resin epoxy tool being weaker than conventionally machined steel tool the moulding parameters were adjusted to avoid damage to the epoxy tool. The moulding parameters for the epoxy tool were temperature of 250°C and pressure of 90Kgcm<sup>-1</sup> and the moulding parameters for the conventional steel tool were temperature of 270°C and a pressure of 100Kgcm<sup>-1</sup>. Mouldings were carried out with PC/ABS resin. It was seen that there were substantial amounts of flashing at the location of the parting surface, which they contribute to the improper use of clay in defining and creating the parting lines. Using clay to define the parting line makes it very difficult to produce high accuracy and perfectly mated surfaces. However, in the post processing of the mould making process, careful finishing operations could be carried out to eradicate the flashing. Another undesired feature seen in the moulded part is a staircase feature which has come from the stereolithography master pattern due to its layer by layer building process. It is emphasized that the quality of the moulded part is only as good as the quality of the master pattern. Improving the quality of the moulded part could be accomplished by extensive effort in finishing and polishing the master pattern before mould production. They conclude that epoxy tool is sufficient for prototyping parts and have the advantage of much shorter turnaround times and lower production costs compared to conventional tooling. Epoxy tooling has the highest desirability in the development stages where a significant number of prototypes parts are required for design and evaluation.

#### **2.4.2.3 Spray Metal Tooling**

Spray metal tooling starts with the creation of a master pattern from a rapid prototyping technique. The rapid prototyping technique used will depend on the accuracy and surface finish required for the tool. A spray gun is used to create a metal shell, spraying atomised droplets of molten metal, which is most commonly a zinc alloy, onto the master pattern which has been coated with a release agent. Tin, aluminium and steel alloys are also used. Flame, arc and plasma are three energy sources that are used to melt the metal. A gas stream of compressed air and nitrogen, atomises the metal and propels the

droplets onto the master pattern. The spraying process continues until a typical layer thickness of between 0.5mm and 5mm is achieved. Once the shell has been completed, reinforcement backing is applied to the shell to add mechanical and thermal strength to the tool. Chemically bonded ceramics, composite epoxy resins, and low melting point alloys are materials typically used for reinforcement. Zinc alloys melt around 420°C and cool very quickly when in droplet form meaning minimal thermal damage to the master pattern. The temperature at the surface of the master pattern does not exceed 50°C when using zinc alloys, which allows the master pattern to be fabricated out of nearly any material that is used within rapid prototyping techniques. Typical part quantities made from injection moulding is between 1,000 and 10,000, depending on the metal alloy and reinforcement material used. A schematic of spray metal tooling is shown in Figure 2.20.

Advantages of spray metal tooling include a 50% reduction in lead times and costs compared to conventional machined tools [68, 69]. Fine detail and accuracy is easily reproduced creating quality moulds. Spray metal tooling has no limitation on mould size but has limitations to the shape of mould that it can manufacture. Small deep features are a problem and often require inserts. The tool life of the mould is relatively short when using low melting point alloys for the shell.

The quality of the sprayed layer depends on six spraying parameters; Spray distance, powder feed rate, travelling speed, cooling air pressure, energy source power, and spray angle. The setting for each parameter depends on the sprayed material and the

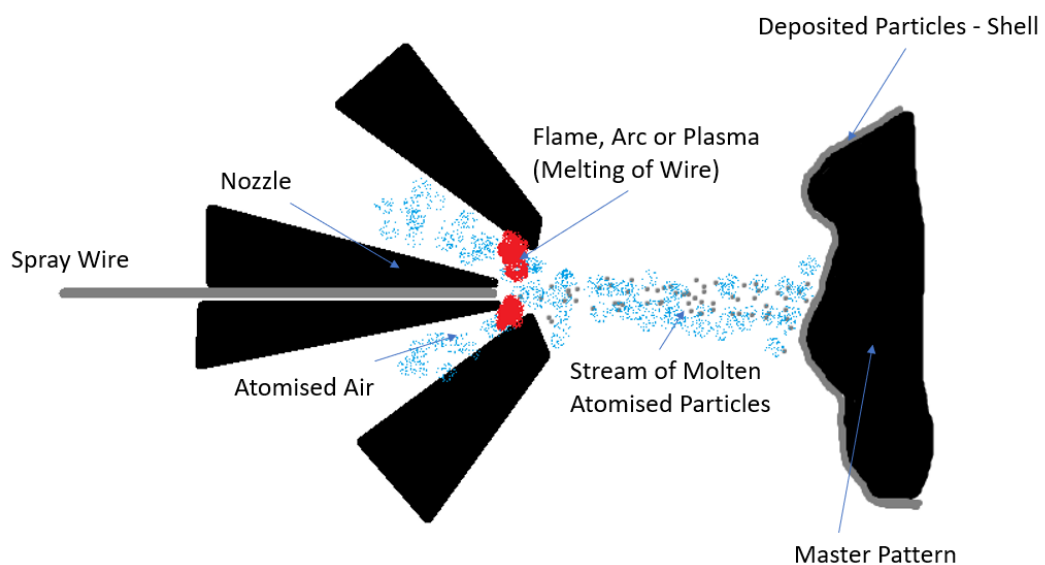


Figure 2.20: Schematic of the spray metal tooling process.

shape and size of the fabricating part [68, 69]. The reinforcement material is arguably the most important part of the tooling that affects its strength and life, which must withstand the pressure and temperature of the manufacturing process [69]. Crucially, the coefficient of thermal expansion, heat transfer, and shrinkage of the reinforcement material and the sprayed metal shell must be similar to avoid any unnecessary internal stresses that contributes to the degradation of the tool. Excellent bonding between the sprayed shell and the backing material is required to maximise the backing material. Composite epoxy resins up to 85wt% aluminium, bismuth-tin-antimony (50%Bi-45%Sn-5%Sn), and iron and sodium silicate are popular reinforcement material for tooling used by injection moulding [68–70].

The master pattern is usually plastic which is inexpensive and quick to fabricate through many rapid prototyping techniques. However, plastic master patterns have low heat resistance which limits the spray material to low melting point materials, such as Zinc alloys to avoid damaging the master pattern. Low melting point alloys have poor wear resistance which limits the use of the manufactured tools to low production runs. Improving the wear resistance of the tooling requires the use of better wear resistance material. Material with good wear resistance also have high melting temperature, which makes them unusable with the common plastic master pattern. Master patterns fabricated from ceramic and metal composites can be used that have the heat resistance to withstand the spraying of high melting temperature alloys [68]. Using a ceramic or metal composite master pattern allows for tools to be fabricated from high wear resistance materials such as stainless steels, tungsten carbide alloys, and iron-nickel-chromium alloys [68].

#### **2.4.2.4 Electroforming Tooling**

Fabrication of Electrical Discharge Machining (EDM) electrodes, moulds and dies is possible by integrating solid freeform fabrication (rapid prototyping) with the electroforming process [71]. Firstly, a master pattern is fabricated by a rapid prototyping technique, commonly by stereolithography. The master pattern must have the desired shape, dimension, accuracy and roughness of the final product as any defects will be mirrored into the moulds. Nickel electrodes are used to metallise the master pattern prior to electroforming, plating to a thickness of  $5\mu\text{m}$  [72]. The metallised master pattern is placed in an electrode bath where a layer of metal, commonly nickel or copper, is deposited until the desired thickness is achieved. Burning out of the master pattern follows to leave only the electroformed shell. Lastly, the electroformed shell is reinforced by material to form the final tool. Tool strength and thermal conductivity are

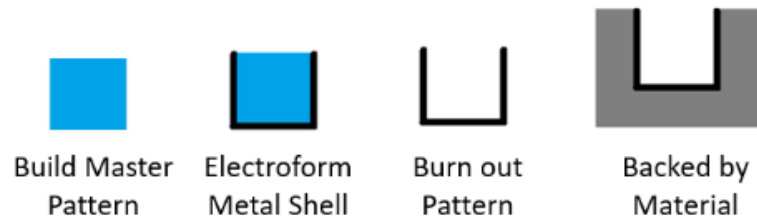


Figure 2.21: Schematic of the electroforming tooling process.

two crucial parameters that is dictated by the reinforcement material used. A schematic of the process is shown in Figure 2.21.

If the master pattern is adequately prepared for electroforming then dimensional tolerances of  $2.5\mu\text{m}$  and surface finish of  $0.05\mu\text{m}$  is achievable for the tool [72]. The main disadvantage of this process is the time required to electroform the shell, which can take up to 2 weeks for a 3mm thick shell [4]. Reducing the thickness of the shell would require a better reinforcement material but would result in shorter electroforming time. Burning out of the master pattern and the applying of the reinforcement material causes thermal deformation to the tool which is a major source of inaccuracy [72].

A reinforcement material with low shrinkage properties is desired as it minimises the internal stresses within the electroformed shell. Chemically bonded ceramics filled with metal particles offer a stiff reinforcement with good thermal conductivity and minimal shrinkage [73]. Epoxy resin composites also offer adequate properties for their use as reinforcement material [74]. The electroformed shell along with the reinforcement material are then placed in a steel mould frame.

#### 2.4.2.5 Cast Metal Tooling

Sand and investment casting are two of the most common casting methods used to produce tooling. Fabrication of a master mould pattern is the first step in the sand casting process, which is accomplished by any of the rapid prototyping techniques. The master pattern is placed in sand and the casting mould is created. On completion of the mould the master pattern is removed, and then the mould cavity is filled with molten metal and allowed to cool. Breaking of the casting mould reveals the finished tooling.

Investment casting requires a ceramic shell to cast molten metal into. There are several different routes available to create the ceramic shell for casting as shown in figure 2.22 [46]. As seen in Figure 2.22, the lead time from CAD design of mould to the finished mould is considerably reduced when incorporating rapid prototyping techniques with investment casting. Direct fabrication of the ceramic shell is one option

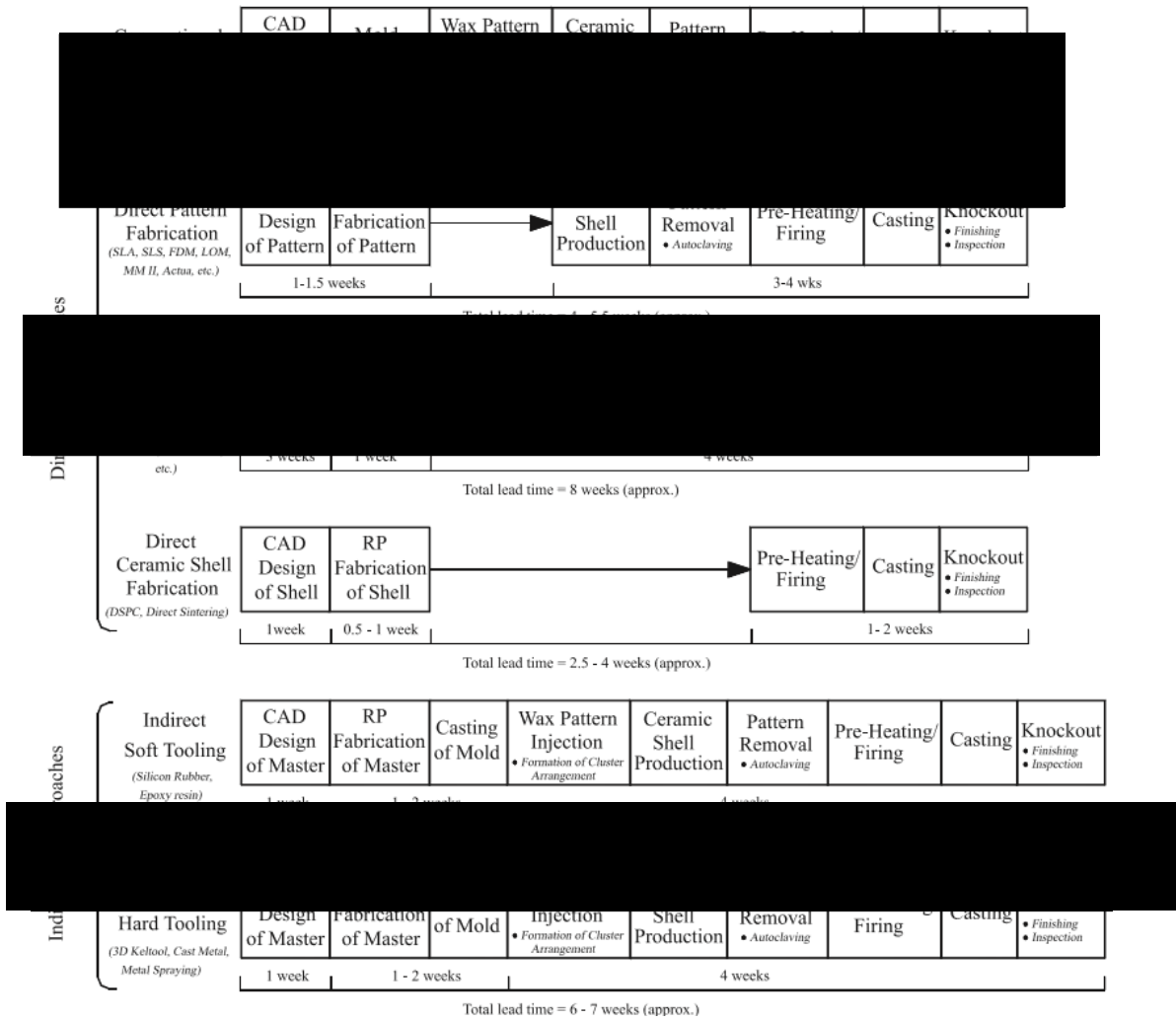


Figure 2.22: Process routes of rapid investment casting [46].

and is described in Section 2.4.1.3. Another option is to fabricate a master pattern and to use this pattern to create the ceramic shell. Incorporating rapid prototyping with investment casting avoids the mould making for wax pattern fabrication which saves considerable time and costs. During part development and prototype testing, design changes are easily accommodated for without incurring high costs of modifying or reproducing hard tooling [75].

Investment casting is often more expensive than sand casting due to the complexity and preparation needed. Although investment casting is more complex and expensive than sand casting, it can produce small and intricate parts that would not be possible by sand casting. The best method will be dependent on the complexity and the size of the desired mould.

Choosing the best material to cast the tool depends on its use. If the tool is going to be used in high volume production then a tool grade steel would be best suited, whilst low

melting metal such as aluminium or zinc would be best suited for tools used for small production runs in product development.

The most crucial part of the direct rapid investment from a rapid prototype pattern is during its removal from the ceramic shell. Heat is used to melt the pattern which flows out of the ceramic shell. Great care is needed when choosing the material for the pattern to avoid damaging the ceramic shell in the removal process. The difference in Coefficient of Thermal Expansion (CTE) of the ceramic and the rapid prototype material is the main problem. Ceramic materials have low CTE whilst common rapid prototyping material, such as ABS has relatively high CTE. To avoid shell cracking, the stress imposed by the expanding pattern must be kept below the modulus of rupture of the shell material [75]. A method to minimise the stress imposed by the expanding pattern on the ceramic shell is to fabricate a hollow pattern. This will allow the pattern to expand inwards during heating, reducing the pressure exerted on the ceramic shell [75].

#### **2.4.2.6 Keltool Tooling**

3D Keltool is a mould making process that produces production moulds within a prototype timeframe. These moulds can produce millions of parts through injection moulding. The process begins with the creating of a master tool pattern, fabricated by stereolithography due to its capabilities of producing highly detailed and accurate parts. As with many other rapid tooling techniques, it is important that the surface finish of the master pattern is satisfactory before proceeding as any defects will be copied into the final mould. RTV transfer mould is produced from the SLA master pattern which is filled with a slurry mixture, which commonly comprises of 70% tool steel powder and 30% epoxy binder [38,46,71,76,77]. Tungsten carbide powder is commonly added to the mixture to improve the hardness and durability of the tool [78]. The mixture is left to cure in the RTV mould before being removed ready for sintering. The green part is then placed in a furnace where the binder material is burned off and the tool steel is sintered, which results in a part which is 70% tool steel and 30% air. The last step is to infiltrate the part with a metal alloy, which is commonly copper. This results in a fully dense part comprising of 70% tool steel and 30% Copper which has physical properties similar to P20 tool steel [77]. Compared to traditional CNC machined steel tools, Keltool offer cost saving of around 25-40% [38]. A schematic of the 3D Keltool process is shown in Figure 2.23.

A typical Keltool tool can withstand moulding temperature greater than 650°C and pressure of 138-172MPa [77]. The Copper increases the thermal conductivity of the

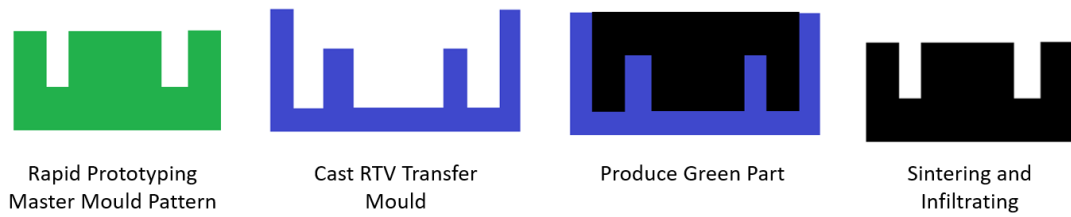


Figure 2.23: Schematic of the 3D Keltool process.

tool, which results in cycle times approximately 30% less than solid steel tools. A disadvantage of the Keltool process is the tooling size, which is limited to around 150 x 215 x 100 mm. Also, thin geometry is very difficult to produce due to the part being very weak in its green state which often break on removal from the RTV mould.

The tooling produced by 3D Keltool is comparable to traditionally machined tooling, which is high praise. During the development of a part it is common to produce prototype part in the quantity of 1 to a usual maximum of 100. This method of producing rapid tooling for prototyping is over engineered and there are faster and cheaper rapid tooling options available for the small quantity of parts that is required during part development.

### 2.4.3 Summary of Rapid Tooling Techniques

The fabrication time, cost, and tool life for each rapid tooling process is summarised in Table 2.4 [4, 38, 46, 52]. Figure 2.24 shows the different rapid tooling processes and their classification.

Table 2.4: Comparison of the different rapid tooling processes.

Rapid Tooling Technique	Fabrication Time	Fabrication Cost	Tool Life (Plastic Injection Moulding)
Resin	Low	Low	100-1000
Metal Powder	High	High	>100,000
Ceramic powder	Low	Low	1 (Expandable Shell)
Laminated Metal	Low	Low\Medium	100,000
LENS	Medium	Medium	100,000
RTV	Low	Low	100-300
Epoxy	Low	Low	100-100,000
Spray Metal	Medium	Medium	1,000-10,000
Electroforming	High	High	>100,000
Cast Metal	Medium	Medium	>200,000
Keltool	High	High	>1,000,000



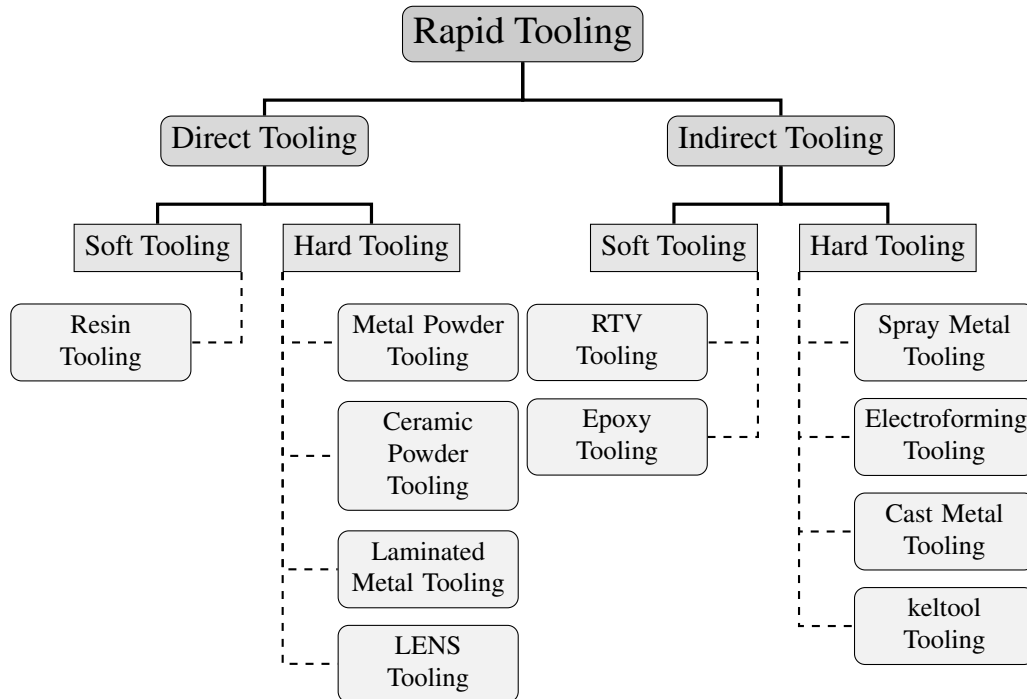


Figure 2.24: Classification of the rapid tooling processes.

## 2.5 Computational Modelling

Utilising rapid tooling can greatly reduce the manufacturing cost and lead time for tool production [5, 52, 79–82]. Tool material, accuracy, surface finish, and mould life are some limitations of rapid tooling [79, 82–84]. Accuracy, thermal conductivity, and mechanical properties of the tool have a significant influence on injection moulding cycle, part quality and geometric complexity [85, 86]. A better understanding of the impact on mould design and the injection moulding process from using rapid prototype tooling is required [5, 80]. Current injection moulding computational simulation packages are not appropriate for simulation of rapid prototype tooling due to the difficulty in predicting the material properties and its variation across different orientations [80]. Computer aided evaluation for rapid tooling process selection and manufacturability for injection moulding has been presented by Nagahanumaiah [79]. A methodology comprising of three major steps; rapid tooling process selection, manufacturability evaluation, and mould cost estimation has been proposed [79]. An integrated quality function deployment (QFD) and analytic hierarchy process (AHP) methods are implemented in a visual C++ program running in windows environment. The purpose of this computer aided evaluation is for an engineer to select the appropriate rapid tooling process and to evaluate the manufacturability and cost of the tool.

Three dimensional computer aided engineering simulation for injection moulding have been around since the 1970s when theoretical principles and fluid mechanical models were applied to computer simulations [87]. Computer Aided Engineering (CAE) and Computer Fluid Dynamics (CFD) are widely used to validate conformal cooling in rapid tooling moulds [88–90]. Whilst a significant amount of work has been done on the thermal validation of rapid prototyping tooling, very little work has been done on their mechanical validation. Computational modelling of the injection moulding process could predict issues and minimises tool iterations.

K M Au et al have performed CAE and CFD validation on rapid tooling for injection moulding of plastic [88]. The rapid tooling they used was metal filled stereolithography (SLA) cavity inserts [91]. Stereolithography rapid prototyping machine is used to fabricate epoxy insert shells directly from CAD data which were then fitted into steel frames and reinforced with aluminium powder and epoxy resin mixture, which is shown in Figure 2.25 [91]. Moldflow Plastic Insight 3.1 was used to identify the optimal cooling system for the rapid tooling and COMSOS/Works was used to evaluate the mechanical properties between solid and scaffolding assembly. The mechanical evaluation compared residual stress, strain, and displacement between simple geometries of a solid cube and a scaffold structure cube which is shown in Figure 2.26 [88]. It was seen that the scaffolding structure had 57% more residual stress, 630% more displacement, and 69% less strain compared to the solid structure [88]. Higher stresses and displacements are seen in the scaffolding structure as it provides less support than a solid volume.

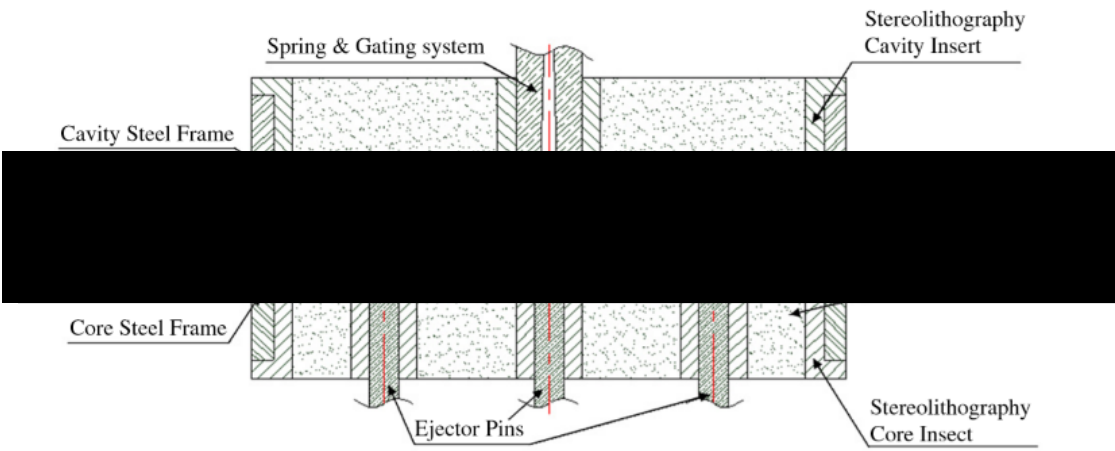
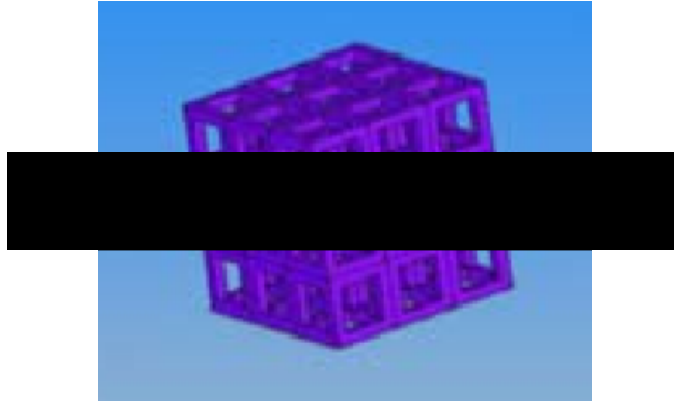


Figure 2.25: Cross sectional view of the stereolithography injection moulding tool inserts [91].



*Figure 2.26: Scaffolding assembly structure used in mechanical evaluation [88].*

Structural analysis of a rapid prototype tooling made from photopolymer with stereolithography has been completed by Huamin Zhou et al [80]. They predict the deformation that occurs in the final part created in the rapid prototype tooling due to the thermal and mechanical loads of the filling process and compare this to experimental testing. Stereolithography injection moulding tooling experimental data was obtained from K Himasekhar et al [86]. To evaluate the performance of the rapid prototype tool they measure the distortion in each axis and the twist in the formed part. Results from their proposed computational model was within 15% to the experimental data for each measurement. In their paper they also highlight the importance of thermal conductivity of the tooling material to ensure a quality part is created.

An accurate three dimensional non-linear coupled thermo-mechanical Finite Element Method (FEM) model has been developed to analyse dimensional accuracy for casting dies using rapid tooling moulds [81]. The FEM analysis is non-linear due to three main attributes; the material, geometry, and boundary conditions [81]. Convergence criterion and time steps directly influence the computational accuracy of the FEM model [81]. Pro-E software on an SGI workstation was used to build the CAD model with the three-dimensional FEM model for half of the die shown in Figure 2.27 [81]. The simulated shrinkage ratio of the part cast in the rapid tooling mould was 1.108% which compares closely to the experimental shrinkage ratio of 1.158% [81].

Work has been done by Miquel Comingo-Espin et al to develop simulations to predict the mechanical properties of rapid prototyped parts, specifically parts made by Fused Deposition Modelling (FDM) [92]. Orientation of the part within the build chamber is one of the most important factors that must be considered with rapid prototype parts, which can influence their surface finish, dimensional accuracy and mechanical properties [92]. All rapid prototype parts are built layer by layer resulting in a non-isotropic

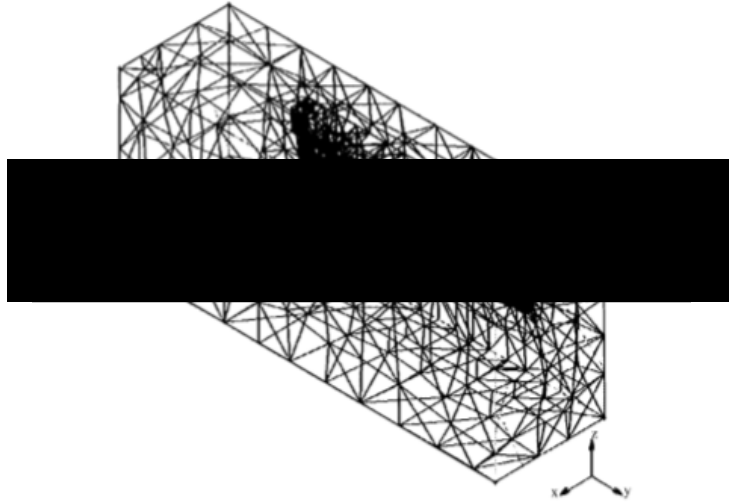


*Figure 2.27: Three-dimensional FEM model for half of the die [81].*

mechanical properties. The mechanical strength of the bonding between layer is of great importance and heavily influences the quality of the part [93–96]. Deformation of the parts were simulated on ANSYS mechanical 15.0 software using isotropic and orthotropic mechanical properties for the part [92]. The isotropic and orthotropic model computational simulations had a mean deviation of 7.30% and 7.12% respectively to the experimental values [92]. The computational model is reasonably accurate with little difference between the isotropic and orthotropic models. It is recommended that orthotropic material is used when the part exceeds the elastic region, as it gives more accurate results in this region when compared to the isotropic model [92]. But when the part only deforms elastically the isotropic model is preferred as it is simpler and gives the same result [92].

## **2.6 Proposed Novel Rapid Tooling Methodology**

There are numerous rapid tooling techniques that could be utilised to manufacture tooling for injection moulding, each with their advantages and disadvantages as described in section 2.4. Metal powder and epoxy rapid tooling techniques are combined to form a new novel rapid tooling technique. Combining metal powder and epoxy rapid tooling techniques will create a more efficient manufacturing process, resulting in cost and time savings.

Similar combinations of rapid tooling techniques have previously been made to maximise the benefits of each rapid tooling technique. Producing cavity inserts (shell) by resin rapid tooling which has been reinforced using epoxy rapid tooling and placed in

a steel frame is a common rapid tooling methodology to produce tooling for injection moulding [2,31,91]. The proposed novel rapid tooling methodology will produce a singular insert (shell) which will be made from a metal using metal powder rapid tooling methodology. Epoxy rapid tooling manufacturing process will be used to reinforce the metal shell. There will be no need for a steel frame for the rapid tooling due to the manufacture of a singular insert (shell) and due to the superior mechanical strength of the metal shell compared to the resin inserts.

Metal powder rapid tooling technique uses selective laser sintering or material binding to directly produce high quality and accurate parts from powdered metals [42, 43, 45, 97]. Depending on part requirement, some post processing might be necessary which increases the lead time and cost of part [42, 43, 45, 97]. Detailed description of metal powder rapid tooling technique can be found in section 2.4.1.2. Epoxy rapid tooling technique is an indirect method, requiring a master mould to be manufactured by any ALM process [63–66]. Epoxy resin is poured into the master mould to produce the desired part. Detailed and accurate parts can be manufactured by epoxy rapid tooling with little time and cost. Detailed description of epoxy rapid tooling technique can be found in section 2.4.2.2.

Figure 2.28 shows the manufacturing route of using the proposed novel combination of metal powder and epoxy rapid tooling techniques to manufacture tooling for injection moulding. Creating a CAD model of the tool is the first step, which is then edited to create a CAD model of the desired manufactured shell. CAD model of the shell will be processed and sent to the appropriate additive layer manufacturing machine to be printed. Once the ALM shell has been manufactured, epoxy resin composite will be poured into the cavity of the shell, creating the final tool. Depending on tool requirements, finishing processes can be applied to improve surface finish and accuracy.

Combining both metal powder and epoxy rapid tooling in the manufacture of tooling for injection moulding utilises the benefits of both techniques. Rapid tooling technique of metal powder produces high quality parts with good mechanical strength, which is perfect for the shell of the tool. Metal powder compared to epoxy resin rapid tooling technique is more expensive and slower, hence minimising the volume of part made from metal powder will reduce the cost and time for the whole tool. Epoxy resin rapid tooling technique will be used to fill the cavity of the shell, reinforcing and adding strength to the tool in little time and cost. Tool design will depend on the injection moulding process parameters, with shell thickness, along with shell and reinforcement material being the main design variables.

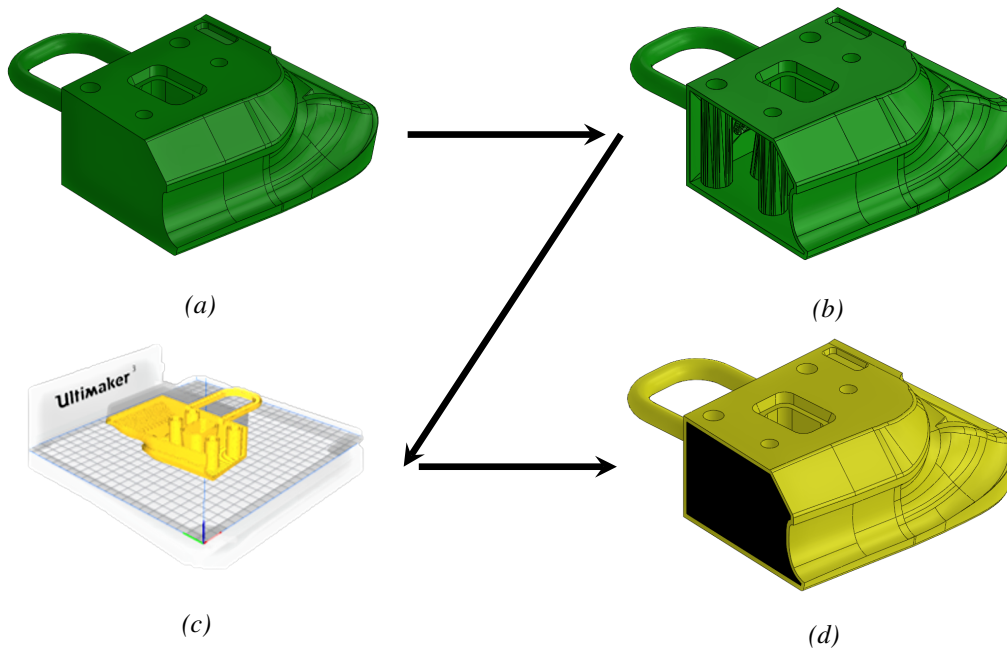


Figure 2.28: Manufacturing route of the proposed novel rapid tooling technique; (a) CAD model of tooling, (b) CAD model of tooling's shell, (c) additive layer manufacture of shell, and (d) filling of shell with epoxy resin.

An example tool made by this proposed novel rapid tooling technique is shown in Figure 2.29. Transparency of the shell has been set to 50% to improve the visualisation of the tool.

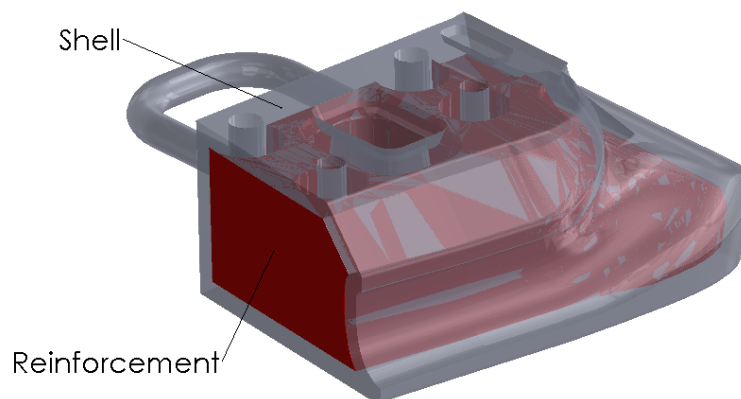


Figure 2.29: Figure of an example tool made by the proposed novel rapid tooling technique.

### 3 ANSYS Computational Method Analysis

#### 3.1 Overview

Mechanical and thermal computational analysis of the proposed rapid prototype tooling will be done on ANSYS 19.1 software. The computational model will represent the manufacturing process of injection moulding of EPDM for exterior automotive seals. There are several different analytical systems available on ANSYS 19.1 that could be used for simulation of injection moulding. Choosing the most appropriate system is important to ensure accurate results within an acceptable computational time. Five different analysis system will be tested, where displacement, stress and computational time results will be compared to choose the most appropriate model. Structural, Computational Fluid Dynamics (CFD) and thermal analytical system will be analysed, separately, in a 1-way coupled Fluid Structure Interaction (FSI), and in a 2-way coupled FSI simulations.

FSI involve coupling of fluid dynamics and structure mechanics analytical systems. Hydrodynamic forces exerted by the fluid flow will deform and change the thermal stresses within a structure, and the deformation of the structure will effect the fluid flow [98–105]. 1-way FSI modelling calculates the hydrodynamic force of the fluid flow and passes this information to the structural model. No update to the fluid flow is needed as it assumes very small deformation of the structure [98–105]. 2-way FSI assumes significant structural deformations and iterates between CFD and structural analytical systems [98–105]. Schematic of information flow in 1-way and 2-way coupled FSI is shown in figure 3.1.

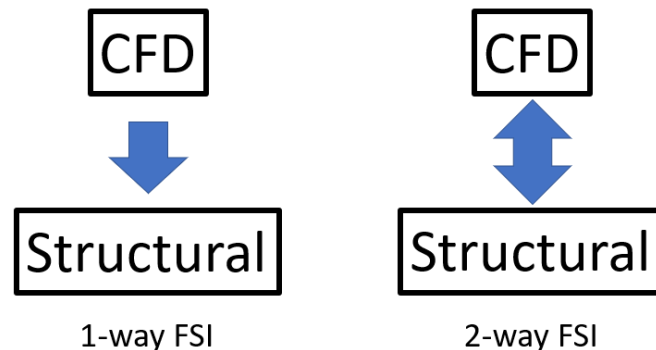


Figure 3.1: Schematic of information flow in 1-way and 2-way coupled fluid structure interaction.

ANSYS CFD fluent analytical solutions, 1-way and 2-way coupled FSI are anticipated to be computationally expensive and have long computation times due to the intricate physics of fluid flow and the complexity of fluid-structure interactions [99–105]. The 2-way coupled FSI model is assumed to be the most accurate model due to its inclusion of mesh displacement at the fluid-solid boundary. A computational model that avoids using CFD analytical models are perceived to be more useful as the computational time is likely to be much smaller, but only if they produce results within an acceptable range to the CFD models.

## 3.2 Methodology

### 3.2.1 Tool Selection

Commercial tooling for injection moulding of EPDM exterior automotive seals is very complex due to the required geometry. Validating ANSYS computational models using a commercial tool would be very complex resulting in unnecessarily high computational time. Simplifying a commercial tool to a constant cross-section geometry two-half tool will reduce the complexity of the simulations and hence the computational time. *6G33 – L20708 – A – 22 – WEATHERSTRIP ASSY~DOOR PRIM* is a commercial EPDM exterior automotive seal part from Aston Martin which will be the benchmark EPDM seal, shown in Figure 3.2. It will be simplified to create the cavity for the tooling used for computational model analysis.

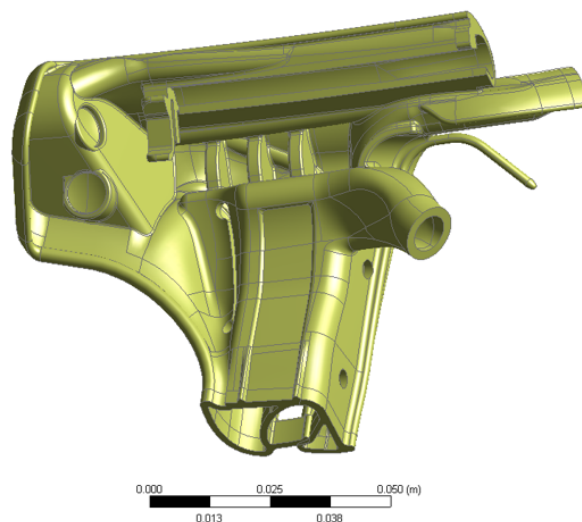


*Figure 3.2: CAD model of Aston Martin 6G33 - L20708 - A - 22 - WEATHER STRIP ASSY – DOOR PRIM exterior automotive seal used as benchmark part for ANSYS computational methods analysis.*



The benchmark EPDM exterior automotive seal from Aston Martin is approximately 120 x 75 x 45 mm in size, with a surface area and volume of 0.032755 m<sup>2</sup> and 3.2933e-05 m<sup>3</sup> respectively. It is important that the simplified part is similar to the original part in these three parameters; size, area, and volume.

The constant cross-section chosen for the simplified part has been taken from the original part and is shown in Figure 3.3. This cross-section is extruded 120 mm to create the simplified part which is approximately 120 x 40 x 20 mm in size, with a surface area and volume of 0.031332 m<sup>2</sup> and 3.1078e-05 m<sup>3</sup> respectively. Figure 3.4 shows the complete simplified part which will be used to create the cavity for the tool used in the computational model analysis.

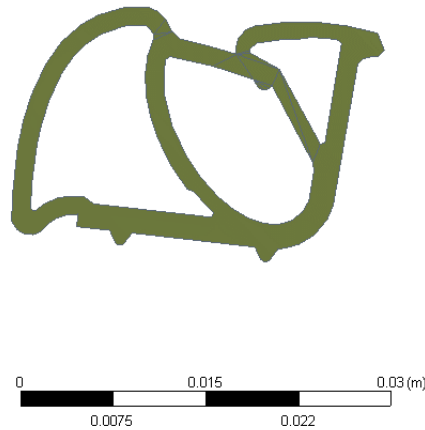


Figure 3.3: Cross-section for simplified part which has been taken from original part.

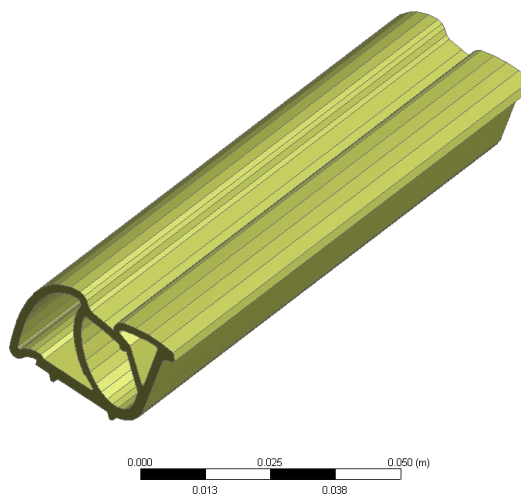
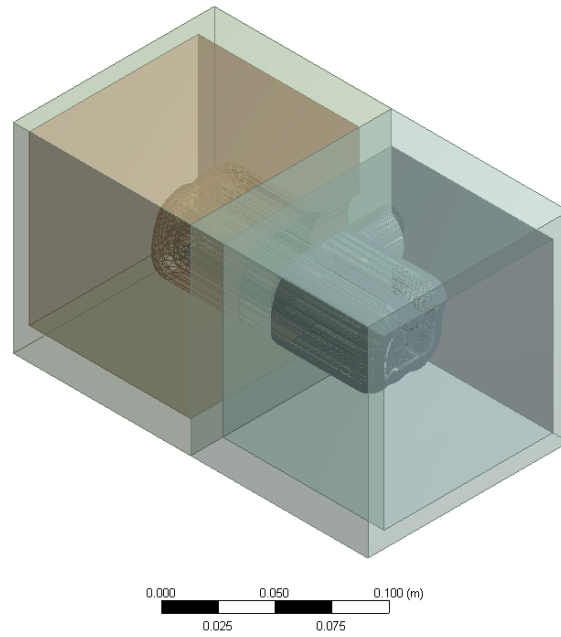


Figure 3.4: Complete simplified part which is used to create the cavity for the mould used in computational model analysis.



*Figure 3.5: Transparent isometric view of the simplified tool for the computational model analysis.*

Tooling for the computational model analysis has two halves (one parting line) and a wall thickness of at least 50mm in every direction. The injection gate is 15mm in diameter and is located at the centre of the tool. It will be a representative tool which is manufactured by the proposed novel rapid prototype tooling methodology, with a shell thickness of 10mm. Tool material will be stainless steel for the shell and epoxy resin for the reinforcement. A transparent isometric view of the simplified tool for the computational model analysis is shown in Figure 3.5.

### **3.2.2 Computational Model**

All computational simulations will be performed on the following system unless otherwise stated, which should be considered when evaluating the computational time. The computer used an Intel(R) Xenon(R) CPU E5-1630 processor at 3.70GHz with 64.0GB RAM. It ran a windows 64-bit operating system with x64-based processor, with 4 cores and 4 available threads. Computational simulations will be performed on ANSYS 19.1 software and all CAD work will be completed in Solidworks 2018 software.

Typical parameters for the injection moulding of EPDM exterior automotive seals are shown in Table 4.1. These values will be used when applicable in the computational models.

Table 3.1: Typical parameters for injection moulding of EPDM exterior automotive seals.

<b>Parameter</b>	<b>Value</b>
<i>Hydraulic Pressure</i>	1400bar (140MPa)
<i>Clamping Pressure</i>	2000bar (200MPa)
<i>Temperature of melt</i>	125°C
<i>Temperature of Plate</i>	200°C
<i>Vulcanisation Time</i>	85s
<i>Melt Material</i>	EPDM Dense 60 shore A
<i>Tool Material</i>	P20 Grade Steel

### 3.2.2.1 Structural

Structural ANSYS components can be simulated either in static (steady-state) or transient systems [101,106]. Static structural analysis uses loading conditions which do not change with time whilst transient structural analysis can use loading conditions which are time dependant. Computational structural models will have a constant loading conditions which are not time dependant, hence a static structural system can be used which is preferred to the transient structural system as it is computationally quicker. Transient structural model will be used for the analysis of 1-way and 2-way FSI computational models, due to the time dependant hydrodynamic loads from the CFD model. Static structural computational model has a constant pressure of 140MPa applied on the fluid-solid interface which represents the hydraulic pressure along with a clamping pressure of 200MPa. Temperature of the system is set to ambient, which is 22°C with no additional heat source applied. Fixed displacement conditions are set along the parting line and at the outer surface of the tool. Along the parting line the x and y axis are free, and the z axis fixed, and at the outer surface the x and y axis are fixed, and the z axis is free. Figure 3.6 shows the static structural computational model with loads and boundary conditions.

Tool cavity (part) is suppressed for the static structural computational model as there is no inclusion of CFD. Contact between the shell and reinforcement components of the rapid prototype tool is set to bonded and the contact between the two halve of the tool is set to rough. Bonded contact allows no sliding and no opening or closing of gaps, whilst rough contact similarly allows no sliding but does allow opening and closing of gaps. Quadratic is the most accurate mesh type available and is used for this analysis. The mesh has 249,502 nodes and 146,931 elements. Analysis will be 1s long with 10-time steps.

Static Structural  
 Times: 1.5  
 21/09/2019 15:45

- A Pressure: 2.e+008 Pa
- B Pressure 2: 2.e+008 Pa
- C Pressure 3: 1.4e+008 Pa
- D Displacement
- E Displacement 2

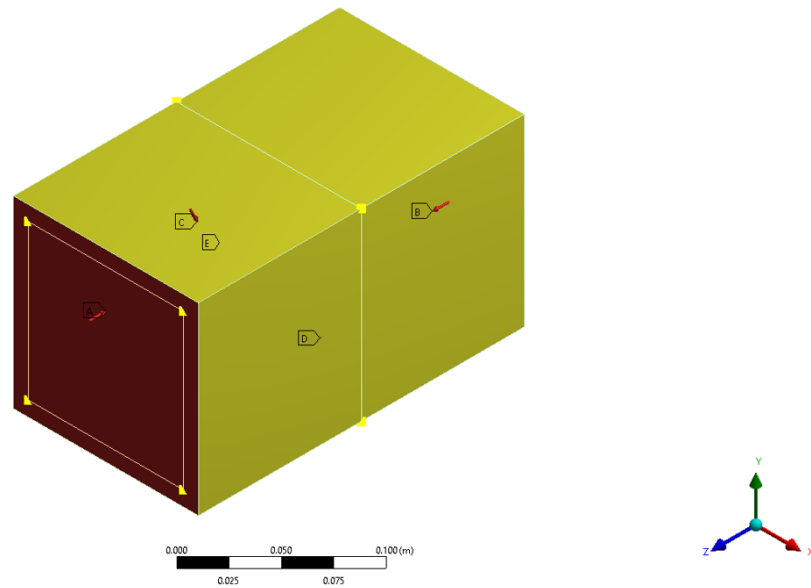


Figure 3.6: Static structural computational model with loads and boundary conditions.

### 3.2.2.2 Thermal-Structural 1-way coupling

The computational model thermal-structural 1-way coupling will have two analysis systems; steady-state thermal and static structural. Firstly, the steady-state thermal component is solved to extrapolate thermal loads. The thermal loads computed from this component will then be imported into the static structural component of the computational model [107]. A project schematic for the 1-way coupled thermal-structural computational model is shown in Figure 3.7.

A thermal-structural 1-way coupling computational model is the structural computational model with the addition of thermal loads. The structural component of the

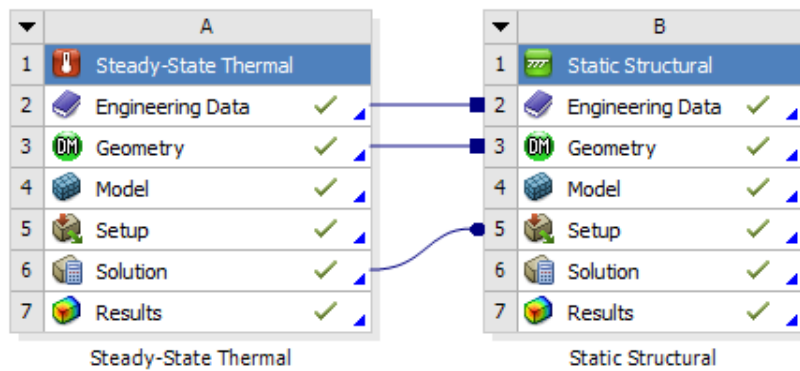


Figure 3.7: Project schematic for the 1-way coupled thermal-structural computational model.

model is set up exactly the same as the structural computational model, with a constant pressure of 140MPa applied to the fluid-solid interface, clamping pressure of 200MPa either side of the tool, and with the same fixed displacements. Contact types, mesh, and analysis settings used are exactly the same as used for the structural computational model.

Thermal components of the thermal-structural 1-way coupling computational model will be performed in steady-state thermal analysis system. A constant temperature of 125°C is applied to the fluid-solid interface which is the same as the melt temperature, and a constant temperature of 200°C is applied to either end of the tool to represent the plate temperature. Contact types, mesh, and analysis settings for the steady-state thermal analysis is exactly the same as for the static structural component. Figure 3.8 shows the steady-state thermal computational model, with A representing the tool-melt interface temperature and B representing the external plate temperature. Figure 3.9 shows the loads and boundary conditions for the structural component of the 1-way coupled thermal-structural computational model, which differs to the structural computational model due to the inclusion of imported body temperature.

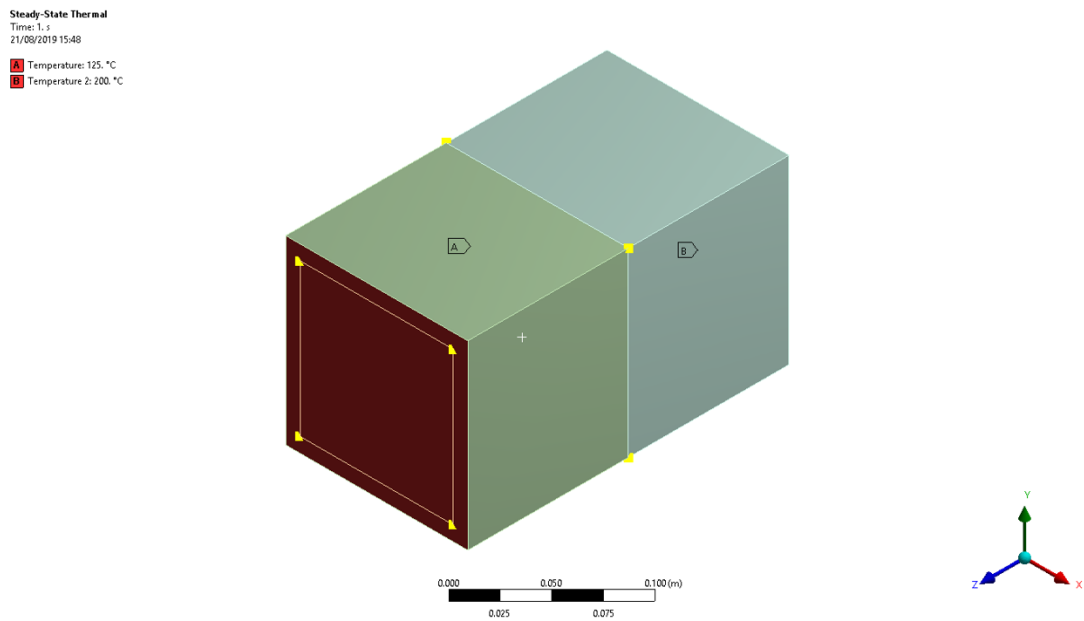


Figure 3.8: Steady-state thermal computational model, with A representing the tool-melt interface temperature and B representing the external plate temperature.

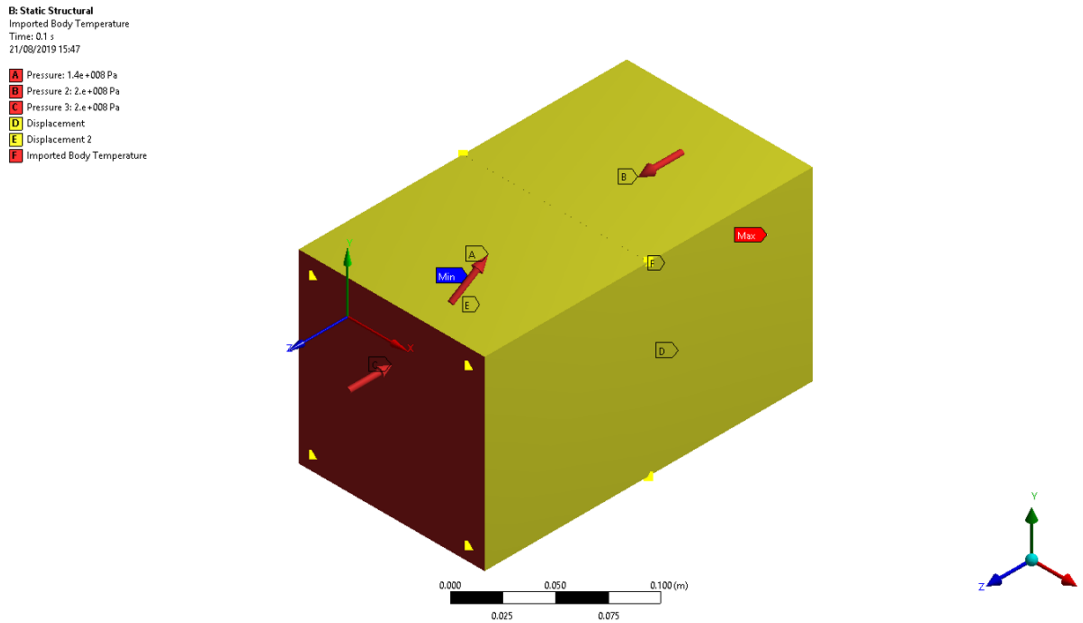


Figure 3.9: Loads and boundary conditions for the structural component of the 1-way coupled thermal-structural computational model, which differs to the structural computational model due to the inclusion of imported body temperature.

**3.2.2.3 Fluent-Structural 1-Way Coupled FSI**

A fluent-structural 1-way coupled FSI computational model will have two analysis systems; fluid flow (fluent) and transient structural. The fluent model will be solved first to extrapolate pressure results from the fluid flow which will be transferred into the transient structural model before solving. A project schematic of the 1-way coupled fluent-structural computational model is shown in Figure 3.10.

The fluent analysis system is only concerned with the cavity of the tool (part). Pressure on the solid-fluid surface due to the hydrodynamic forces of the fluid flow will be

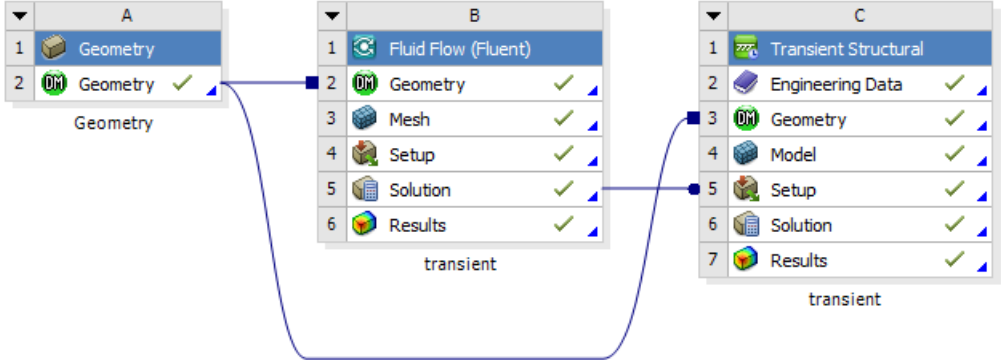


Figure 3.10: Project schematic of the 1-way coupled fluent-structural computational model.

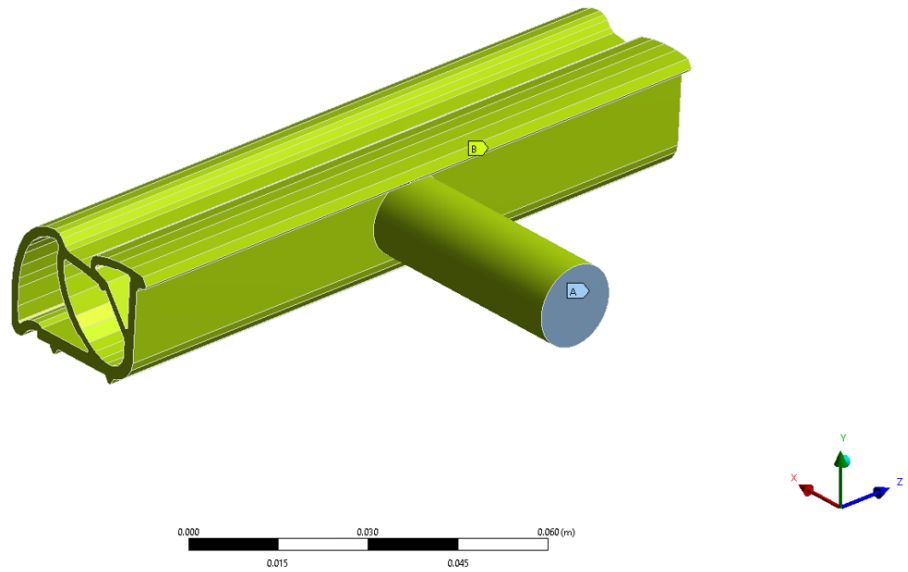


Figure 3.11: Model for the fluent simulations along with its named selections; inlet and fluid-tool boundary.

computed which will be exported and used in the transient structural analysis system. EDPM dense 60 shore A will be the fluid material, which has a density of  $1800 \text{ kg/m}^3$  and viscosity of  $250 \text{ kg/m.s}$ . Figure 3.11 shows the fluent model along with its named selections; inlet and solid-fluid boundary. A linear mesh is used for the fluent model which has 4008 nodes and 14627 elements.

Fluent simulation will run with three models; multiphase volume of fluid, energy, and viscous k-epsilon. There will be two materials used for the simulation, air to fill the cavity at the start of model and EPDM which is injected into the cavity. The patch function will be used to ensure that at the start of the simulation only air is present in the cavity, and that only EPDM is injected into the cavity.

Boundary conditions for the fluent simulation is as follows; the solid-fluid boundary is a wall, and the inlet is a velocity inlet. A velocity inlet is chosen over a pressure inlet due to the complexity required for the pressure inlet simulation. If a pressure inlet was chosen then a pressure outlet must be present to allow the occupying air to escape, creating a pressure difference and allowing fluid to flow into the cavity. The required pressure outlet would occur at the parting line and would be very small. Including a very small area would require a significantly finer mesh to be used which would be computationally very expensive. Velocity inlet does not require and outlet as it assumes that the air is being replaced by the EPDM. Injection time is commonly

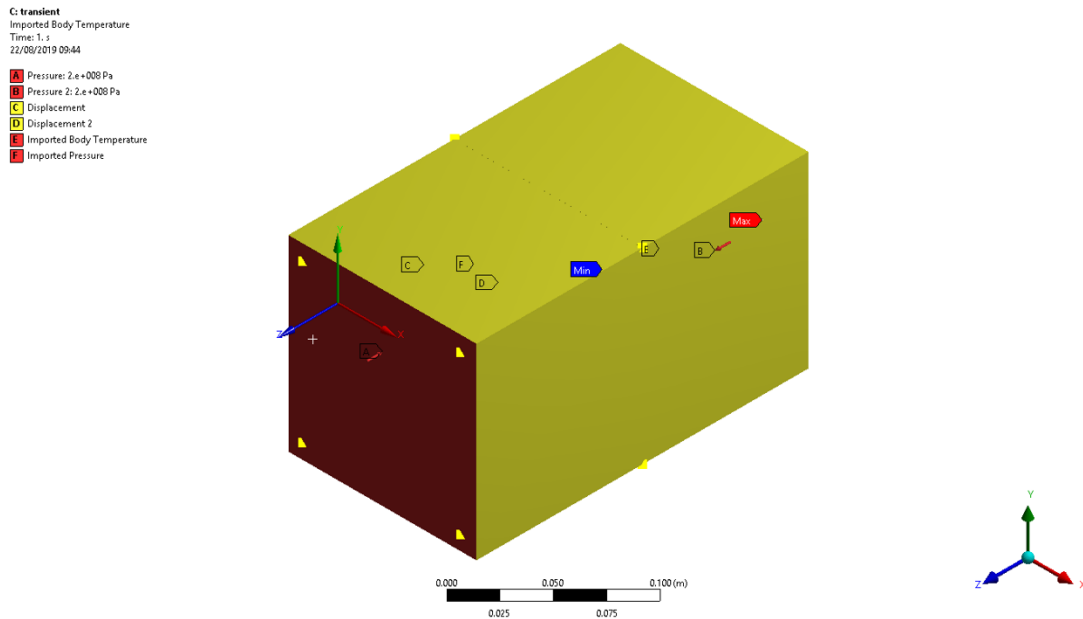


Figure 3.12: Loads and boundary conditions for the transient structural component of the 1-way coupled fluent-structural computational model.

2s for a EPDM seal of this size, which requires an inlet velocity magnitude of 0.1m/s. The velocity inlet boundary condition will have a velocity of 0.1m/s, gauge pressure of 140MPa, and a temperature of 125°C.

The fluent simulation will run with an adaptive stepping method until the end time of 2s is reached. Maximum and minimum time steps are set to 1e-03s and 1e-07s respectively and a max iteration per time step is set to 5.

The transient structural component of the 1-way coupled fluent-structural computational model is set up similarly to the static structural models used in previous computational models. Contact type and mesh are kept exactly the same. The analysis setting is synced to the analysis time used by the fluent simulation. The clamping pressure is still applied at the ends of the tool but there is no solid-fluid interface pressure applied as this is imported from the fluent simulation. Body temperature is also imported from the fluent simulation. Fixed geometries are the same as for the previous structural computational models. Figure 3.12 shows the loads and boundary conditions for the transient structural component of the 1-way coupled fluent-structural computational model.

**3.2.2.4 Fluent-Thermal-Structural 1-Way Coupled FSI**

Fluent-thermal-structural 1-way coupled FSI computational model will have three analysis systems; fluid flow (fluent), transient thermal, and transient structural. Fluent



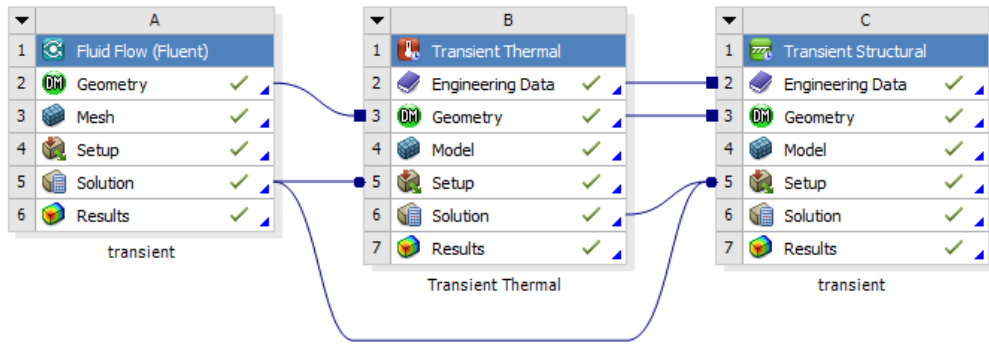


Figure 3.13: Project schematic of the 1-way coupled fluent-thermal-structural computational model.

model will be solved first to extrapolate pressure and thermal results at the fluid-solid interface. The transient thermal model will be solved secondly after importing the thermal results from the fluent simulation. Thermal results from the transient thermal model and pressure results from the fluent simulation will be imported into the transient structural model which then will then be solved, giving the final result of the fluent-thermal-structural 1-way coupled FSI computational model. A project schematic of the 1-way coupled fluent-thermal-structural computational model is shown in Figure 3.13.

Analysis systems for the fluent-thermal-structural 1-way coupled FSI computational model are very similar the fluent-structural 1-way coupled FSI computational model but with the inclusion of the transient thermal analysis system. Transient thermal model is very similar to the steady-state transient model used in the thermal-structural 1-way coupling computational model. The only differences are that the fluid-solid interface temperature is imported from the fluent simulation and the analysis time is synced to the fluent simulation. Thermal load from the heated plate, contact types, and mesh are exactly the same. The fluent model is exactly the same as the one used in the fluent-structural 1-way coupled FSI computational model. The only difference between the transient structural model in the fluent-thermal-structural 1-way coupled FSI and fluent-structural 1-way coupled FSI computational models is that the thermal load is imported from the transient thermal model and not the fluent model. Everything else is exactly the same. Figure 3.14 shows the loads and boundary conditions for the transient structural component of the 1-way coupled fluent-thermal-structural computational model.

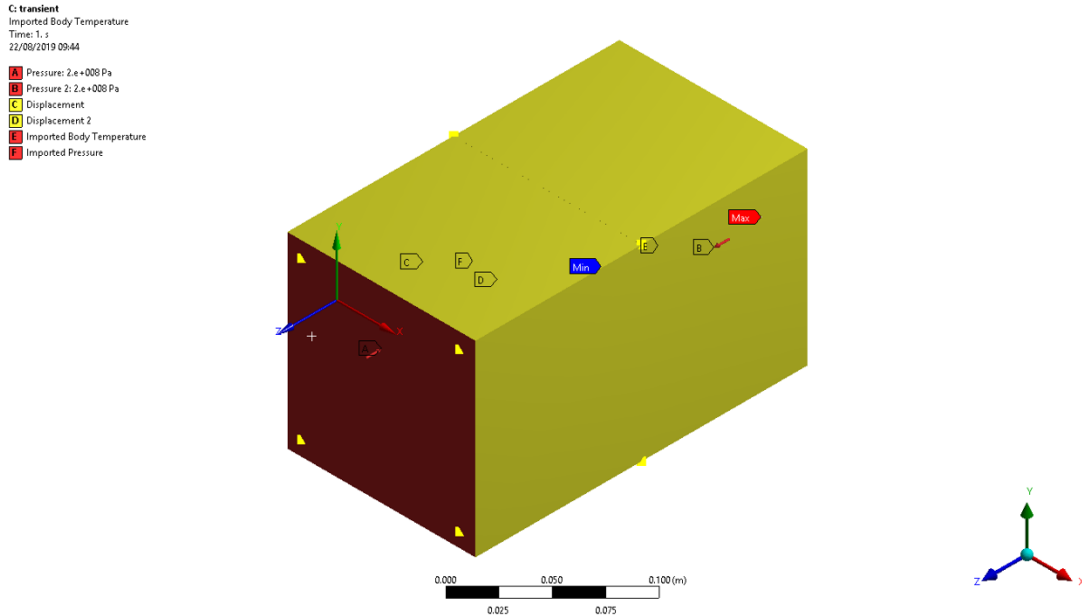


Figure 3.14: Loads and boundary conditions for the transient structural component of the 1-way coupled fluent-thermal-structural computational model.

### 3.2.2.5 Flunet-Structural 2-Way Coupled FSI

A single 2-way coupled FSI computational model will be analysed consisting of a fluid flow (fluent) and transient structural analysis systems. An addition of a system coupling component is needed to run the 2-way coupled FSI simulation [100, 102–105]. The system coupling component is required for co-simulation between the CFD fluent and mechanical transient structural models and ensures constant time duration

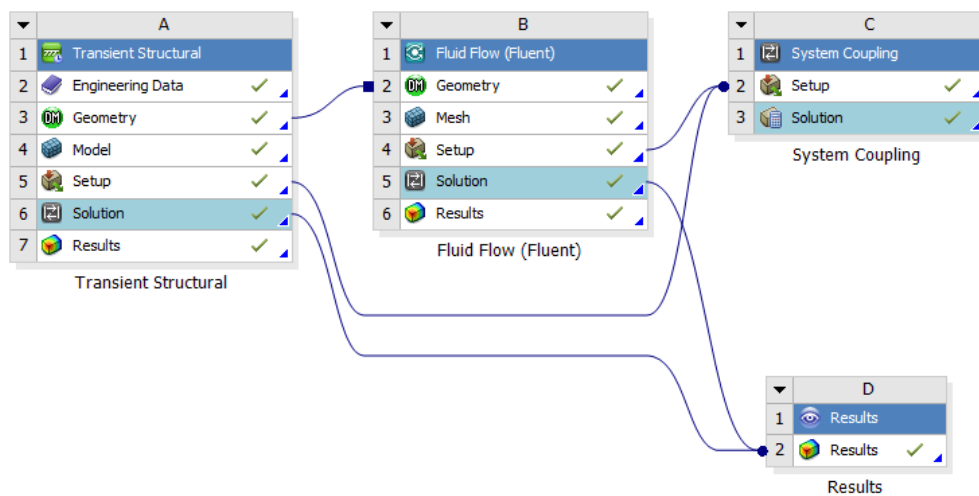


Figure 3.15: Project schematic of the 2-way coupled fluent-structural computational model.

and time step settings across both models [100, 102–105]. Force data from the fluent simulation is transferred to the structural model, and the displacement data from the structural simulation is transferred to the fluent model. Data transfer links are created in the system coupling between fluid-solid surfaces selected in both fluent and structural analysis systems. The transfer of data is done at every time step. Figure 3.15 shows the project schematic of the 2-way coupled fluent-structural computational model.

There are a few important differences between the fluent and structural analysis systems in 2-way and 1-way coupled computational models. In the structural analysis system, the fluid-solid interface needs to be selected to receive the force data from the fluent analysis system. End time of the coupled simulation cannot exceed the end time selected in the structural analysis system. The fluid flow (fluent) analysis system requires a dynamic mesh to allow for the variation in displacement received from the structural analysis system. System coupling is the type of dynamic mesh used and is used in the fluid-solid boundary zone. There is no need to apply analysis settings in the fluent analysis system as it is over written by the analysis setting in the system coupling.

All boundary conditions and loads in the 2-way coupled fluid-structural computational model are exactly the same as in the 1-way coupled fluent-structural computational model. The only difference between the two computational models is the analysis setting, which for the 2-way coupled FSI computational model will run for 2s with a constant time step of 0.001s and maximum iteration each time step of 10.

### **3.3 Results**

Displacement, stress, and computational time results for each computational model has been extrapolated from the simulations. Locations of the maximum and minimum displacement and stress for each computational model have also been noted. Table 3.2 summarises the results of the ANSYS computational model analysis. It shows the maximum and average displacement and stress values at the fluid-solid interface, along with the computational time for each model. Visualisation of these results are shown in Figures 3.16, 3.17, and 3.18. Maximum and average displacement results from each computational model is shown in Figure 3.16, maximum and average stress results from each computational model is shown in Figure 3.17, and computational time for each computational model is shown in Figure 3.18.

2-way coupled FSI fluent-structural computational model produced the largest maxi-

imum displacement and stress results of all models. The smallest maximum displacement and stress results are produced by the structural computational model, which is within 14% of the largest maximum results produced by the 2-way coupled FSI fluent-structural model. 1-way coupled FSI thermal-structural model produced the largest average displacement result whilst the 2-way coupled FSI fluent-structural model produced the smallest average displacement result. The largest average stress result was produced by the 1-way coupled FSI fluent-thermal-structural model whilst the smallest average stress result was produced by the 1-way coupled FSI thermal-structural model.

Table 3.2: Summary of the ANSYS computational model analysis, displaying maximum and average displacement and stress values at the fluid-solid interface, along with the computational time for each model.

Computational Model		Displacement (m)		Stress (Pa)		Computational Time (h/m/s)
		Maximum	Average	Maximum	Average	
Structural	Static	0.981e-04	4.613e-05	1.136e+09	2.569e+08	0/11/37
1-way coupled FSI	Thermal-Structural	1.067e-04	5.838e-05	1.275e+09	2.344e+08	0/34/17
	Fluent-Structural	0.983e-04	4.567e-05	1.222e+09	2.579e+08	1/42/48
	Fluent-Thermal-Structural	1.099e-04	4.203e-05	1.301e+09	3.764e+08	2/08/22
2-way coupled FSI	Fluent-Structural	1.129e-04	4.188e-05	1.319e+09	2.693e+08	8/24/31

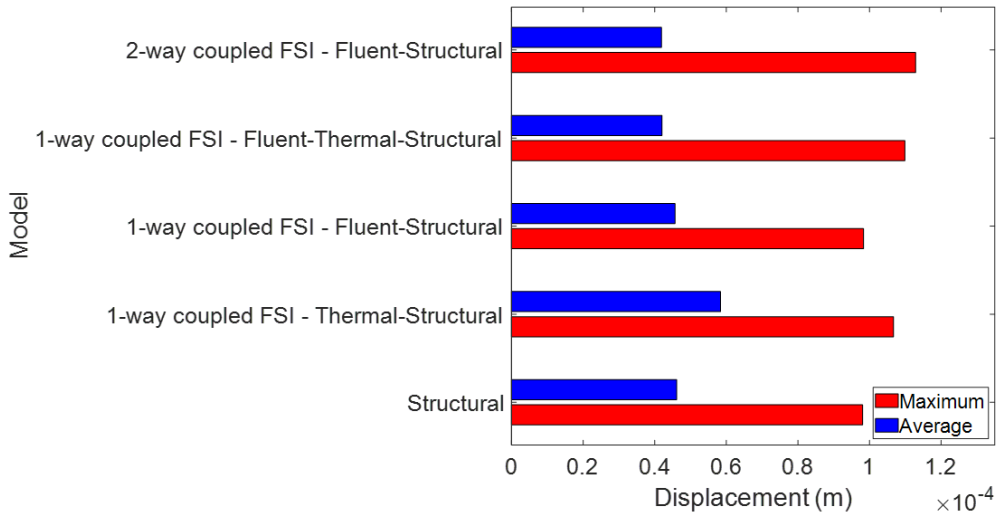


Figure 3.16: Maximum and average displacement results from each computational model at fluid-solid interface.

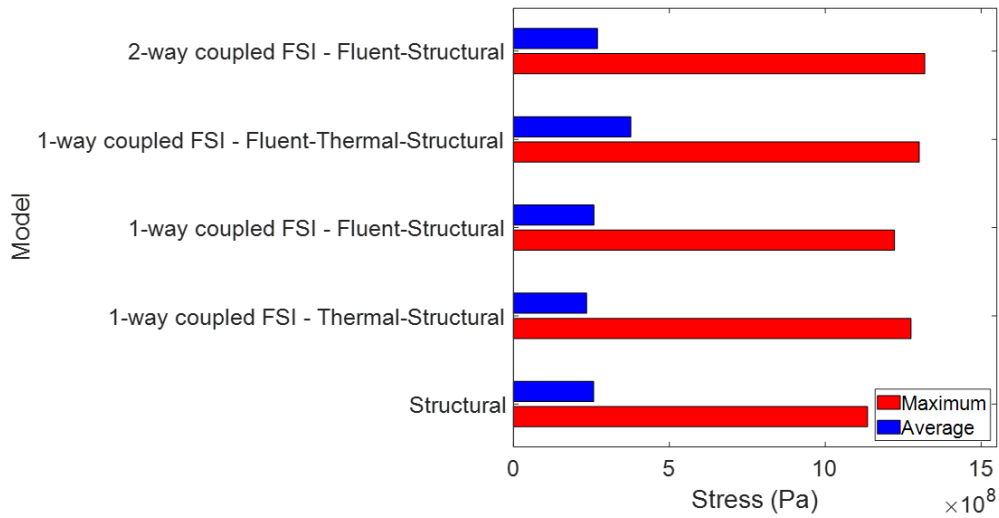


Figure 3.17: Maximum and average stress results from each computational model at fluid-solid interface.

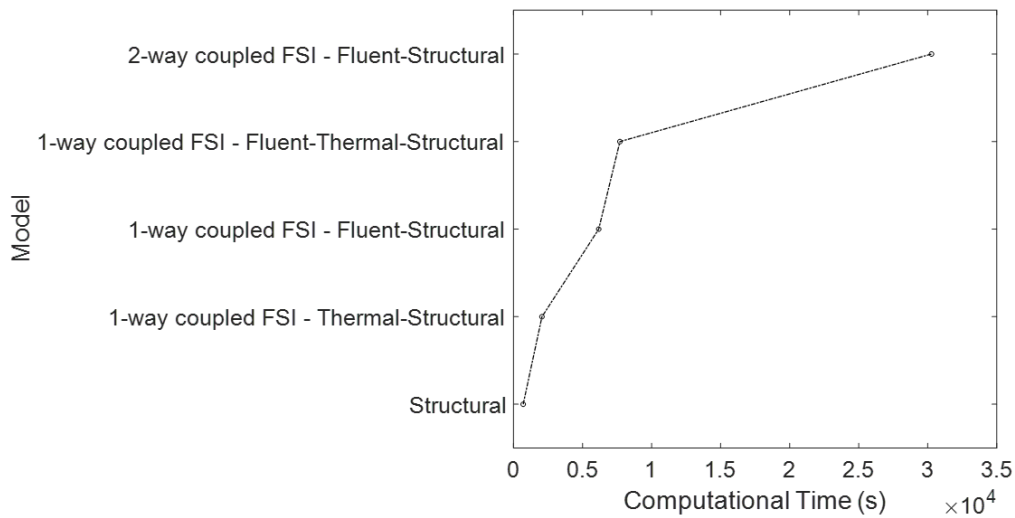


Figure 3.18: Computational time for each computational model.

The differences between the largest and smallest average results are less than 38%. It is seen that the maximum displacement and stress results increase with the inclusion of thermal or CFD fluent analysis components. The thermal analysis system adds thermal loads to the computational model which results in higher maximum results. Higher maximum results are seen with the inclusion of the CFD fluent analysis system due to localised high pressure. The structural computational model has a constant pressure acting on the surface of the fluid-tool interface whilst the computational models which include the fluent analysis systems have varying pressure along the fluid-solid interface. Varying pressure is seen in CFD models which results in areas with higher

or lower pressure compared to the constant pressure in the structural computational model. The higher maximum displacement and stress results seen in computational models which include fluent analysis system is due to the areas of high pressure.

Location of maximum and minimum displacement and stress at the fluid-solid interface was also evaluated from the computational models results. Displacement plots which include location of maximum and minimum displacement for the structural, 1-way coupled FSI fluent-thermal-structural, and 2-way coupled FSI fluent-structural computational models are shown in Figures 3.19, 3.20, and 3.21 respectively. Red markers are used to locate the maximum displacement whilst the blue markers locate the minimum displacement.

Displacement plots are very similar for all computational models and follow the same pattern as seen in Figures 3.19, 3.20, and 3.21. Locations for maximum and minimum displacement for each computational model are all in the same area. The minimum is seen at the inlet whilst the maximum is seen near the outer edges. The structural computational model locates the maximum displacement at the other end of the tool to the other models, but this is of no concern as the tooling is symmetrical and similar displacements are expected at opposite ends of the centre line.

Pressure plots for the structural, 1-way coupled FSI fluent-thermal-structural, and 2-way coupled FSI fluent-structural computational models are shown in Figures 3.22, 3.23, and 3.24 respectively. Red markers are used to locate the maximum stress whilst the blue markers locate the minimum stress.

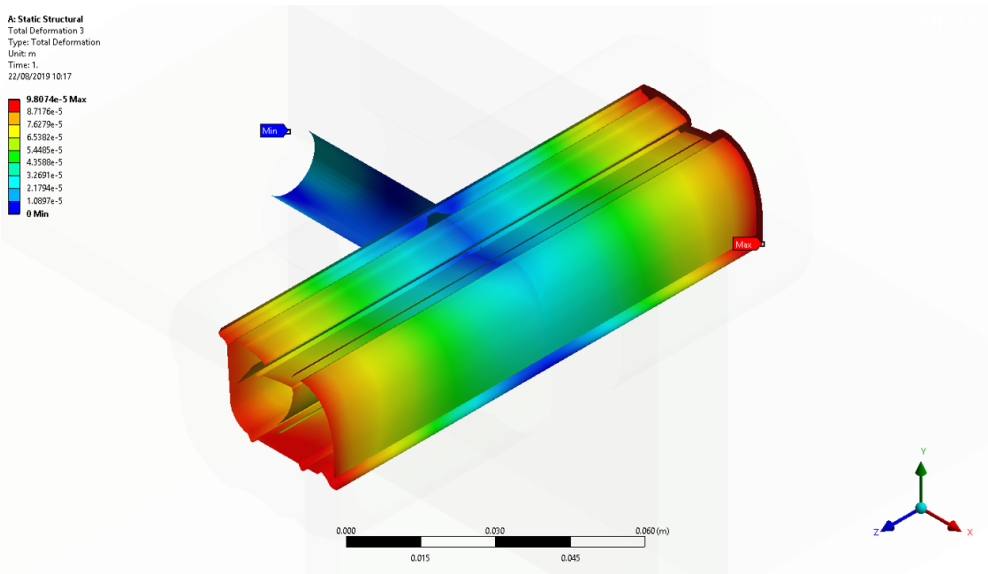


Figure 3.19: Displacement plot including location of maximum and minimum displacement for the structural computational model.

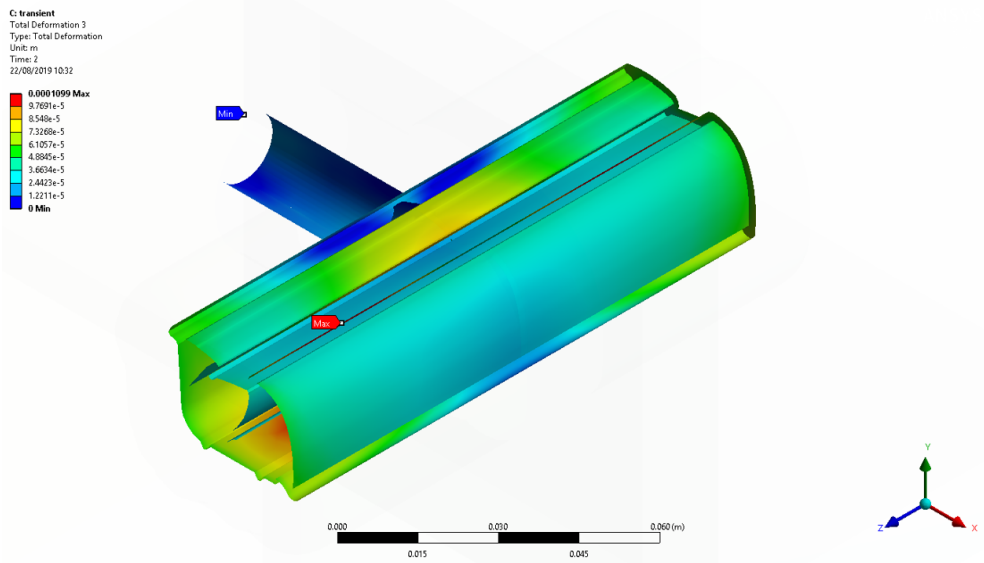


Figure 3.20: Displacement plot including location of maximum and minimum displacement for the 1-way coupled FSI fluent-thermal-structural computational model.

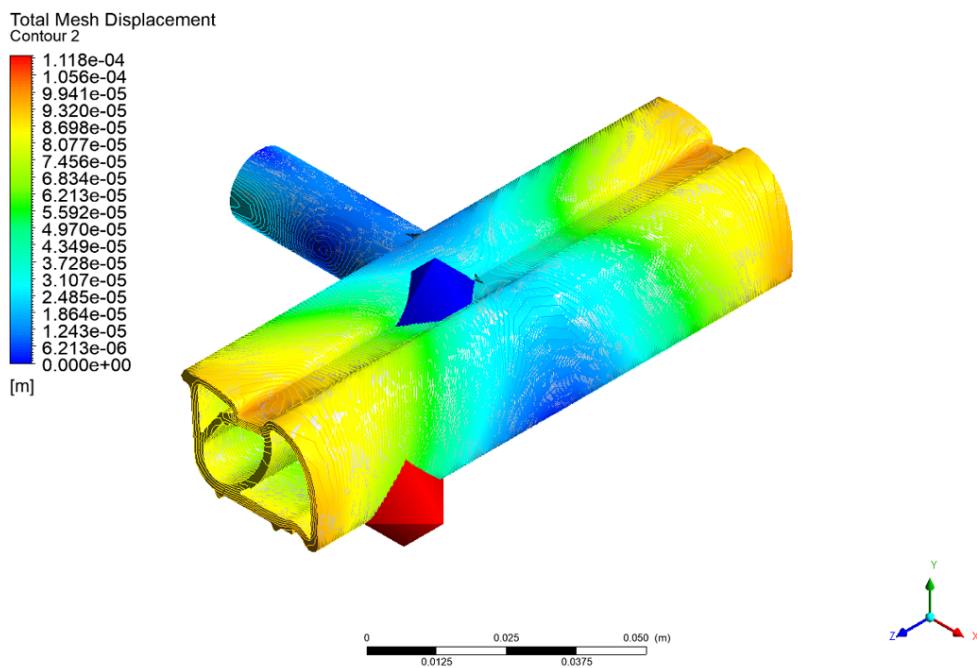


Figure 3.21: Displacement plot including location of maximum and minimum displacement for the 2-way coupled FSI fluent-structural computational model.

Computational models which have CFD fluent components have a less uniform stress plot. The stress plot seen from the structural computational model is much more uniform than the one seen from the 2-way coupled FSI fluent-structural model as seen in Figures 3.22 and 3.24. This is due to the variation in pressure that arises from the fluid flow which is not seen in the static pressure used in the structural model. All

models have the minimum stress located at the center of the tool. The maximum stress is located in the same area for all models except for the 2-way coupled FSI fluent-structural model. A different location for maximum stress in the 2-way coupled FSI fluent-structural model can be attributed to the mesh deformation along this fluid-solid boundary. A slight change in geometry could cause a stress concentration and a new location for the maximum stress.

There is little difference in displacement and stress results obtained by the different

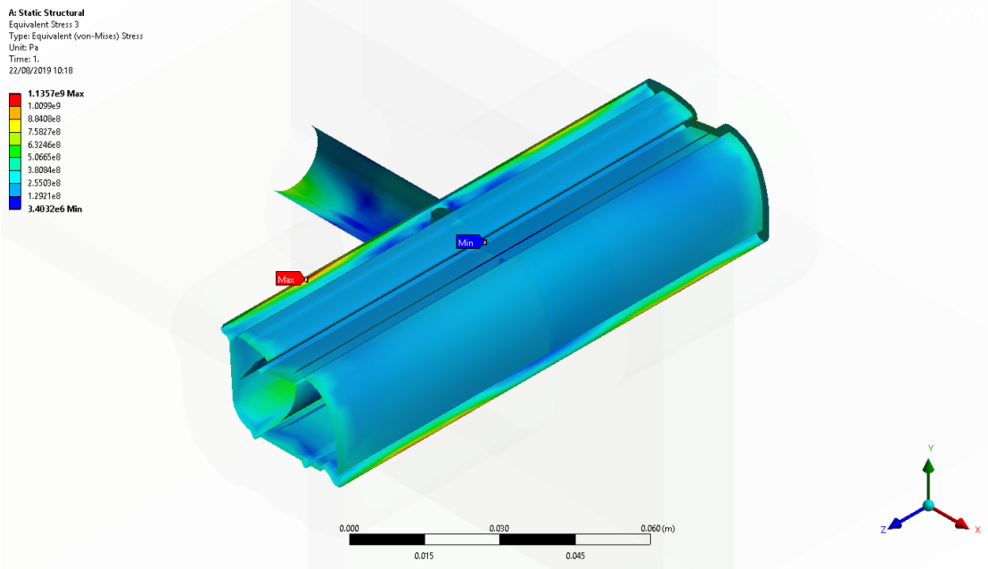


Figure 3.22: Stress plot including location of maximum and minimum stress for the structural computational model.

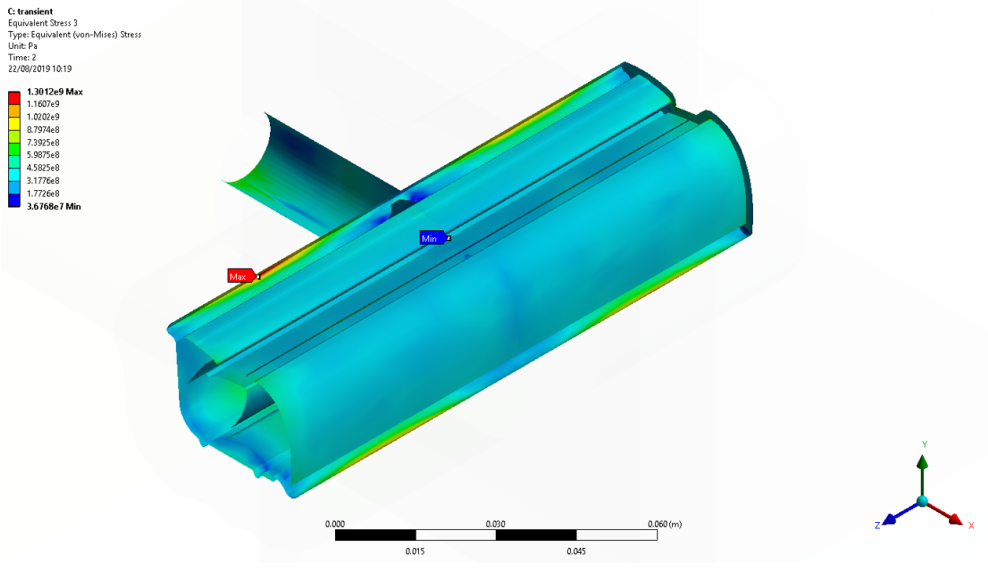


Figure 3.23: Stress plot including location of maximum and minimum stress for the 1-way coupled FSI fluent-thermal-structural computational model.



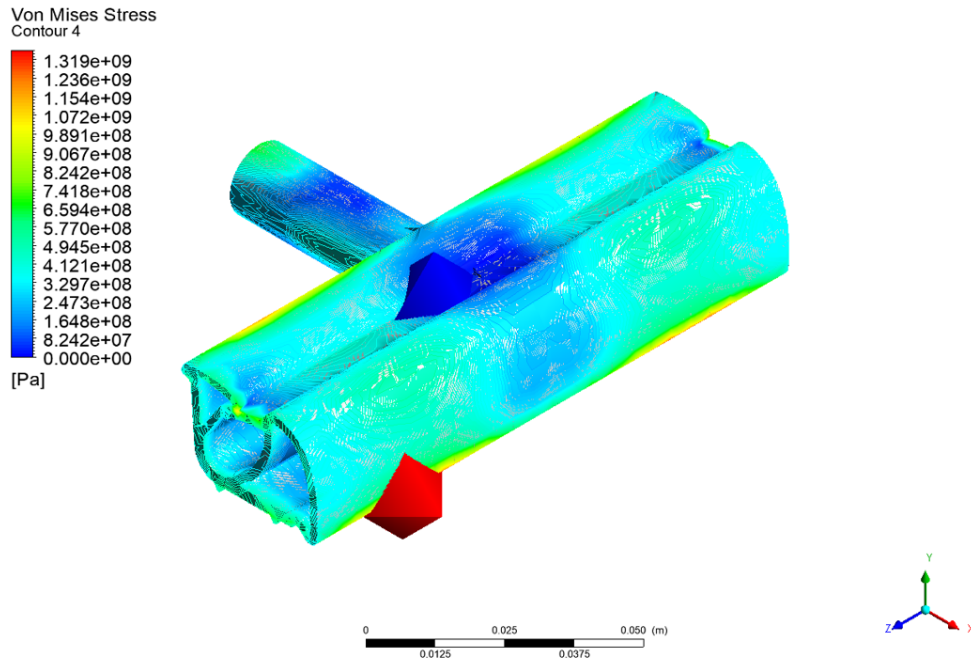


Figure 3.24: Stress plot including location of maximum and minimum stress for the 2-way coupled FSI fluent-structural computational model.

computational models. It is assumed that the 2-way coupled FSI fluent-structural computational model is most accurate due to the inclusion of the mesh deformation at the fluid-solid boundary. 1-way coupled FSI fluent-thermal-structural computational model is accepted to be nearly as accurate as the deformation of the fluid-solid boundary mesh is very small.

Computational time will be used to choose the most appropriate model as the displacement and stress results from each computational model are similar. As seen in Figure 3.18 there is a large difference in computational time between models. The structural computational model takes the least amount of time to compute, taking 697s, while the 2-way coupled fluent-structural computational model takes the longest to compute, taking 30,271s (8hours, 24minutes, and 31seconds). Including a thermal analysis system to the structural computational model adds 1,360s to the computational time, a 295% increase. Adding a fluent analysis system to the thermal-structural 1-way coupled computational model increases the computational time by a further 4,111s, a 300% increase.

All results for the structural and 2-way coupled FSI fluent-structural computational models are within 13.9% of each other. A deviation of 13.9% in displacement and stress will have no adverse effect on the final outcomes of this research. It is impressive that the structural computational model produces results that is within a small range to

the anticipated most accurate model with a computational time that is 43 times smaller. The structural computational model is chosen as the most appropriate to simulate the injection moulding of EPDM.

### 3.4 Conclusion

An evaluation of all applicable computational models available on ANSYS 19.1 software for the simulation of EPDM injection mould has been made. Displacement and stress results along with the computational time for each computational model was used for comparison.

1. Maximum displacement and stress results from all computational models were within 14% of each other. 2-way coupled FSI fluent-structural computational model had the largest maximum displacement and stress results whilst the structural computational model had the smallest maximum displacement and stress results.
2. Average results for displacement and stress were within 38% for all computational models. 1-way coupled FSI thermal-structural model produced the largest average displacement result whilst the 2-way coupled FSI fluent-structural model produced the smallest average displacement result. Largest average stress result was produced by the 1-way coupled FSI fluent-thermal-structural model whilst the smallest average stress result was produced by the 1-way coupled FSI thermal-structural model.
3. Displacement plots for all computational models are very similar with the maximum and minimum values located in the same area. Stress plots differ between computational models which do or do not include the CFD fluent analysis system. The difference in the stress plot is due to the unsteady pressure caused from the fluid flow in the CFD fluent computational models when compared to the static pressure used in the non CFD fluent computational models.
4. Computational time varies significantly from the smallest time, 697s for the structural computational model, to the largest time, 30,271s for the 2-way coupled FSI fluent-structural computational model. Adding a thermal analysis system to the structural computational model approximately increases the computational time by 295%. Adding a further fluid flow (fluent) analysis system to a

1-way coupled thermal-structural computational model approximately increases the computational time by 300%.

5. A structural computational model is chosen as the most appropriate computational model for the analysis of EPDM injection moulding. All displacement and stress results from the structural computational model were within 13.9% of the results from the 2-way coupled FSI computational model which is assumed to be the most accurate model. Computational time for the structural computational model is also significantly smaller than any other model, especially computational models which have fluid flow (fluent) analysis systems.

## **4 Computational Validation of Proposed Novel Rapid Tooling**

### **4.1 Overview**

Following the ANSYS computational method analysis in Section 3, the structural computational model has been chosen as most appropriate computational model to simulate the injection moulding of EPDM. The computational model will run on ANSYS 19.1 using the static structural analysis system for the mechanical validation, and the transient thermal analysis system for the thermal validation.

This section will validate the suitability of the proposed novel rapid prototype tooling to be used in the injection moulding of EPDM. Validation will be based on a commercially used injection moulding 614690 – 1 – AM305 roadster header mould tool by Aston Martin. Due to the complexity of the tool it was necessary to simplify the tool down to a single part for the computational model.

The computational model will determine the best parameters for the rapid prototype tooling, which includes materials and shell thickness. Titanium, aluminium, and stainless steel alloys are the material chosen for the shell, whilst epoxy resin composites are chosen for the reinforcement material. Shell thickness will vary between 2mm and 12mm to determine the optimum thickness. Displacement, stress, and thermal results will be used to determine the suitability of the proposed novel rapid tooling and will be directly compared to a commercially used tooling, the benchmark which is made from P20 grade steel.

### **4.2 Methodology**

#### **4.2.1 Physical Model**

Validation of the novel rapid prototype tooling will be done on a pre-existing injection moulding tool that has been used commercially by Aston Martin, 614690 – 1 – AM305 roadster header mould tool which is shown in Figure 4.1. It is very complex, containing 34 individual components. Typical injection moulding parameters for this tool are summarised in Table 4.1.

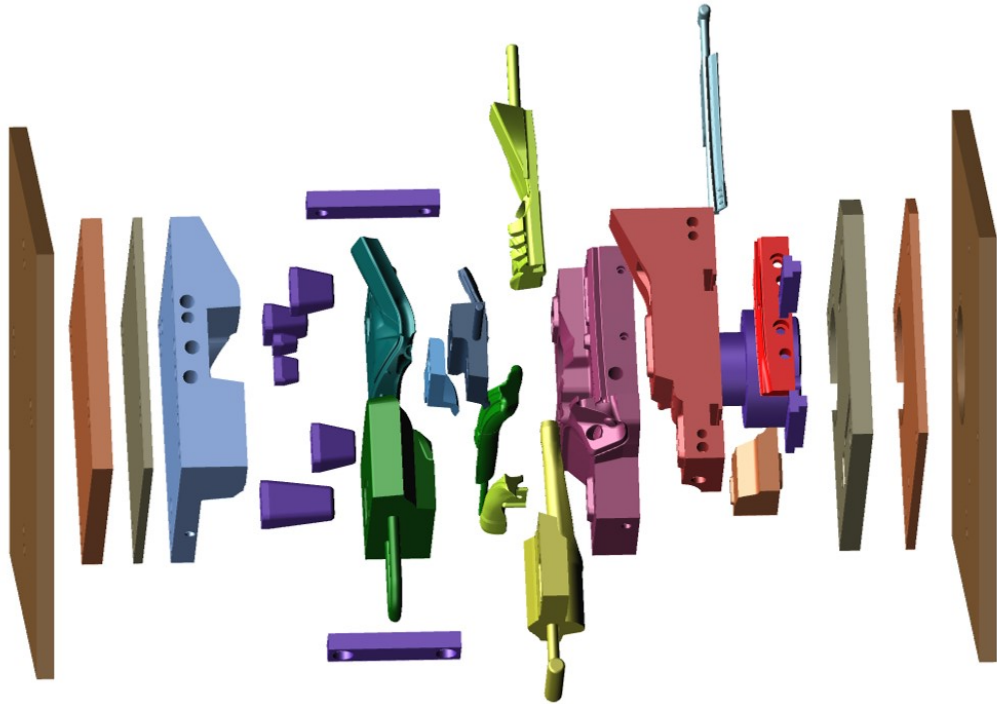


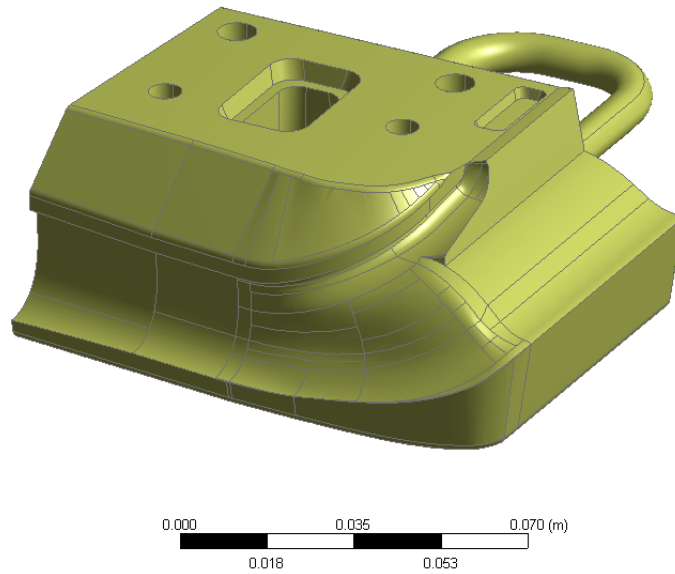
Figure 4.1: Exploded view of the Aston Martin 614690 – 1 – AM305 roadster header mould tool.

Table 4.1: Typical parameters for injection moulding of EPDM using Aston Martin 614690 – 1 – AM305 roadster header mould tool.

<b>Parameter</b>	<b>Value</b>
<i>Hydraulic Pressure</i>	1400bar (140MPa)
<i>Clamping Pressure</i>	2000bar (200MPa)
<i>Temperature of melt</i>	125°C
<i>Temperature of Plate</i>	200°C
<i>Vulcanisation Time</i>	85s
<i>Melt Material</i>	EPDM Dense 60 shore A
<i>Tool Material</i>	P20 Grade Steel

#### 4.2.2 Computational Model

All subsequent computational simulations will be performed on the following system unless otherwise stated, which is the same system used for the ANSYS computational method analysis in Section 3. The computer used an Intel(R) Xenon(R) CPU E5-1630 processor at 3.70GHz with 64.0GB RAM. It ran a windows 64-bit operating system with x64-based processor, with 4 cores and 4 available threads. ANSYS 19.1 software



*Figure 4.2: Isometric view of a CAD model of the single part chosen from the commercial tool for computational validation.*

using static structural and transient thermal analysis systems will be used to simulate the mechanical and thermal properties of the novel rapid tooling. Solidworks is used to modify the original CAD model to create a representative tool that would be manufactured by the novel rapid tooling method.

It would be unrealistic to run simulations on the whole tool as it is very complex and would result in excessive computational time. A single part of the tool was chosen for validation, shown in Figure 4.2. This part is very representative of most parts in the tool in terms of size and complexity.

Material assigned to the shell and reinforcement was chosen from commonly used and available sources. Renishaw was used to obtain data for powdered material commonly used for ALM, which included generic wrought material data and mechanical properties of additively manufactured components [108]. Reinforcement material data was attained from Resin Systems Corporation [109]. Table 4.2 summarises the materials and their properties used in the computational simulations.

For the following simulations, shell thickness, shell material, and reinforcement will be the independent parameters, whilst displacement and stress will be the dependent parameters. Shell thicknesses between 2mm and 12mm will be tested with the three chosen material from Renishaw, all with and without reinforcement. A benchmark part will be simulated which will be a solid part made from P20 grade steel. Results from the novel rapid tooling parts will be compared directly to this benchmark part.

Table 4.2: Material and their properties to be used in computational simulations.

Material Name	P20 Grade Steel	Ti6Al4V ELI-0406	AlSi10Mg	SS 316L-0407	RS-2243 High Temperature Epoxy
	Steel	Titanium	Aluminium	Stainless Steel	Epoxy Resin
<i>Use</i>	Benchmark	Shell	Shell	Shell	Reinforcement
<i>Density (g/cm<sup>3</sup>)</i>	7.85	4.42	2.68	7.99	1.8
<i>Thermal Conductivity (W/m°C)</i>	46.5	8	190	16.2	0.85
<i>Melting Range (°C)</i>	1460	1635	570	1371	170
<i>Coefficient of Thermal Expansion (μ/°C)</i>	11.8	9	21	16.0	32.4
<i>Ultimate Tensile Strength (MPa)</i>	927	1085	366	624	34.3
<i>Yield Strength (MPa)</i>	716	985	220	494	27.5
<i>Youngs Modulus (GPa)</i>	204	126	64	190	9.61
<i>Specific Heat Capacity (J/kg°C)</i>	471	528	994	490	1200
<i>Emissivity</i>	0.4	0.25	0.15	0.15	0.9

#### 4.2.2.1 Mechanical

Mechanical simulations will be performed in ANSYS static structural analysis system. Static structural system is chosen over the transient structural system due to the steady state nature of the problem. A constant pressure of 140MPa will be applied at the fluid interaction face to represent the hydraulic pressure. Fixed geometry will be applied to faces which are in contact with other parts of the tool. Figure 4.3 shows the physical set up of the mechanical simulation which includes a pressure and fixed geometries.

Contact setting between the two components of the part, the shell and reinforcement, in the computational model is set to bonded. Bonded contact means that there is no slip or peeling. Analysis setting will be set to run for 1s with 10-time steps. Mesh sensitivity tests will be run to evaluate which mesh is most appropriate for this simulation, with consideration towards computational time and accuracy of results. Average and maximum results for displacement and stress will be extracted from the simulations to evaluate the mechanical properties of the ALM tools which will be compared against the benchmark tool.

E: Copy of Transient Structural  
Transient  
Time: 1. s  
22/08/2019 11:22  
Pressure: 1.4e+008 Pa  
Fixed Support 3

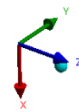
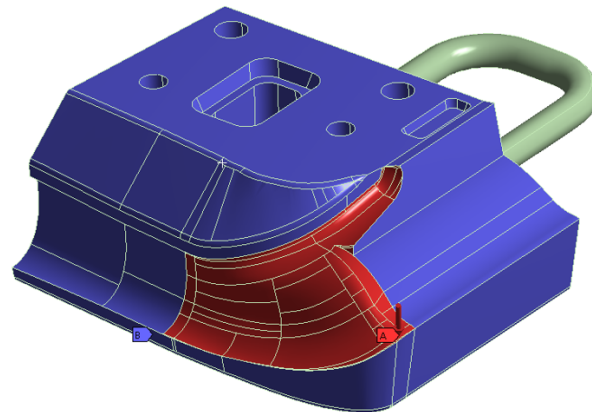


Figure 4.3: Physical setup of the mechanical simulation which includes a pressure and fixed geometries.

#### 4.2.2.2 Thermal

Thermal simulations will be performed in ANSYS transient thermal. Varying temperature will be applied at the fluid-solid interface to represent the contact between the

A: Transient Thermal  
Transient Thermal  
Time: 150. s  
22/08/2019 11:27  
Temperature: 25. °C  
Radiation: 22. °C, 0.4

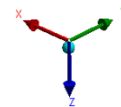
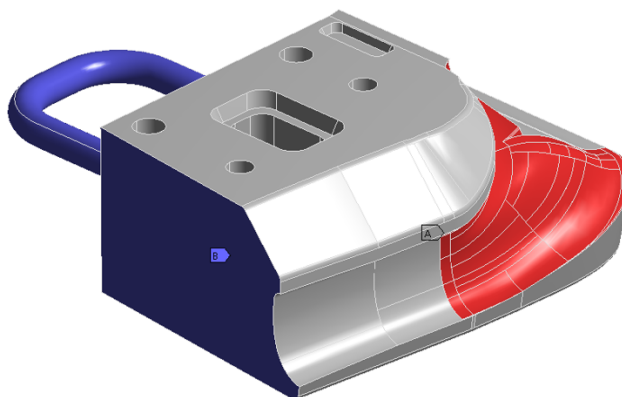
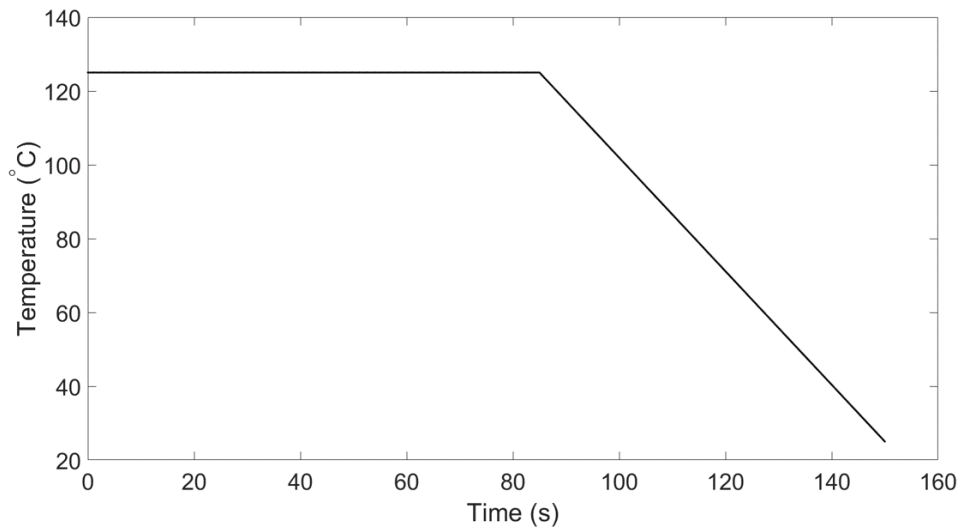


Figure 4.4: Physical setup of the thermal simulation which includes a temperature and thermal radiation.





*Figure 4.5: Temperature profile at the fluid-solid interface.*

melt material and the tool. Radiation is applied on surfaces which are exposed to atmosphere, where the ambient temperature is set to 22°C. Figure 4.4 shows the physical set up of the thermal simulation which includes the temperature and thermal radiation. Temperature profile at the melt tool interface is shown in Figure 4.5. Temperature is set to 125°C for the first 85s, the vulcanisation time, and then is decreased linearly down to 25°C over 65s, which is typically the cooling time for injection moulding of EPDM parts.

Thermal simulations will be carried out on tools which have shown to have adequate mechanical properties in the mechanical simulations. The analysis setting will be set to run for 150s with 300-time steps. Contact between part components will be bonded, the same as for the mechanical simulations. Mesh sensitivity test will also be performed for thermal simulations as there is often a different optimum mesh setting for mechanical and thermal simulations. Average and maximum temperature will be extrapolated from the simulations to evaluate the thermal footprint of the ALM tools which will be compared to the benchmark tool.

## **4.3 Results**

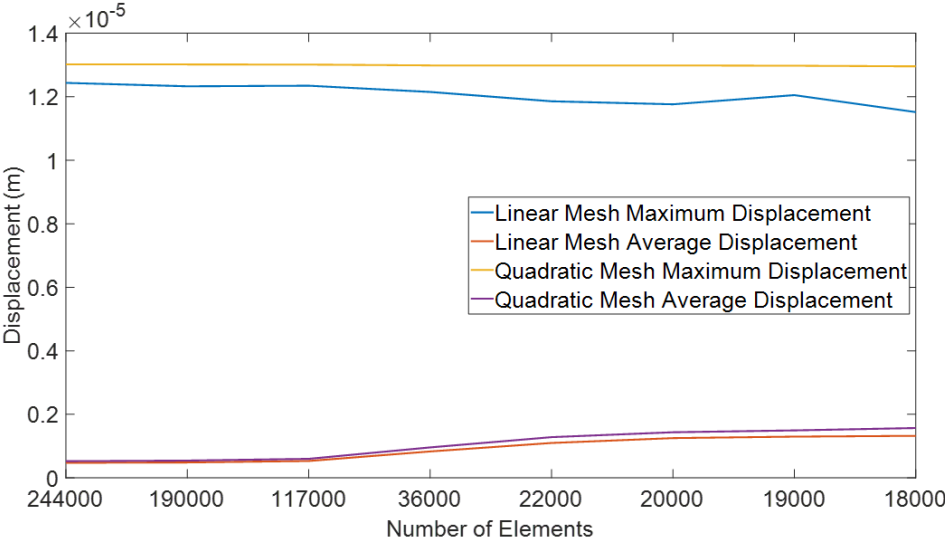
### **4.3.1 Mechanical**

#### **4.3.1.1 Mesh Sensitivity Analysis**

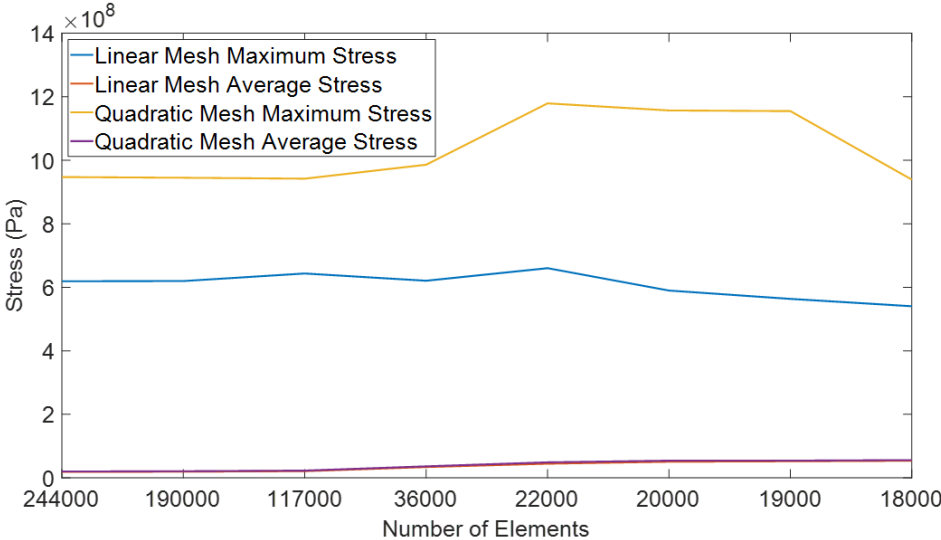
Mesh sensitivity analysis for the mechanical simulations were performed on the benchmark tool, which is a solid part made from P20 grade steel. Figure 4.6 summarises the

mesh sensitivity analysis, comparing maximum and average displacement and stress, and computational time against number of elements for a linear and quadratic type mesh.

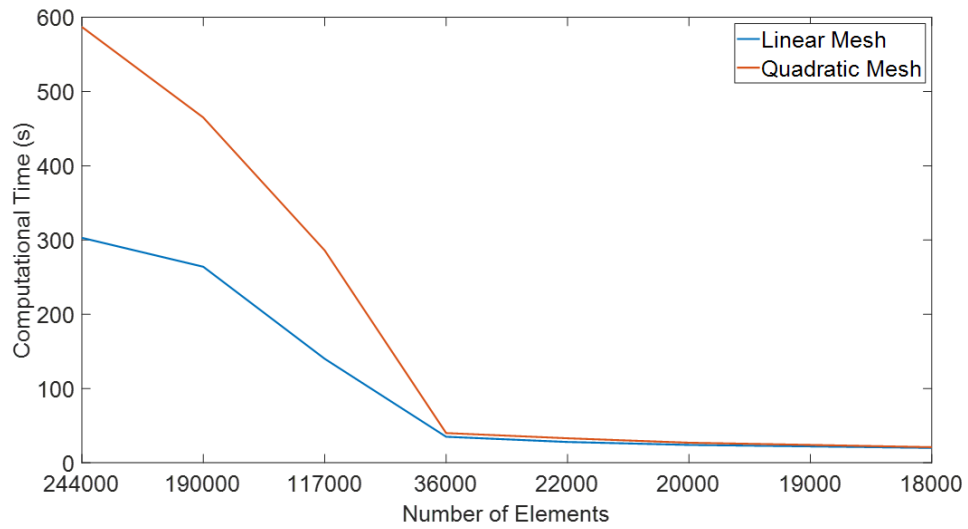
A mesh which has at least 117000 elements produces converged results for both the displacement and stress simulations, irrespective of the mesh type used. Computational time for the linear mesh is always smaller than for the quadratic mesh, with the difference increasing with number of elements. Excluding the maximum stress results, both mesh types give the same results. When looking at the converged maximum stress results, the linear mesh result is around 35% smaller than for the quadratic mesh which is a significant deviation in results.



(a)



(b)



(c)

Figure 4.6: Summary of the mechanical mesh sensitivity analysis, comparing (a) maximum and average displacement, (b) maximum and average stress, and (c) computational time against number of elements for linear and quadratic type mesh.

Figure 4.7 is a histogram of stress results in each node for the linear and quadratic mesh. The linear mesh has 117,196 elements and 30,890 nodes, whilst the quadratic mesh has 117,264 elements and 199,808 nodes. Stress is plotted on the x axis whilst percentage of mesh nodes within each stress range is plotted on the y axis which is log scaled. Both linear and quadratic meshes have a similar node stress distribution pattern up to stress vales of 650MPa. The number of nodes with stress greater than

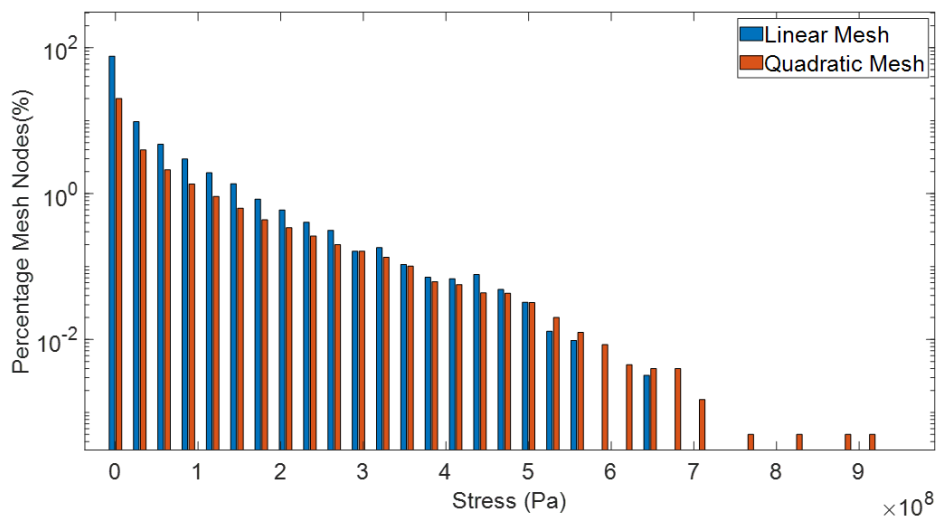
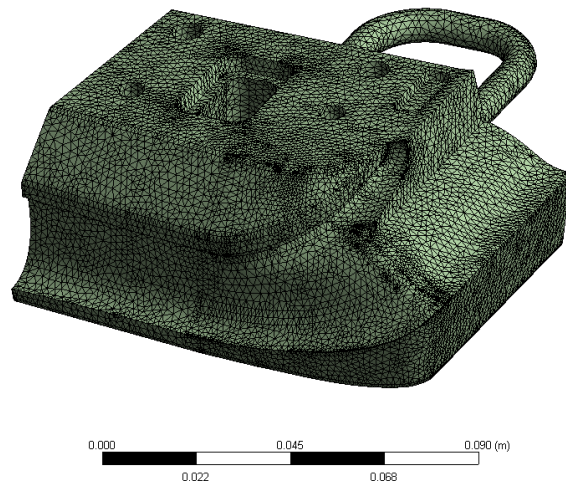


Figure 4.7: Histogram of node stress in the linear and quadratic mesh.



*Figure 4.8: Mesh used for the mechanical simulations of an 8mm thick shell without reinforcement.*

650MPa was zero for the linear mesh and 18 for the quadratic mesh, which is an insignificant number of nodes, accounting for only 0.009% of the total quadratic mesh nodes. As seen in figure 4.7, the quadratic mesh has a small number of rouge nodes which drastically increases the maximum stress value attained, resulting in inaccurate and non-representative results. Linear mesh has no rouge nodes and will be used for the mechanical simulations.

Figure 4.8 shows an example mesh, specifically used for the mechanical simulations of an 8mm thick shell without reinforcement rapid prototype tooling. This is a linear mesh with 30,890 nodes and 117,196 elements. The computational time for this mesh was 124s.

#### **4.3.1.2 Displacement**

Figures 4.9 and 4.10 compare maximum and average displacement respectively of parts with different shell thicknesses, materials, and with or without reinforcement. There is a large difference in maximum displacement between parts with and without reinforcement material. An increase in maximum displacement of 17.8 times was seen with the 2mm thick aluminium shell rapid prototype tooling when no reinforcement was used. As the shell thickness increases there is a reduction in the difference in maximum displacement between parts with and without reinforcement, but the part with reinforcement always has the smaller maximum displacement compared to the same part without reinforcement. This is due to the mechanical strength that the reinforcement adds to the part.

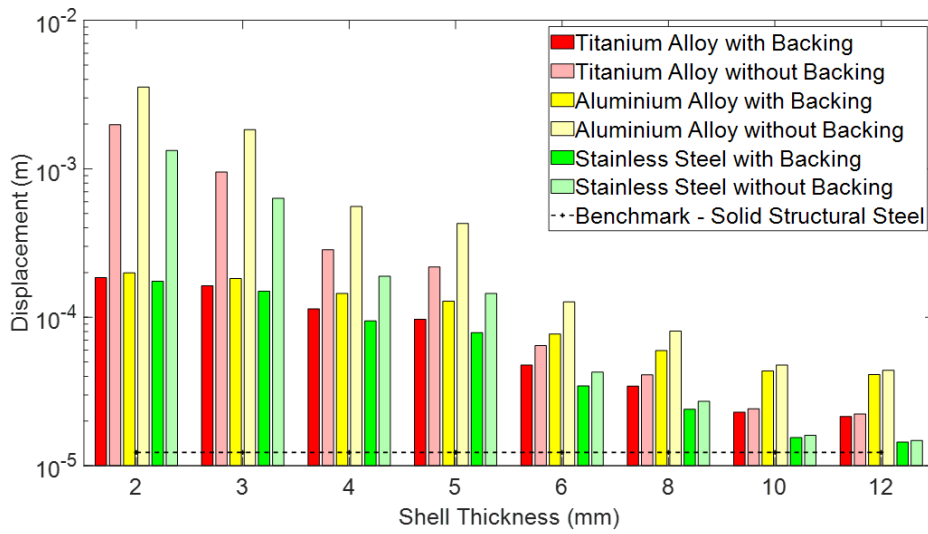


Figure 4.9: Comparison of maximum displacement of additive layer manufactured parts with different shell thicknesses, material, and with or without reinforcement.

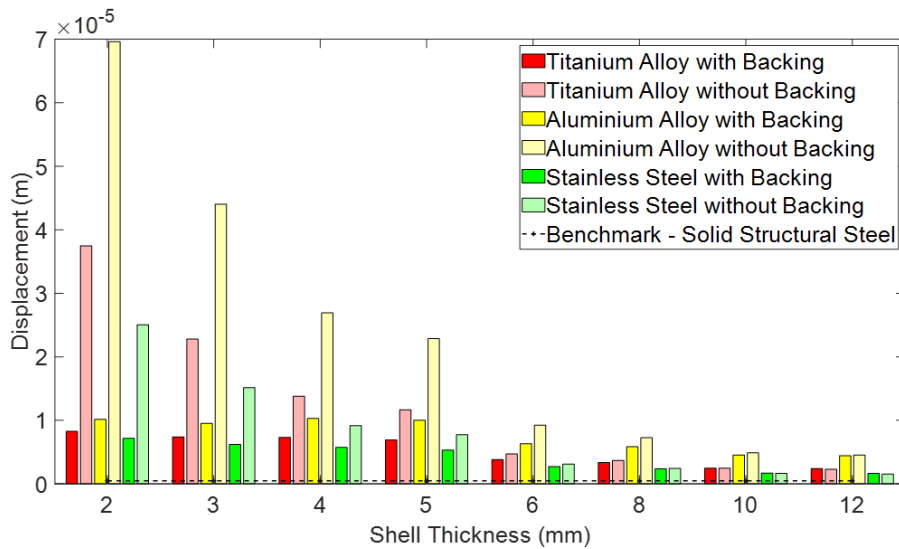


Figure 4.10: Comparison of average displacement of additive layer manufactured parts with different shell thicknesses, material, and with or without reinforcement.

There is also a correlation between shell thickness and displacement. As predicted the displacement reduces with an increase in shell thickness. Maximum and average displacement in the ALM parts is always higher than the benchmark part. In parts that have reinforcement this can be attributed to the lower mechanical properties of the reinforcement material compared to the P20 grade steel or ALM metal components. As for the parts with no reinforcement, this can be attributed to the material volume. In the solid benchmark part, there are sections where there is very little deformation which results in lowering the average displacement. Due to the smaller volume of

material in the ALM parts with no reinforcement, there is less material with very little deformation, resulting in higher average displacement.

### 4.3.1.3 Stress

Figures 4.11 and 4.12 compare maximum and average stress of parts with different thicknesses, materials, and with or without reinforcement. As seen in Figures 4.9, 4.10, 4.11, and 4.12 the stress results follow the same trends as the displacement results. ALM parts which have reinforcement have considerably lower maximum and average stress compared to parts which have no reinforcement, with the difference in maximum and average stress between parts with, and without reinforcement decreases as the shell thickness increases. It is also seen that the maximum and average stress in the parts decrease with an increase in shell thickness.

Comparing the ALM and benchmark parts we see very similar maximum stress in parts with shell thickness of 10mm or more regardless of material. Average stress of ALM parts are very similar to the benchmark part for all shell thicknesses when reinforcement is included. For the ALM parts without reinforcement the average stress is comparable to the benchmark part at shell thicknesses above 8mm.

It is more informative to compare parts stress against its UTS, which is shown in Figure 4.13. The plot shows the percentage of nodes with stress greater than the materials UTS. As expected, the percentage of nodes with stress greater than its materials UTS decreases with an increase in shell thickness, and with the inclusion of reinforcement.

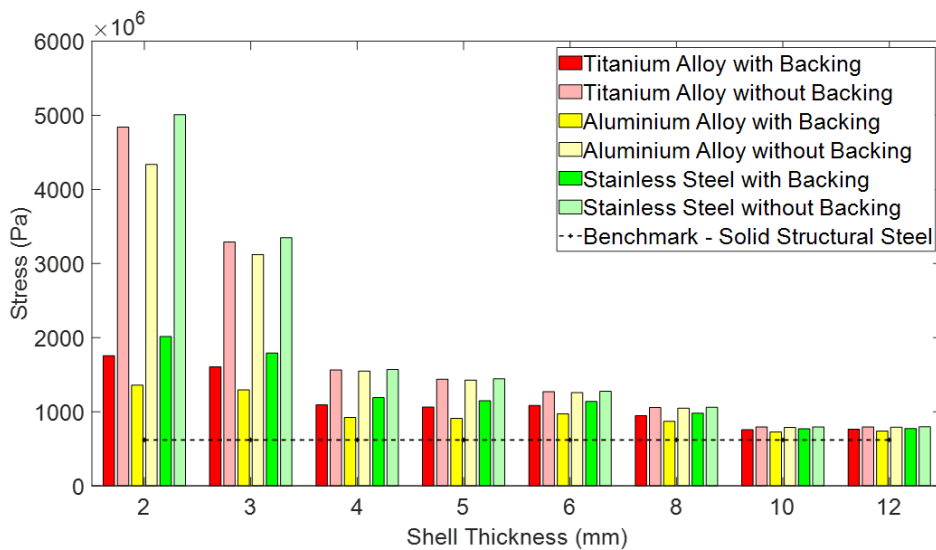


Figure 4.11: Comparison of maximum stress of additive layer manufactured parts with different shell thicknesses, material, and with or without reinforcement.

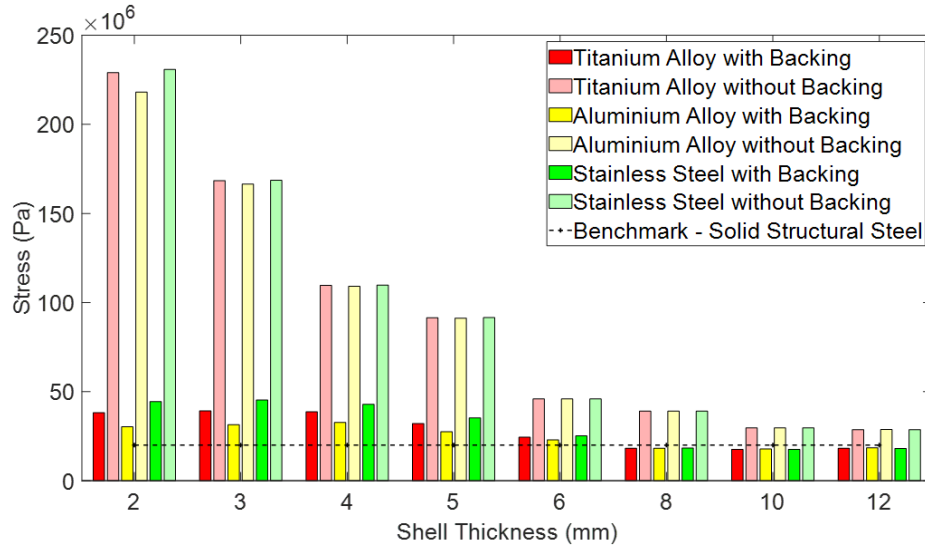


Figure 4.12: Comparison of average stress of additive layer manufactured parts with different shell thicknesses, material, and with or without reinforcement.

Figure 4.14 is an exact plot of Figure 4.13 but with a safety factor of 2. As seen in Figures 4.13 and 4.14, the titanium shell rapid prototype tooling performs best, having significantly less nodes with stress over its material UTS compared to the aluminium and stainless-steel rapid prototype tooling. No exceeding of UTS stress is seen in the rapid prototype tooling with a titanium shell over 5mm thick, with reinforcement and stainless-steel shell over 10mm thick with reinforcement. The rapid prototype tooling with the smallest shell thickness with no stress exceeding its UTS is the 5mm thick

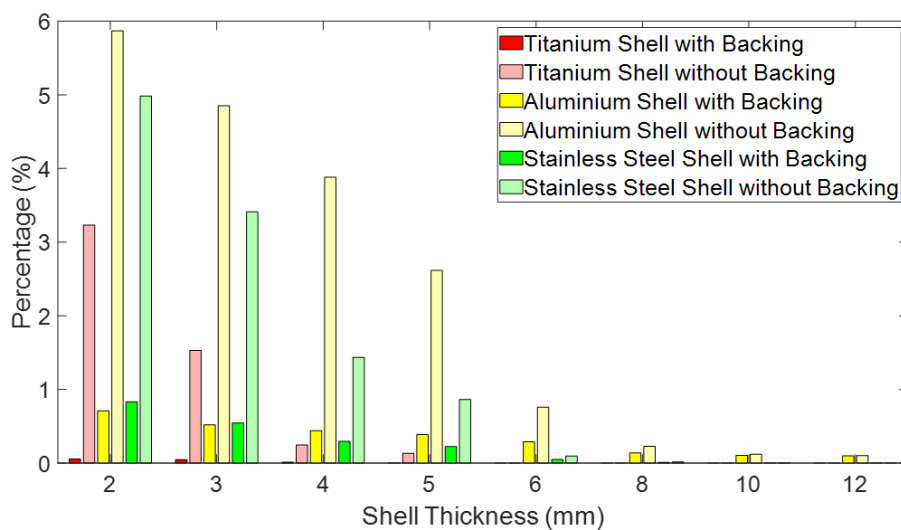


Figure 4.13: Percentage of mesh nodes with stress greater than the ultimate tensile strength of the material.

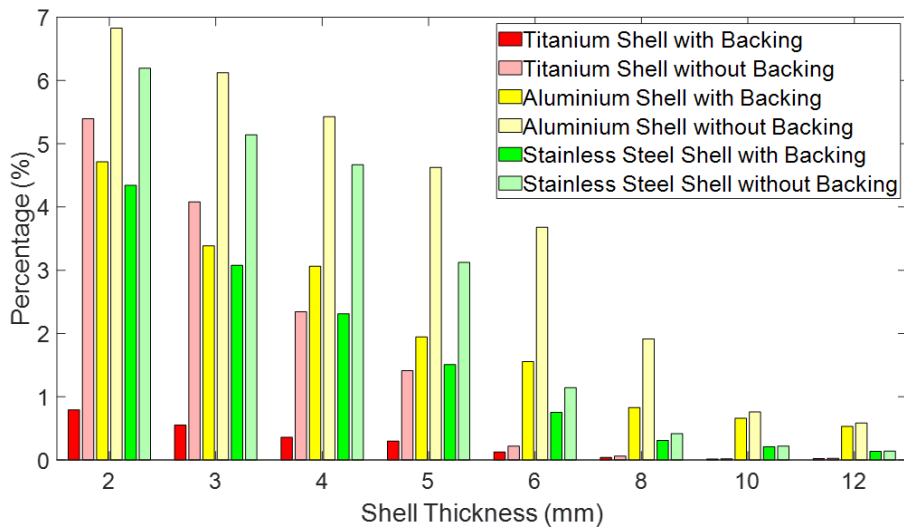


Figure 4.14: Percentage of mesh nodes with stress greater than the ultimate tensile strength of the material with a safety factor of 2.

titanium shell with reinforcement.

#### 4.3.1.4 Mechanical Results Discussion

Consideration of part objective is necessary when evaluating the mechanical results. ALM tools are designed to manufacture a small number of prototype parts, up to a 100, differing to the benchmark which is designed for the manufacture 50,000+ of production parts. The majority of the ALM parts have similar maximum and average stress to the benchmark part as seen in Figures 4.11 and 4.12. However, the ALM parts do not have similar maximum or average displacement to the benchmark part as seen in Figures 4.9 and 4.10. The large displacements would be of concern if the requirements for the ALM parts was the same as the benchmark, but due to the limited number of parts that is required from the ALM tool then it is of little concern.

Due to the findings in Figure 4.13 it is suggested from the mechanical analysis that the optimal rapid prototype tooling is a 5mm thick titanium shell with reinforcement. The 5mm thick titanium shell with reinforcement is the ALM part which has the smallest shell volume that has no stress over its UTS.

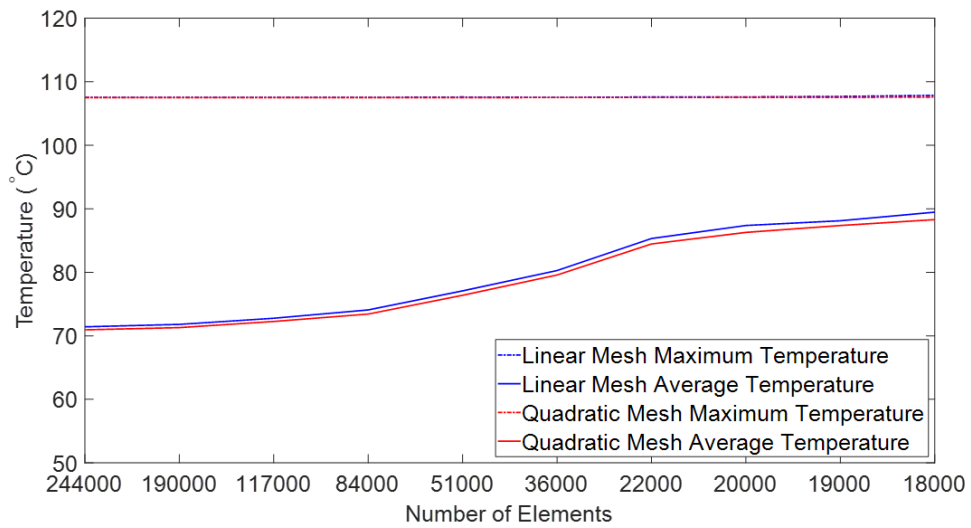
Thermal simulations will be run on a 2mm thick shell with reinforcement and 8mm thick shell without reinforcement ALM parts for all three materials. All mechanical results are similar between the 2mm thick shell with reinforcement and 8mm thick shell without reinforcement ALM parts. Completing thermal simulations on ALM parts which have and have not got reinforcement will give a good idea of how the reinforcement influences the thermal footprint of the ALM part.



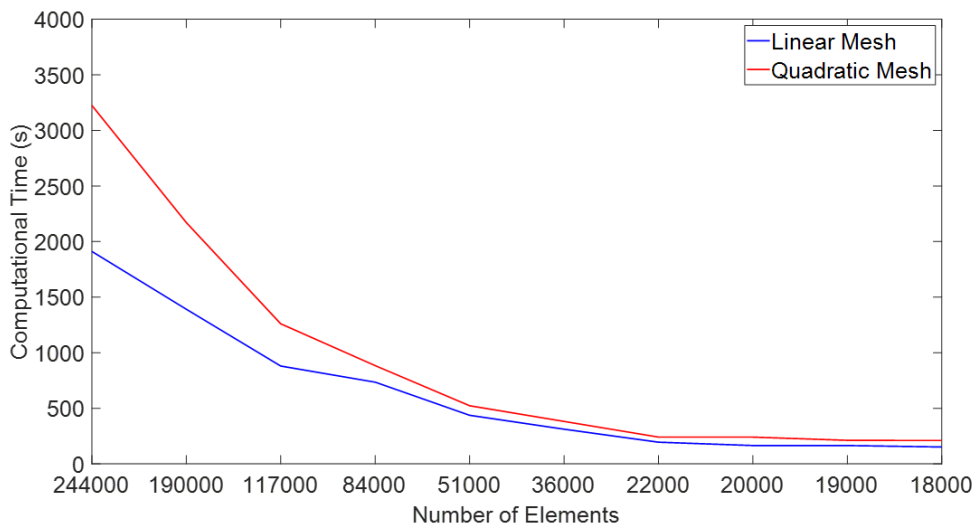
## 4.3.2 Thermal

### 4.3.2.1 Mesh Sensitivity Analysis

Mesh sensitivity analysis for the thermal simulations were performed on the benchmark tool, which is a solid part made from P20 grade steel. Temperature values have been extrapolated at 100s. Figure 4.15 summarises the mesh sensitivity analysis, comparing maximum and average temperature, and computational time against number of



(a)



(b)

Figure 4.15: Summary of the thermal mesh sensitivity analysis, comparing (a) maximum and average temperature, and (b) computational time against number of elements for linear and quadratic type mesh.

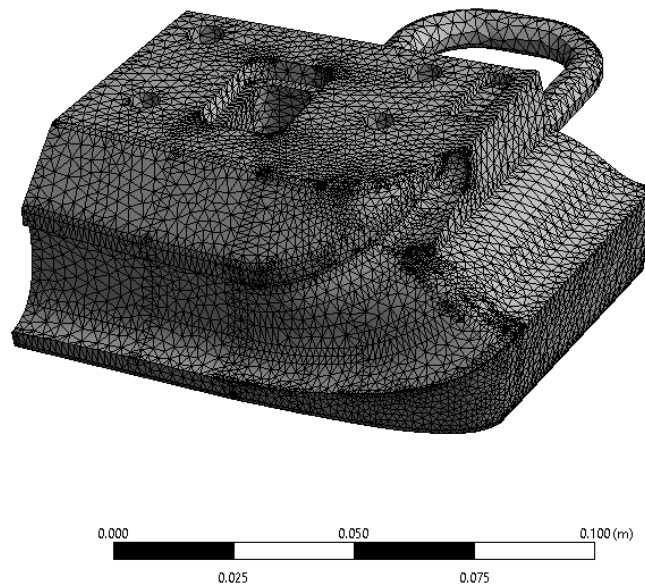


*Figure 4.16: Mesh used for the thermal simulations of an 8mm thick shell without reinforcement rapid prototype tooling.*

elements in mesh. The effect of the mesh on maximum temperature is very little but is significant for the average temperature. It takes a mesh with at least 190,000 elements to converge the average temperature. Temperature results are very similar between the linear and quadratic type mesh, but computational time for the linear mesh is considerably smaller. Thermal simulations will be meshed with a linear mesh that has greater than 190,000 elements.

Figure 4.16 shows an example mesh, specifically used for the thermal simulation of an 8mm thick shell without reinforcement rapid prototype tooling. This is a linear mesh with 49,931 nodes and 190,380 elements. The computational time for this mesh was 1,426s.

#### **4.3.2.2 Temperature**

As previously mentioned in Section 4.3.1.4, 2mm thick shell with reinforcement and 8mm thick shell without reinforcement for all three shell materials are the rapid prototype tooling chosen for thermal analysis. Figure 4.17 is a plot of maximum and average temperature against time for 2mm thick shell with reinforcement rapid prototype tooling along with the benchmark, whilst maximum and average temperature against time for 8mm thick shell without reinforcement rapid prototype tooling along with the benchmark is shown in Figure 4.18.

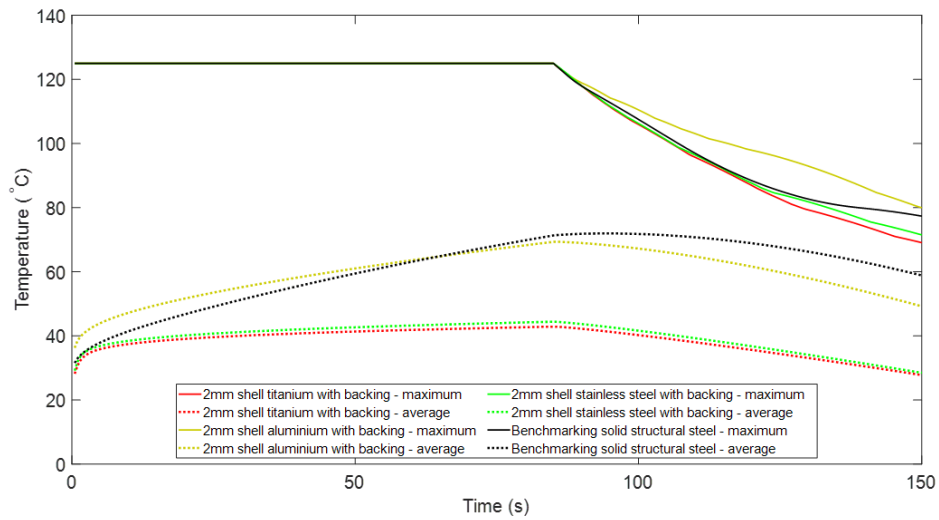


Figure 4.17: Maximum and average temperature profile for 2mm thick shell with reinforcement rapid prototype tooling.

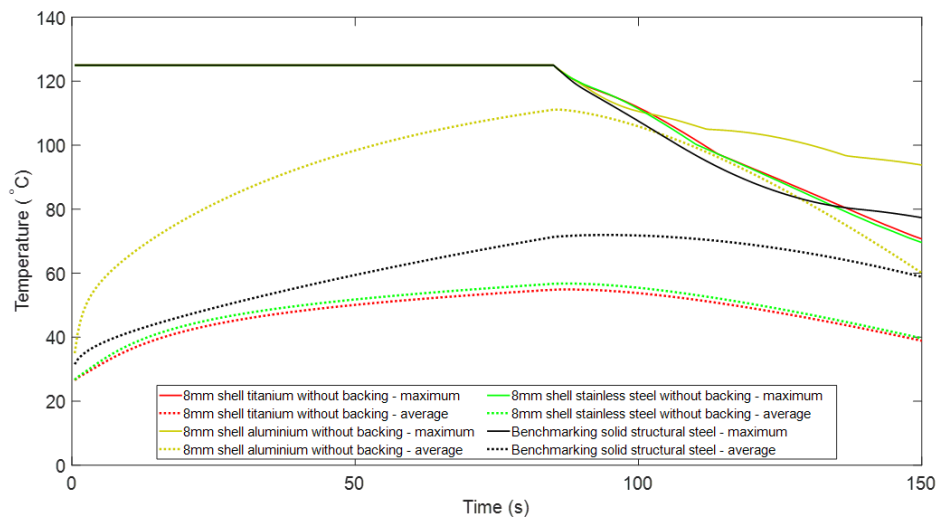


Figure 4.18: Maximum and average temperature profile for 8mm thick shell ALM parts without reinforcement.

Heating and cooling of parts depends on the thermal conductivity and specific heat capacity of the material. Aluminium has the highest thermal conductivity of the tested materials, resulting in aluminium parts having the quickest heating and cooling rates. There is a significant thermal footprint difference between the 2mm thick shell with reinforcement and 8mm thick shell without reinforcement rapid prototype tooling due to the reinforcement material. Heating and cooling of the reinforcement material is slow compared to all shell material due to its lower thermal conductivity and higher specific heat capacity. Average heating rate was  $0.557^{\circ}\text{C/s}$  and  $1.048^{\circ}\text{C/s}$  whilst aver-

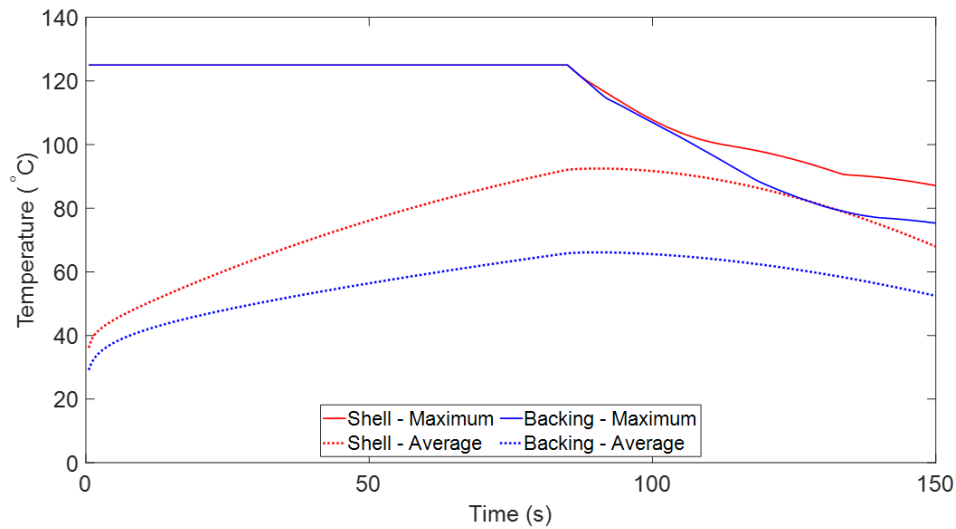
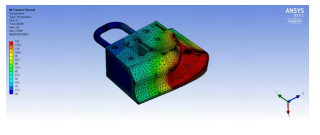
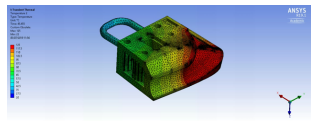
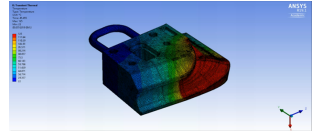
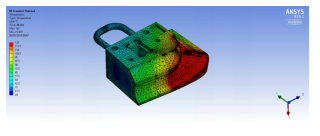
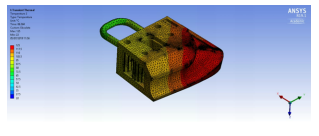
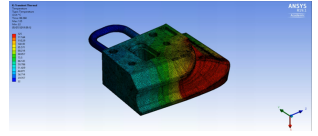
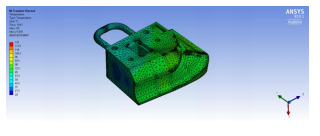
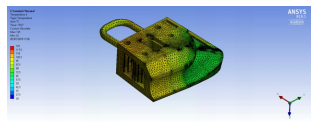
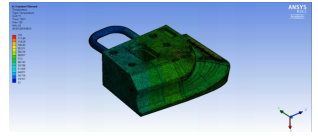
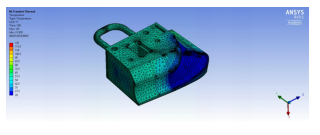
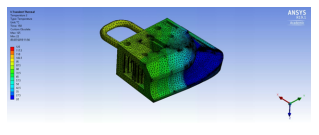
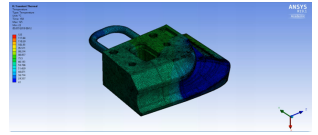


Figure 4.19: Temperature profile of the two components, shell and reinforcement, in the 2mm thick aluminium shell with reinforcement rapid prototype tooling.

age cooling rate was  $0.309^{\circ}\text{C/s}$  and  $0.785^{\circ}\text{C/s}$  for the 2mm thick aluminium shell with reinforcement and the 8mm thick aluminium shell without reinforcement respectively. Temperature profile of the two components, shell and reinforcement, in the 2mm thick aluminium shell with reinforcement rapid prototype tooling is shown in Figure 4.19. During heating, the maximum temperature of the shell and reinforcement is very similar, whilst the average temperature of the shell is around  $10^{\circ}\text{C}$  greater than the backing but increasing at a similar rate. During cooling the maximum and average temperature of the shell decreases much quicker than the backing due to its material properties. Rapid prototype tooling without reinforcement heats and cools quicker than rapid prototype tooling with reinforcement as seen in Figures 4.17 and 4.18. A tool which heats and cools quicker is preferred as it improves the injection moulding process, hence rapid prototype tooling which do not include reinforcement are preferred to rapid prototype tooling with reinforcement.

Table 4.3 shows the temperature in the 2mm thick aluminium with reinforcement rapid prototype tooling, 8mm thick aluminium without reinforcement rapid prototype tooling, and benchmark part at 45s, 86s, 120s, and 150s. Figures in Table 4.3 visually shows what is seen in Figures 4.17, 4.18, and 4.19. It shows that the rate of heating and cooling of the part depends on the thermal properties of its material. Minimising the heating and cooling time of a ALM tool would shorten the cycle times of the injection moulding process, resulting in prolonging the tool life.

Table 4.3: Thermal Footprint of 2mm thick aluminium shell with backing rapid prototype tooling, 8mm thick aluminium shell without backing rapid prototype tooling, and benchmark part at 45s, 86s, 120s, and 150s.

Time (s)	Part		
	2mm Aluminium with Backing	8mm Aluminium without Backing	Benchmark
45			
86			
120			
150			

#### 4.3.2.3 Evolution of Part Design

Rapid prototype tooling which has reinforcement has a worse thermal footprint compared to rapid prototype tooling without reinforcement due to the thermal properties of the reinforcement material which is epoxy resin. Improving the thermal properties of the reinforcement material would improve the thermal footprint of the rapid prototype tooling. Including aluminium powder in the epoxy resin composite would greatly improve the thermal properties of the reinforcement, and also its mechanical properties. Figure 4.20 shows the average temperature of 2mm thick aluminium shell rapid prototype tooling with reinforcement material of epoxy resin composite including 0vol.%, 10vol.%, 30vol.%, and 50vol.% aluminium powder, compared against 8mm thick aluminium shell without reinforcement rapid prototype tooling and benchmark parts. Figure 4.21 shows the same plot as Figure 4.20 but for titanium shell rapid prototype tooling. The results for stainless steel and titanium rapid prototype tooling are very similar. Table 4.4 summarises the heating and cooling rates for Figure 4.20. Increasing the vol.% of aluminium powder in the epoxy resin composite rises the thermal conductivity of the backing material, which is responsible for the rate of heating and cooling of the rapid prototype tooling. As seen in Figures 4.20 and 4.21, and Ta-

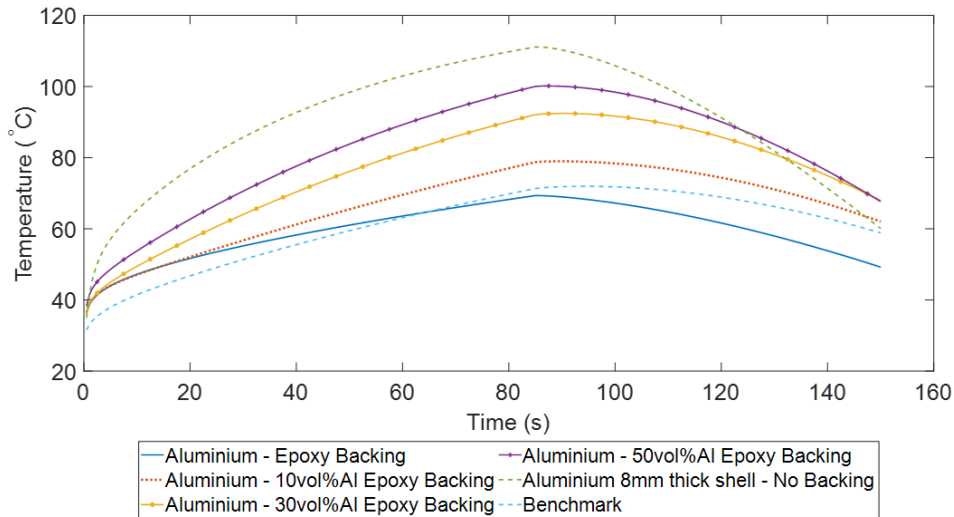


Figure 4.20: Average temperature of rapid prototype tooling 2mm thick aluminium shell with reinforcement material of epoxy composite including 0vol.%, 10vol.%, 30vol.%, and 50vol.% aluminium powder, compared against 8mm thick aluminium shell without reinforcement rapid prototype tooling and benchmark parts.

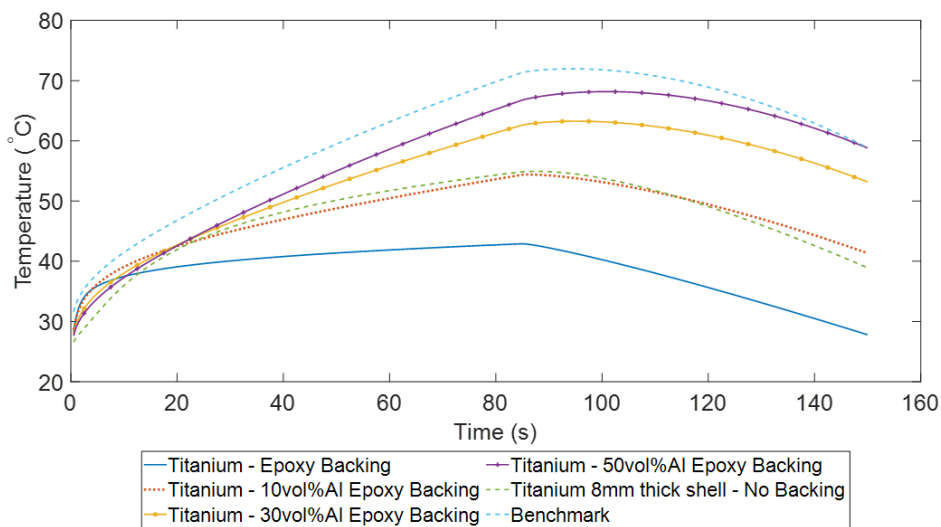


Figure 4.21: Average temperature of rapid prototype tooling 2mm thick titanium shell with reinforcement material of epoxy composite including 0vol.%, 10vol.%, 30vol.%, and 50vol.% aluminium powder, compared against 8mm thick titanium shell without reinforcement rapid prototype tooling and benchmark parts.

ble 4.4, the rate of heating and cooling of rapid prototype tooling increase with vol.% of aluminium powder included in the reinforcement material. Increasing the vol.% of aluminium powder in the reinforcing material of the 2mm thick aluminium shell rapid prototyping tool from 0vol.% to 50vol.% increased the heating and cooling rates by over 60%.

Table 4.4: Average heating and cooling rates of various aluminium rapid prototype and benchmark tooling.

<b>Part</b>	<b>Reinforcement Material</b>	<b>Heating Rate (°C/s)</b>	<b>Cooling Rate (°C/s)</b>
<i>2mm thick aluminium shell with reinforcement</i>	Epoxy Resin	0.557	0.309
<i>2mm thick aluminium shell with reinforcement</i>	Epoxy Resin with 10vol.% Aluminium	0.668	0.327
<i>2mm thick aluminium shell with reinforcement</i>	Epoxy Resin with 30vol.% Aluminium	0.825	0.371
<i>2mm thick aluminium shell with reinforcement</i>	Epoxy Resin with 50vol.% Aluminium	0.918	0.498
<i>8mm thick aluminium shell without reinforcement</i>	N/A	1.048	0.785
<i>Benchmark - Production tool made from P20 grade steel</i>	N/A	0.581	0.192

All aluminium rapid prototype tooling has a better thermal footprint than the benchmark tool, with faster heating and cooling rates. The 2mm thick aluminium shell with 50vol% aluminium reinforcement rapid prototype tooling has a similar thermal footprint to the 8mm thick aluminium shell without reinforcement rapid prototype tooling. The 2mm thick titanium shell with 10vol.% aluminium reinforcement rapid prototype tooling has very similar thermal footprint to the 8mm thick titanium shell without reinforcement rapid prototype tooling. A comparison thermal footprint to the benchmark part is seen with the 2mm thick titanium with 50vol.% aluminium reinforcement. A significant increase in rate of heating and cooling is achieved with the small addition of aluminium powder in the reinforcement material. Rapid prototype tooling with 2mm thick shell with 50vol.% aluminium reinforcement would require only 284g of aluminium powder for the reinforcement material, incurring minimal increase in tool expense.

## 4.4 Conclusion

Computational validation has been performed on ANSYS 19.1 software to validate the suitability of the novel rapid tooling methodology to manufacture tooling for the injection moulding of EPDM exterior automotive seals.

1. The structural computational model was used to validate the mechanical suitability of the proposed rapid prototype tooling for injection moulding of EPDM.
2. Increasing the shell thickness or adding reinforcement both decreased the displacement and stress in the rapid prototype tooling.
3. Out of the three shell materials, titanium was the best as it had the lowest percentage of nodes with stress greater than its UTS.
4. The 5mm thick titanium shell with reinforcement is proposed as the optimum rapid prototype tool from the mechanical testing.
  - (a) The 5mm thick titanium shell with reinforcement rapid prototype tooling had maximum and average displacement of  $96.91\mu\text{m}$  and  $6.902\mu\text{m}$  respectively. The maximum and average stress of  $1063\text{MPa}$  and  $32.14\text{MPa}$  respectively during the simulation of injection moulding of EPDM.
5. Thermal evaluation showed that inclusion of the reinforcement had a negative effect on the thermal properties of the rapid prototype tooling. Improvements to the thermal properties of the reinforcement material by adding aluminium powder drastically improved the thermal footprint of the tooling.
  - (a) Improvements of 65% and 61% in heating and cooling rates respectively was achieved with the 2mm thick aluminium shell with reinforced rapid prototype tooling when the aluminium powder vol.% in the reinforcement material was raised from 0vol.% to 50vol.%.
6. 5mm thick titanium shell with reinforcement is suggested as the optimum rapid prototype tooling following the mechanical and thermal analysis. The reinforcement material would be an epoxy resin composite with 50vol.% aluminium powder.



## 5 Evaluation of Proposed Novel Rapid Tooling

### 5.1 Tool Life

It is essential for the rapid prototype tooling to have a minimum of 100 cycles before failure, as specified by Aston Martin. This would be a sufficient quantity for prototype testing or for small production runs required for limited edition vehicles programs. Due to the complexity of the rapid prototype tooling it is difficult to comprehensively deduce the number of cycles it could last before failure without undertaking experimental testing. Tool material, melt material, operator, and tool maintenance are the most important parameters that influences the life of the tool [110–113]. Hardness of the tool material is a significant factor that determines the life of a tool, with harder materials incurring much smaller wear compared to softer materials. Certain melt materials can have properties which are damaging to the tool. This could include materials which have abrasive components such as glass or ceramic particles, or materials which cause corrosion of the tool material. The operator has a significant role in prolonging the life of the tool. Correct setting of the injection moulding machine is critical to avoid unnecessary damage to the tool. Over-clamping, alignment, ejector stroke, over pressurisation, and lubrication are some of the important settings that the operator controls. Maintenance of the tool can also massively increase the tools life, which would include daily cleaning of tool faces and lubricating appropriate surfaces.

Estimation of possible rapid prototype tooling cycle life can be made by using a stress to cycles to failure (S-N) curves [114, 115]. S-N curves are predominantly used for high cycle fatigue (HCF), commonly over  $10^4$  cycles to failure and not for low cycle fatigue (LCF) failures as is expected for the rapid prototype tooling. LCF occurs when the maximum stress in the cycle is exceeding the yield strength of the material, resulting in plastic deformation.

From displacement and stress results in Section 4 the 5mm thick titanium shell with reinforcement is suggested as the optimum rapid prototype tooling. During the injection of melted material into the cavity, a maximum stress value of 1063MPa is seen in the rapid prototype tooling. Zero stress is assumed in tooling between part ejection and closing of the mould. A stress range for the tool is estimated as 1063MPa which will be used to approximate the number of cycles before failure. ALM Ti-6Al-4V has a yield strength of 985MPa which is lower than the maximum stress, likely resulting in a LCF failure.

S-N curve for solution treated aged Ti-6Al-4V is shown in Figure 5.1 which has been

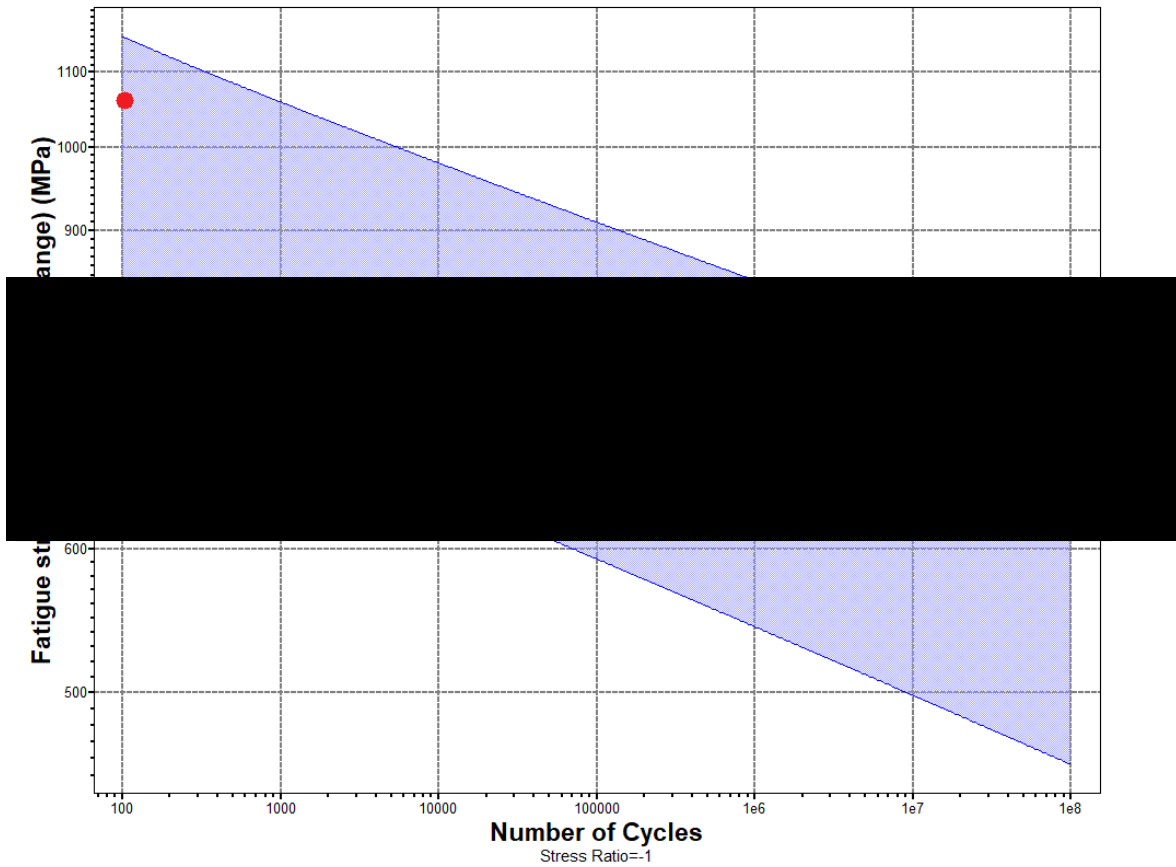


Figure 5.1: S-N curve for solution treated aged Ti-6Al-4V [7].

taken from CES EduPack 2018 [7]. As seen in Figure 5.1 there is a large range between the lower and higher curves. At 100 number of cycles to failure, a stress range of 1063MPa which is anticipated for the rapid prototype tooling is located between the upper and lower ranges. Due to the large range of the S-N curve a exact number of cycles to failure is hard to predict but and estimation can be made that the number of cycles before failure would be in the region of 100 .

## 5.2 Production Cost

Calculating and comparing the production cost of tooling manufactured by ALM or traditional machining is difficult, hence the costs are only an estimation. The following production cost estimations do not include finishing costs and the tolerances of the parts are set to  $\pm 0.1mm$ . Comparison of the production cost between using ALM or traditional manufacturing techniques will be done for a single part of the tool, used in the computational analysis in Section 4, and also for the whole tool.

### 5.2.1 Individual Part

Production cost estimation will be undertaken for the manufacture method by ALM and traditional machining of a single part tool used for the computational analysis in Section 4. Manufacturing costs for the ALM shell component are summarised in Table 5.1 for thicknesses of 2mm and 8mm for aluminium, titanium and stainless steel material. These costs are for the ALM process of selective laser sintering and quotes received from Swansea University. In terms of total cost, titanium is the cheapest material with aluminium being the most expensive. Titanium has the highest material cost but its superior processability means that the build time and manufacturing costs are smaller than for aluminium and stainless steel.

*Table 5.1: Summary of the manufacturing cost for the ALM shell components of 2mm and 8mm thickness.*

	Material	Aluminium		Titanium		Stainless Steel	
	Shell Thickness (mm)	2	8	2	8	2	8
	Build Time (h/m/s)	23/50/59	46/12/38	7/44/24	15/58/56	11/48/18	21/47/12
Cost (£)	Setup	100.56	100.56	100.56	100.56	100.56	100.56
	Capital Equipment	445.99	864.14	144.74	242.77	220.76	407.41
	Material	24.64	49.57	78.85	158.63	72.32	145.5
	Waste	45.71	13.96	45.71	13.96	47.71	13.96
	Consumable	40.89	40.89	54.60	54.60	40.89	40.89
	Energy	286	5.55	0.93	1.56	1.42	2.61
	Gas	4.95	5.85	4.31	4.52	4.47	4.87
	Post processing	160	160	160	160	160	160
	Total Cost	779.89	1,226.55	543.98	722.63	600.41	841.85

Additional cost of the reinforcement will be added to each 2mm thick shell ALM part. Material cost for the reinforcement is estimated to be less than a pound, with the only major costs coming from labour and equipment. An approximation that filling the cavity of the shell will have a total cost of £100. Table 5.2 summarises the total cost for the manufacture of the complete rapid prototype tooling. There are three rapid prototype tooling which have similar manufacture cost, the 2mm thick titanium shell with reinforcement, 8mm thick titanium shell without reinforcement, and 2mm thick stainless steel shell with reinforcement.

*Table 5.2: Total cost for the manufacture of complete rapid prototype tooling.*

Material	Aluminium		Titanium		Stainless steel	
Shell Thickness (mm)	2	8	2	8	2	8
Total Cost (£)	879.89	1,226.55	643.94	722.63	700.41	841.85

5mm thick titanium shell with reinforcement was suggested as the optimum rapid prototype tooling from the mechanical computational model in section 4. Approximation of the production cost of this part is £742.24, and summarised in Table 5.3.

Table 5.3: Production cost for the 5mm thick titanium shell with reinforcement rapid prototype tooling.

Component	Cost (£)
<i>Shell</i>	642.24
<i>Reinforcement</i>	100
<i>Total</i>	742.24

Estimation of manufacturing costs of the commercial "benchmark" part by traditional machining is achieved through various quotations. Material for the benchmark part is P20 grade steel with tolerance of  $\pm 0.1mm$  with no finishing processes applied. Swansea University estimates that it would take 30 hours of machining to produce the benchmark part, estimating a cost of £1,600. They also estimated a total cost of £2,500 if heat treatment and polishing post processing was completed. Build time for the shell of the 5mm thick titanium shell with reinforcement rapid prototype tooling is 10 hours which is a third of the estimated machining time for the benchmark part. Table 5.4 summarises the traditional machining manufacturing cost for the benchmark part from various companies.

Table 5.4: Traditional machining manufacturing cost for the benchmark part form various companies.

Company	Xometry	Protolabs	Swansea University
<i>Total Cost (£)</i>	1,570.00	1,641.26	1,600.00

All three quotations for the manufacture of the benchmark part by traditional machining are within 5% to each other. There is a significant cost difference, around £850 between the manufacture of the 5mm thick titanium with reinforcement rapid prototype tooling and the benchmark part by traditional machining. This equates to a cost saving of 210% when using rapid prototypeing tooling instead of traditional machining for the manufacture of the benchmark part. Only tool parts with significantly complex geometries would be manufactured by ALM with simpler parts being manufactured using traditional machining techniques. Combining the manufacturing of complex parts with ALM, and simple parts by traditional machining will give the best cost saving.

## 5.2.2 Whole Tool

The production costs for Aston Martin 614690 – 1 – AM305 Vantage Roadster header mould tool in 2015 was £35,000. An exploded view of the mould tool is shown in Figure 4.1 in Section 4.2.1. The tool is made from 34 individual components, with each component varying in complexity. Depending on component complexity, it could be cheaper and quicker to manufacture by either ALM or traditional machining techniques. There are several components that would be cheaper and quicker to manufacture through traditional manufacturing techniques. Examples of such components are shown in Figure 5.2. These components have simple geometry that could easily be manufactured by a milling operation which would be significantly cheaper and quicker than using any ALM technique.

Out of the 34 components that make up Aston Martin 614690 – 1 – AM305 Vantage Roadster header mould tool, 16 are estimated to be of sufficient complexity that their manufacture through ALM techniques would offer cost and time saving compared to traditional machining techniques. One of these parts has already been seen in Figure 4.2 in Section 4. Examples of other components within the tool with complex geometry is shown in Figure 5.3. It would be cheaper to manufacture these components by using ALM techniques compared to traditional machining as estimated in Section 5.2.1.

An approximate cost saving of £850 is achievable for each complex component when manufactured using ALM compared to traditional machining. In the case of manufacturing a small number of complex parts, as we have here, ALM is cheaper than traditional machining as it is easier to set up. If the number of parts to be manufactured increased, there will come a point where traditional machining will become economically more viable than ALM. There are 16 complex components in the whole

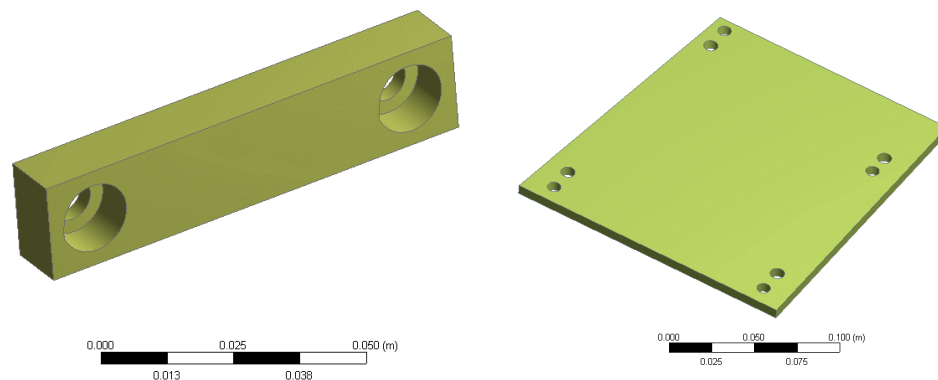


*Figure 5.2: CAD drawings of simple components from the Aston Martin 614690 – 1 – AM305 Vantage Roadster header mould tool.*

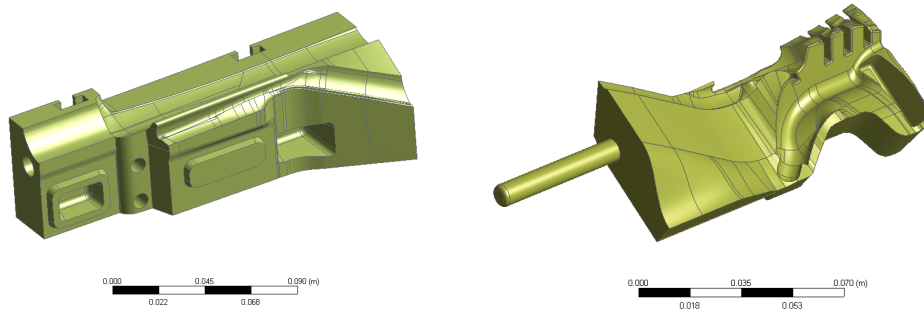


*Figure 5.3: CAD drawings of complex components from the Aston Martin 614690 – 1 – AM305 Vantage Roadster header mould tool.*

tool which would result in a total cost saving of £13,600. Combining traditional machining and ALM to manufacture simple and complex tool components could result in cost saving of 39%.

## 6 Conclusion

### 6.1 Project Outcomes

The overall outcomes of this project are listed below.

1. A novel rapid prototype tooling methodology has been proposed for the manufacture of tooling for injection moulding of EPDM. It has two components, an outer metal shell which is reinforced by an inner epoxy resin composite.
2. Computational models developed in ANSYS 19.1 software which simulate the injection moulding process of EPDM have been tested and evaluated. Accuracy of results along with computational time was used to determine the most appropriate model, which was the static structural model.
3. The structural computational model was used to validate the mechanical suitability of the proposed rapid prototype tooling for injection moulding of EPDM. All rapid prototype tooling with reinforcement and rapid prototype tooling with a shell thickness greater than 6mm without reinforcement is sufficient for injection moulding of EPDM. The 5mm thick titanium shell with reinforcement is proposed as the optimum rapid prototype tool from the mechanical testing.
  - (a) The 5mm thick titanium shell with reinforcement rapid prototype tooling had maximum and average displacement of  $96.91\mu\text{m}$  and  $6.902\mu\text{m}$  respectively and maximum and average stress of  $1063\text{MPa}$  and  $32.14\text{MPa}$  respectively during the simulation of injection moulding of EPDM.
4. Thermal evaluation of the rapid prototype tooling was done using transient thermal analysis system in ANSYS 19.1 software. It showed that inclusion of the reinforcement had a negative effect on the thermal properties of the rapid prototype tooling. Improvements to the thermal properties of the reinforcement material by adding aluminium powder drastically improved the thermal footprint of the tooling.
  - (a) Improvements of 65% and 61% in heating and cooling rates respectively was achieved with the 2mm thick aluminium shell with reinforcement rapid prototype tooling when the aluminum powder vol.% in the epoxy resin composite was raised from 0vol.% to 50vol.%.

5. Following the mechanical and thermal analysis, rapid prototype tooling of a 5mm thick titanium shell with reinforcement is proposed as an optimum tool for injection moulding of EPDM. The reinforcement material would be epoxy resin composite with 50vol.% of aluminium powder.
6. Evaluation of the expected tool life, specifically for the 5mm thick titanium shell with reinforcement rapid prototype tooling was done using an S-N curve. From the maximum stress value obtained in the computational model it was estimated that the rapid prototype tooling would achieve upwards of 100 cycles before failure.
7. Production cost for the tooling was compared between the proposed rapid prototype tooling methodology and traditional machining techniques. A cost saving of £850 per complex tool component is achievable when using the proposed rapid prototype tooling methodology instead of traditional machining techniques. A total saving of £13,600, 39% is possible for the whole tool when using ALM instead of traditional machining for the manufacture of complex tool components.

## **6.2 Future Work**

1. Experimental testing is needed to validate the computational simulation. This could be done with a whole tool or more practically with a single tool component.
2. Behavior of the bond between the shell and reinforcement need to be examined closer. This information will help to better estimate the mechanical and thermal properties of the rapid prototype tooling and its potential life.
3. Evaluation of best material for the reinforcement is needed to optimise the rapid prototype tooling. Potential research could look at the using pressurised fluid as the reinforcement as it is incompressible.
4. This work has looked at a constant thickness shell. Further work is needed to look at how varying the thickness and including ribs in the shell could improve the performance of the rapid prototype tooling. This could potentially increase the mechanical properties of the rapid prototype tooling whilst reducing the volume of the shell, optimising the design and reducing cost and time.



## References

- [1] X. Yan and P. Gu, "A review of rapid prototyping technologies and systems," 1996.
- [2] D. T. Pham and S. S. Dimov, *Rapid manufacturing: the technologies and applications of rapid prototyping and rapid tooling*. Springer-Verlag London, 2001.
- [3] M. Gurr and R. Mülhaupt, "Rapid Prototyping," *Reference Module in Materials Science and Materials Engineering*, 2016.
- [4] A. Rosochowski and A. Matuszak, "Rapid tooling: the state of the art," *Journal of Materials Processing Technology*, vol. 106, no. 1-3, pp. 191–198, 2000.
- [5] C. K. Chua, S. M. Chou, and T. S. Wong, "Rapid prototyping technologies and limitations," *The International Journal of Advanced Manufacturing Technology*, vol. 14, pp. 146–152, 1998.
- [6] J.-P. P. Kruth, M. C. Leu, and T. Nakagawa, "Progress in additive manufacturing and rapid prototyping," *CIRP Annals - Manufacturing Technology*, vol. 47, no. 2, pp. 525–540, 1998.
- [7] Granta Design, "CES EduPack," 2018.
- [8] M. V. Duin, "Chemistry of EPDM Cross-linking," *KGK Kautschuk Gummi Kunststoffe*, vol. 55, no. 4, pp. 150–156, 2002.
- [9] Plastics and Rubber Institute, *Rubber Technology and Manufacture*, second ed. ed., C. M. Blow and C. Hepburn, Eds. Butterworth Scientific, 1982.
- [10] CPMA, "Chemicals & Petrochemicals Manufacturers' Association, India," 2012. [Online]. Available: <http://cpmaindia.com/epdm.php>
- [11] K. Naskar, U. Gohs, U. Wagenknecht, and G. Heinrich, "PP-EPDM thermoplastic vulcanisates (TPVs) by electron induced reactive processing," *Express Polymer Letters*, vol. 3, no. 11, pp. 677–683, 2009.
- [12] N. R. Legge, G. Holden, and H. F. Schroeders, "Thermoplastic Elastomer: A Comprehensive Review," *Hanser, Munich*, 1987.
- [13] A. Y. Coran and R. P. Patel, *Rubber-Thermoplastic Compositions. Part 1. EPDM-Polypropylene Thermoplastic Vulcanisates.*, 53rd ed. Rubber Chemistry and Technology, 1980.
- [14] W. Jiang, C.-h. Liu, Z.-g. Wang, L.-j. An, H.-j. Liang, X.-h. Wang, and H.-x. Zhang, "Brittle-tough transition in PP/EPDM blends: Effects of interparticle distance and temperature," *Polymer*, vol. 39, no. 14, pp. 3285–3288, 1998.
- [15] W. Jiang, S. C. Tjong, and R. K. Li, "Brittle-tough transition in PP/EPDM blends: Effects of interparticle distance and tensile deformation speed," *Polymer*, vol. 41, no. 9, pp. 3479–3482, 2000.
- [16] H. Yang, Q. Zhang, M. Guo, C. Wang, R. Du, and Q. Fu, "Study on the phase structures and toughening mechanism in PP/EPDM/SiO<sub>2</sub> ternary composites," *Polymer*, vol. 47, no. 6, pp. 2106–2115, 2006.
- [17] L. B. de Paiva, A. R. Morales, and F. R. Valenzuela Díaz, "Organoclays: Properties, preparation and applications," *Applied Clay Science*, vol. 42, no. 1-2, pp. 8–24, dec 2008.
- [18] A. Usuki, A. Tugigase, and M. Kato, "Preparation and properties of EPDM–clay hybrids," *Polymer*, vol. 43, no. 8, pp. 2185–2189, apr 2002.
- [19] S. J. Ahmadi, Y. Huang, and W. Li, "Fabrication and physical properties of EPDM–organoclay nanocomposites," *Composites Science and Technology*, vol. 65, no. 7-8, pp. 1069–1076, jun 2005.
- [20] P. Ghosh and A. Chakrabarti, "Conducting carbon black filled EPDM vulcanizates: assessment of dependence of physical and mechanical properties and conducting character on variation of filler loading," *European Polymer Journal*, vol. 36, no. 5, pp. 1043–1054, may 2000.

- [21] K. M. Jäger, D. H. McQueen, I. A. Tchmutin, N. G. Ryvkina, and M. Klüppel, "Electron transport and ac electrical properties of carbon black polymer composites," *Journal of Physics D: Applied Physics*, vol. 34, no. 17, pp. 2699–2707, 2001.
- [22] C.-H. Yao and I. Manas-Zloczower, "Study of Mixing Efficiency in Roll-Mills," *Polymer Engineering and Science*, vol. 36, no. 3, pp. 305–310, 1996.
- [23] L. N. Carli, C. R. Roncato, A. Zanchet, R. S. Mauler, M. Giovanela, R. N. Brandalise, and J. S. Crespo, "Characterization of natural rubber nanocomposites filled with organoclay as a substitute for silica obtained by the conventional two-roll mill method," *Applied Clay Science*, vol. 52, no. 1-2, pp. 56–61, apr 2011.
- [24] K. Singha, "A Review on Coating & Lamination in Textiles: Processes and Applications," *American Journal of Polymer Science*, vol. 2, no. 3, pp. 39–49, 2012.
- [25] M. Biron, "Thermoset Processing," *Thermosets and Composites*, pp. 269–297, 2014.
- [26] J. E. Mark, B. Erman, and C. M. Roland, *The Science and Technology of Rubber*, 4th ed. Elsevier Inc, 2013.
- [27] R. Orza, "Investigation of peroxide crosslinking of EPDM rubber by solidstate NMR," *Eindhoven University of Technology*, pp. 1–18, 2008.
- [28] D. T. Pham and R. S. Gault, "A comparison of rapid prototyping technologies," *International Journal of Machine Tools and Manufacture*, vol. 38, no. 10-11, pp. 1257–1287, 1998.
- [29] K. Thrimurthulu, P. M. Pandey, and N. Venkata Reddy, "Optimum part deposition orientation in fused deposition modeling," *International Journal of Machine Tools and Manufacture*, vol. 44, no. 6, pp. 585–594, 2004.
- [30] G. Wu, N. A. Langrana, S. Rangarajan, R. Mccuiston, R. Sadanji, S. Danforth, and A. Safari, "Fabrication of Metal Components using FDM: Fused Deposition of Metals," *Proceedings of Solid Freeform Fabrication Symposium*, 1999.
- [31] S. Masood and W. Song, "Development of new metal/polymer materials for rapid tooling using Fused deposition modelling," *Materials & Design*, vol. 25, no. 7, pp. 587–594, oct 2004.
- [32] D. Ahn, J.-H. Kweon, J. Choi, and S. Lee, "Quantification of surface roughness of parts processed by laminated object manufacturing," *Journal of Materials Processing Technology*, vol. 212, no. 2, pp. 339–346, 2012.
- [33] M. Feygin and S. S. Pak, "Laminated Object Manufactureing Apparatus and Method," *U.S. patent 5976719*, 1999.
- [34] K. V. Wong and A. Hernandez, "A review of additive manufacturing," *International Scholarly Research Network*, 2012.
- [35] P. K. Gokuldoss, S. Kolla, and J. Eckert, "Additive manufacturing processes: Selective laser melting, electron beam melting and binder jetting-selection guidelines," *Materials*, vol. 10, no. 6, 2017.
- [36] X. Xu, S. Meteyer, N. Perry, and Y. F. Zhao, "Energy Consumption Model of Binder jetting Additive Manufacturing Process," *International Journal of Production Research*, vol. 53, no. 23, pp. 7005–7015, 2014.
- [37] R. Ippolito, L. Iuliano, and A. Gatto, "Benchmarking of Rapid Prototyping Techniques in Terms of Dimensional Accuracy and Surface Finish," *CIRP Annals*, vol. 44, no. 1, pp. 157–160, 1995.
- [38] C. K. Chua, K. H. Hong, and S. L. Ho, "Rapid tooling technology. Part 1. A comparative study," *International Journal of Advanced Manufacturing Technology*, vol. 15, no. 8, pp. 604–608, 1999.
- [39] J. W. Halloran, M. Griffith, and T.-M. Chu, "Stereolithography Resin for Rapid Prototyping of Ceramics and Metals," no. 19, pp. 50–55, 1999.
- [40] J. H. Sandoval and R. B. Wicker, "Functionalizing stereolithography resins: Effects of dispersed multi-walled carbon nanotubes on physical properties," *Rapid Prototyping Journal*, 2006.

- [41] I. H. Tavman, "Thermal and Mechanical Properties of Aluminium Powder-Filled High Density Polyethylene Composites," *Journal of Applied Polymer Science*, vol. 62, pp. 2161–2167, 1996.
- [42] I. P. Ilyas, "Production of Plastic Injection Moulding Tools using Selective Laser Sintering and High Speed Machining," 2007.
- [43] F. Abe, K. Osakada, M. Shiomi, K. Uematsu, and M. Matsumoto, "The manufacturing of hard tools from metallic powders by selective laser melting," *Journal of Materials Processing Technology*, vol. 111, no. 1-3, pp. 210–213, 2001.
- [44] W. Meiners, C. Over, K. Wissenbach, and R. Poprawe, "Direct Generation of Metal Parts and Tools by Selective Laser Powder Remelting (SLPR)," *Proceedings of the SFF Symposium*, 1999.
- [45] J. P. Kruth, L. Froyen, J. Van Vaerenbergh, P. Mercelis, M. Rombouts, and B. Lauwers, "Selective laser melting of iron-based powder," *Journal of Materials Processing Technology*, vol. 149, no. 1-3, pp. 616–622, 2004.
- [46] C. M. Cheah, C. K. Chua, C. W. Lee, C. Feng, and K. Totong, "Rapid prototyping and tooling techniques: A review of applications for rapid investment casting," *International Journal of Advanced Manufacturing Technology*, vol. 25, no. 3-4, pp. 308–320, 2005.
- [47] Y. Tang, J. Fuh, H. Loh, Y. Wong, and L. Lu, "Direct laser sintering of a silica sand," *Materials & Design*, vol. 24, no. 8, pp. 623–629, dec 2003.
- [48] E. Sachs, M. Cima, and J. Cornie, "Three dimensional printing: ceramic shells and cores for casting and other applications," *International Conference on Rapid Prototyping*, pp. 39–53, 1991.
- [49] F. Klorke and C. Freyer, "Fast Manufacture, Modification and Repair of Molds Using Controlled Metal Build Up (CMB)," *Rapid Prototyping Journal*, pp. 6–8, 2001.
- [50] A. H. Alami, "Using Laminated Metal Tooling (LMT) in die manufacturing for clay moulding," *Proceeding of the 5th International Symposium on Mechatronics and its Applications, ISMA 2008*, no. June 2008, 2008.
- [51] D. I. Wimpenny, B. Bryden, and I. R. Pashby, "Rapid laminated tooling," *Assembly Automation*, vol. 23, no. 4, pp. 372–381, 2003.
- [52] G. N. Levy, R. Schindel, and J. P. Kruth, "Rapid manufacturing and rapid tooling with layer manufacturing (LM) technologies, state of the art and future perspectives," *CIRP Annals - Manufacturing Technology*, vol. 52, no. 2, pp. 589–609, 2003.
- [53] T. Himmer, T. Nakagawa, and M. Anzai, "Lamination of metal sheets," *Computers in Industry*, vol. 39, no. 1, pp. 27–33, 1999.
- [54] T. Sinmazçelik, E. Avcu, M. Ö. Bora, and O. Çoban, "A review: Fibre metal laminates, background, bonding types and applied test methods," *Materials and Design*, vol. 32, no. 7, pp. 3671–3685, 2011.
- [55] J.-Y. Jeng and M.-C. Lin, "Mold fabrication and modification using hybrid processes of selective laser cladding and milling," *Journal of Materials Processing Technology*, vol. 110, no. 1, pp. 98–103, mar 2001.
- [56] L. Costa, R. Colaco, T. Reti, A. M. Deus, and R. Vilar, "Tempering Effects in Steel Parts Produced by Additive Fabrication Using Laser Powder Deposition," *Proceeding of VR*, p. 249, 2003.
- [57] J. O. Milewski, G. K. Lewis, D. J. Thoma, G. I. Keel, R. B. Nemeç, and R. A. Reinert, "Directed light fabrication of a solid metal hemisphere using 5-axis powder deposition," *Journal of Materials Processing Technology*, vol. 75, no. 1-3, pp. 165–172, 1998.
- [58] E. C. Santos, M. Shiomi, K. Osakada, and T. Laoui, "Rapid manufacturing of metal components by laser forming," *International Journal of Machine Tools and Manufacture*, vol. 46, no. 12-13, pp. 1459–1468, 2006.
- [59] L. Ceyzeriat, "Room Temperature Curable Siloxane Compositions "United States Patent Office" ' 3,133,891," pp. 3–5, 1951.

- [60] S. Kemaloglu, G. Ozkoc, and A. Aytac, "Properties of thermally conductive micro and nano size boron nitride reinforced silicon rubber composites," *Thermochimica Acta*, vol. 499, no. 1-2, pp. 40–47, 2010.
- [61] W. Zhou, S. Qi, C. Tu, H. Zhao, C. Wang, and J. Kou, "Effect of the particle size of Al<sub>2</sub>O<sub>3</sub> on the properties of filled heat-conductive silicone rubber," *Journal of Applied Polymer Science*, vol. 104, no. 2, pp. 1312–1318, 2007.
- [62] M. A. Raza, A. Westwood, A. Brown, N. Hondow, and C. Stirling, "Characterisation of graphite nanoplatelets and the physical properties of graphite nanoplatelet/silicone composites for thermal interface applications," *Carbon*, vol. 49, no. 13, pp. 4269–4279, 2011.
- [63] R. P. Atkins, C.-S. Wang, and T. J. Dearlove, "High Temperature Epoxy Tooling Composition of Bifunctional Epoxy, Trifunctional Epoxy, Anhydride, Imidazole and Interstitially Matched Filler," no. 19, pp. 3–6, 1990.
- [64] L. Yue, G. Pircheraghi, S. A. Monemian, and I. Manas-Zloczower, "Epoxy composites with carbon nanotubes and graphene nanoplatelets - Dispersion and synergy effects," *Carbon*, 2014.
- [65] Q. F. Cheng, J. P. Wang, J. J. Wen, C. H. Liu, K. L. Jiang, Q. Q. Li, and S. S. Fan, "Carbon nanotube/epoxy composites fabricated by resin transfer molding," *Carbon*, vol. 48, no. 1, pp. 260–266, 2010.
- [66] J. Zhu, H. Peng, F. Rodriguez-Macias, J. L. Margrave, V. N. Khabashesku, A. M. Imam, K. Lozano, and E. V. Barrera, "Reinforcing epoxy polymer composites through covalent integration of functionalized nanotubes," *Advanced Functional Materials*, vol. 14, no. 7, pp. 643–648, 2004.
- [67] H. S. Ong, C. K. Chua, and C. M. Cheah, "Rapid moulding using epoxy tooling resin," *International Journal of Advanced Manufacturing Technology*, vol. 20, no. 5, pp. 368–374, 2002.
- [68] H. Zhang, G. Wang, Y. Luo, and T. Nakaga, "Rapid hard tooling by plasma spraying for injection molding and sheet metal forming," *Thin Solid Films*, vol. 390, no. 1-2, pp. 7–12, 2001.
- [69] C. K. Chua, K. H. Hong, and S. L. Ho, "Rapid Tooling Technology. Part 2. A Case Study Using Arc Spray Metal Tooling," pp. 609–614, 1999.
- [70] D. Milovich and R. H. Nelson, "Composite Backing Structure for Spray Metal Tooling," *U.S. patent 5976719*, 1991.
- [71] Y. Luo, M. C. Leu, and Z. Ji, "Assessment of Enviromental Performance of Rapid Prototyping and Rapid Tooling Processes," *In Proceedings of Solid Freeform Fabrication Symposium*, pp. 783–792, 1999.
- [72] B. Yang and M. C. Leu, "Integration of Rapid Prototyping and Electroforming for Tooling Application," *CIRP Annals - Manufacturing Technology*, vol. 48, no. 1, pp. 119–122, 1999.
- [73] J. McGeough, M. Leu, K. Rajurkar, A. De Silva, and Q. Liu, "Electroforming Process and Application to Micro/Macro Manufacturing," *CIRP Annals*, vol. 50, no. 2, pp. 499–514, 2001.
- [74] M. D. Monzon, M. D. Marrero, A. N. Benitez, P. M. Hernandez, and J. F. Cardenes, "A technical note on the characterization of electroformed nickel shells for their application to injection molds," *Journal of Materials Processing Technology*, vol. 176, no. 1-3, pp. 273–277, 2006.
- [75] C. W. Lee, C. K. Chua, C. M. Cheah, L. H. Tan, and C. Feng, "Rapid investment casting : direct and indirect approaches via fused deposition modelling," *Int J Adv Manuf Technol*, vol. 23, pp. 93–101, 2004.
- [76] N. Hanumaiah, B. Ravi, and N. P. Mukherjee, "Rapid Hard Tooling Process selection Using QFD-AHP Methodology," *Journal of Manufacturing Technology Management*, vol. 17, no. 3, pp. 332–350, 2006.
- [77] Wohlers Associates Inc, "3D Keltool," *Rapid Prototyping, Tooling & Manufacturing State of the Industry*, vol. 3, pp. 2–3, 2003.

- [78] 3D, “3D keltool - How it Works.” [Online]. Available: [http://www.3dsystems.ru/products/productiontooling/3dkeltool/products{\\\_}3dkel{\\\_}howitworks.asp.htm](http://www.3dsystems.ru/products/productiontooling/3dkeltool/products{\_}3dkel{\_}howitworks.asp.htm)
- [79] Nagahanumaiah, K. Subburaj, and B. Ravi, “Computer aided rapid tooling process selection and manufacturability evaluation for injection mold development,” *Computers in Industry*, vol. 59, no. 2-3, pp. 262–276, mar 2008.
- [80] H. Zhou and D. Li, “Integrated simulation of the injection molding process with stereolithography molds,” *International Journal of Advanced Manufacturing Technology*, vol. 28, pp. 53–60, 2006.
- [81] Y. Song, Y. Yan, R. Zhang, Q. Lu, and D. Xu, “Three dimensional non-linear coupled thermo-mechanical FEM analysis of the dimensional accuracy for casting dies in rapid tooling,” *Finite Elements in Analysis and Design*, vol. 38, no. 1, pp. 79–91, dec 2001.
- [82] R. J. M. Hague, *Unlocking the design potential of rapid manufacturing*, 2006.
- [83] A. K. Sood, R. K. Ohdar, and S. S. Mahapatra, “Improving dimensional accuracy of fused deposition modelling processed part using grey Taguchi method,” *Mater. Des.*, vol. 30, no. 10, pp. 4243–4252, 2009.
- [84] S. Saqib and J. Urbanic, *An experimental study to determine geometric and dimensional accuracy impact factors for fused deposition modelled parts: Enabling manufacturing competitiveness and economic sustainability*. Berlin Heidelberg: Springer, 2012.
- [85] N. Iyer and K. Ramani, “A study of localized shrinkage in injection molding with high thermal conductivity molds,” *Injection Moulding Technology*, vol. 6, no. 2, pp. 73–90, 2002.
- [86] K. Himasekhar, J. Lottey, and K. K. Wang, “CAE of mold cooling in injection moulding using a three dimensional numerical simulation,” *Journal of engineering for industry*, vol. 114, no. 2, pp. 213–221, 1992.
- [87] S.-W. Kim and L.-S. Turng, “Developments of three dimensional computer aided engineering simulation for injection moulding,” *Journal of modelling and simulation in materials science and engineering*, vol. 12, pp. 151–173, 2004.
- [88] K. M. Au and K. M. Yu, “A scaffolding architecture for conformal cooling design in rapid plastic injection moulding,” *International Journal of Advanced Manufacturing Technology*, vol. 34, no. 5-6, pp. 496–515, 2007.
- [89] R. Aluru, M. Keefe, and S. Advani, “Simulation of injection moulding into rapid-prototyped molds,” *Rapid Prototyping Journal*, vol. 7, no. 1, pp. 42–51, 2001.
- [90] L. Q. Tang, K. Pochiraju, C. Chassapis, and Manoochehri, “A computer-aided optimization approach for the design of injection mold cooling system,” *Journal of mechanical design*, vol. 120, no. 2, pp. 165–174, 1998.
- [91] S. Rahmati and P. Dickens, “Rapid tooling analysis of Stereolithography injection mould tooling,” *International Journal of Machine Tools and Manufacture*, vol. 47, no. 5 SPEC. ISS., pp. 740–747, 2007.
- [92] M. Domingo-Espin, J. M. Puigoriol-Forcada, A.-A. Garcia-Granada, J. Llumà, S. Borros, and G. Reyes, “Mechanical property characterization and simulation of fused deposition modeling Polycarbonate parts,” *Materials & Design*, vol. 83, pp. 670–677, oct 2015.
- [93] J. Kotliniski, “Mechanical properties of commercial rapid prototyping materials,” *Rapid prototyping journal*, vol. 20, no. 6, pp. 499–510, 2014.
- [94] I. Gibson and D. Shi, “Material properties and fabrication parameters in selective laser sintering process,” *Rapid prototyping journal*, vol. 3, pp. 129–136, 1997.
- [95] C. Majewski and N. Hopkinson, “Effect of section thickness and build orientation on tensile properties and material characteristics of laser sintered nylon-12 parts,” *Rapid prototyping journal*, vol. 17, no. 3, pp. 176–180, 2011.

- [96] A. K. Sood, R. K. Ohdar, and S. S. Mahapatra, "Experimental investigation and empirical modelling of FDM process for compressive strength improvement," *Journal of advanced research*, vol. 3, no. 1, pp. 81–90, 2012.
- [97] W. Meiners, K. Wissenbach, and R. Poprawe, "Direct generation of metal parts and tools by selective laser powder remelting (SLPR)," *International Congress on Applications of Lasers & Electro-Optics*, vol. 31, pp. E31—E37, 1998.
- [98] Y. Y. Perng, "Modeling Fluid Structure Interactions," 2011. [Online]. Available: <https://support.ansys.com/staticassets/ANSYS/Conference/Confidence/Houston/Downloads/modeling-fluid-structure-interactions.pdf>
- [99] F. K. Benra, H. J. Dohmen, J. Pei, S. Schuster, and B. Wan, "A comparison of one-way and two-way coupling methods for numerical analysis of fluid-structure interactions," *Journal of applied mathematics*, pp. 1–16, 2011.
- [100] H. Schmucker, F. Flemming, and S. Coulson, "Two-way coupled fluid structure interaction simulation of a propeller turbine," *International Journal of Fluid Machinery and Systems*, vol. 3, no. 4, pp. 342–351, 2010.
- [101] P. Stopford, "ANSYS fluid structure interaction for thermal management and aeroelasticity," 2011. [Online]. Available: <https://support.ansys.com/staticassets/ANSYSUK/staticassets/ANSYSFSIforThermalManagementandAeroelasticity11thMay2011.pdf>
- [102] J. San, "System coupling 14.0 - two-way FSI with ANSYS fluent and ANSYS mechanical," in *ANSYS regional conferenc.* ANSYS, 2012. [Online]. Available: <https://support.ansys.com/staticassets/ANSYS/Conference/Confidence/SanJose/Downloads/multiphysics-systems-coupling-2.pdf>
- [103] D. B. Velcea, "Study of a flammable fluid passing through a mixing t-junction by using the ANSYS fluid structure interaction capabilities," *Naval Academy Scientific Bulletin*, vol. 14, no. 2, pp. 335–340, 2015.
- [104] S. Chitrakar, M. Cervantes, and B. S. Thapa, "Fully coupled FSI analysis of Francis turbines exposed to sediment erosion," *International journal of fluid machinery and systems*, vol. 7, no. 3, pp. 101–109, 2014.
- [105] S.-s. Khalid, L. Zhang, X.-w. Zhang, and K. Sun, "Three-dimensional numerical simulation of a vertical axis tidal turbine using the two-way fluid structure interaction approach," *Journal of Zhejiang University science and applied physics and engineering*, vol. 14, no. 8, pp. 574–582, 2013.
- [106] Mechead, "Difference between static and transient analysis?" 2019. [Online]. Available: <http://www.mechead.com/difference-between-static-and-transient-analysis/>
- [107] R. Silva, "Direct coupled thermal-structural analysis in ANSYS workbench," in *ESSS conference & ANSYS userd meeting.* Atibaia, Brasil: ESSS, 2013.
- [108] Renishaw, "Data Sheets - Additive manufacturing," 2019. [Online]. Available: <https://www.renishaw.com/en/data-sheets-additive-manufacturing--17862>
- [109] Resin Systems Corporation, "RS-2243-High Temp Epoxy," 2019. [Online]. Available: [http://resinsystems.com/?page{\\\_}id=1217](http://resinsystems.com/?page{\_}id=1217)
- [110] E. Bienk and N. Mikkelsen, "Application of advanced surface treatment technologies in the modern plastics moulding industry," *Wear*, vol. 207, no. 1-2, pp. 6–9, jun 1997.
- [111] R. A. Witik, J. Payet, V. Michaud, C. Ludwig, and J.-A. E. Månson, "Assessing the life cycle costs and environmental performance of lightweight materials in automobile applications," *Composites Part A: Applied Science and Manufacturing*, vol. 42, no. 11, pp. 1694–1709, nov 2011.
- [112] R. Folgado, P. Peças, and E. Henriques, "Life cycle cost for technology selection: A Case study in the manufacturing of injection moulds," *International Journal of Production Economics*, vol. 128, no. 1, pp. 368–378, nov 2010.

- [113] P. Peças, I. Ribeiro, R. Folgado, and E. Henriques, “A Life Cycle Engineering model for technology selection: a case study on plastic injection moulds for low production volumes,” *Journal of Cleaner Production*, vol. 17, no. 9, pp. 846–856, jun 2009.
- [114] M. Janecek, F. Novy, P. Hrcuba, J. Strasky, L. Trsko, M. Mhaede, and L. Wagner, “The very high cycle fatigue behaviour of Ti-6Al-4V Alloy,” *International symposium on physics of materials*, vol. 128, no. 4, pp. 497–502, 2015.
- [115] A. Kirchner, B. Kloden, T. Weissgarber, B. Kieback, A. Schoberth, S. Bagehorn, and D. Greite-meier, “Mechanical properties of Ti-6Al-4V additively manufactured by electron beam melting,” *Euro PM2015 - AM - Electron Beam Melting*, 2015.